The Synthesis and Optimization of Conjugated Polymers for Photovoltaic Applications

Samuel Chesson Price

A dissertation submitted to the faculty of the University of North Carolina at Chapel Hill in partial fulfillment of the requirements for the degree of Doctor of Philosophy in the Department of Chemistry.

Chapel Hill
2011

Approved by

Edward Samulski

Wei You

Marcey Waters

Thomas Meyer

David Nicewicz

Abstract

Samuel Chesson Price: The Synthesis and Optimization of Conjugated Polymers for Photovoltaic Applications

(Under the direction of Professor Wei You)

Conjugated polymer solar cells have the potential to be a cheap, light weight, robust source of solar power and could contribute to solving the energy problems our future faces. The primary limiting factor for commercialization of these devices is the power conversion efficiency, which is governed by the conjugated polymer semiconductor in the active layer of these devices. However, the current state of the art materials are not optimized, and progress in the design of conjugated polymers must be made for these devices to be financially viable. Synthetic modification of the polymer p-type semiconductor is necessary to fully understand the structure-property relationships that govern the underlying principle performance criteria of these polymer photovoltaic cells. By synthesizing new conjugated polymers with a variety of chemical structures, more insight can be gained into the factors that govern the band gap, oxidation and reduction potential, hole mobility, and phase separation behavior of the conjugated polymer is achieved. The culmination of this knowledge allows for the synthesis of new polymer materials which show exceptionally high photovoltaic efficiency of 7%.

Additionally, these polymers are able to form exceptionally thick films and still maintain high efficiencies. The exceptional performance of these materials grants a unique insight that will affect polymer design strategies in the future.

To David Vernon, my high school chemistry teacher.

Acknowledgements

First & foremost, I'd like to thank my advisor, Wei You. Wei is likely the most patient professor I've ever encountered, and he gave me the space to develop intellectually on my own (aka, propose a ton of bad ideas that ultimately fail). I can recall several days where Wei and I were extremely busy, and yet I still found myself in Wei's office for hours, discussing some interesting paper or result that just came in. If all the supervisors I ever have are like Wei, I would be truly blessed.

Secondly, I want to thank David Vernon, my high school chemistry teacher. Vernon set this whole ridiculous chemistry trip in motion. He changed my attitude towards school by introducing me to a subject that was analytical, yet far more practical than any of the other math or science classes I had before. Vernon is still the best chemistry educator I've ever experienced, and I attribute part of my current success to the knowledge foundation I gained in his class.

I also want to thank Jeremy Niskala, who accompanied me as Wei's first class of graduate students. Jeremy is an excellent friend and researcher, and being around his incredible work ethic was inspiring.

I want to thank Huaxing Zhou, Liqiang Yang, Andrew Stuart, Rycel Uy, Phil Hamilton, Jason Dyke, Nabil Kleinhenz, Paul Hoertz, and Shengqiang Xiao. I've thoroughly enjoyed working with all of you, and each of you have contributed to this thesis.

Finally, I want to thank my family and Olivia. Without Olivia's support through all the frustrating times I've encountered, I would surely have quit long before now.

Table of Contents

Chapter 1: Introduction

The rising cost of traditional, non-renewable energy sources have placed increased public attention on the development of renewable, cheap energy sources for economic and national security reasons. Photovoltaic cells based upon polymer semiconductors are expected to be part of the solution to alternative energy needs for the future, and power conversion efficiencies of such devices are currently nearing the range for commercial application.

Polymer solar cells will provide two distinct potential advantages over current silicon based technology. First, polymer photovoltaics are expected to be lightweight, flexible, and mechanically robust when compared to polycrystalline silicon cells. Secondly, polymer photovoltaics may be manufactured using rapid roll-to-roll, solution printing techniques, rather than the slow, low yielding, thermally inefficient processes which characterize current solar cell manufacturing. Therefore despite modest power conversion efficiencies when compared to inorganic semiconductor solar cells, drastic cost reductions and more potential applications drives the current research interest in polymer solar cells.

Additionally, polymer photovoltaic cells offer the opportunity for extensive modification through chemical synthesis. The typical film thickness for a polymer photovoltaic cell is less than one micro, which would require less than one gram of polymer semiconductor to make a solar cell of one square meter. Significant synthetic modification of the polymer material is not expected to significantly drive up the cost of the final device, given the small amount of material required. Therefore, the chemical synthesis and optimization of conjugated polymers for use in these photovoltaic applications has the potential to dramatically affect the energy technology landscape.

Preliminary Organic Photovoltaics

The first organic photovoltaic cell was developed in 1985 by C. W. Tang at the Eastman Kodak Corporation using copper phthalocyanine (CuPc) dye as the p-type, electron donating semiconductor, and a perylene derivative (1) as the n-type semiconductor.[1] This bilayer device was roughly 1% efficient, however it was manufactured using high vacuum evaporation methods to deposit the films used for the cell.

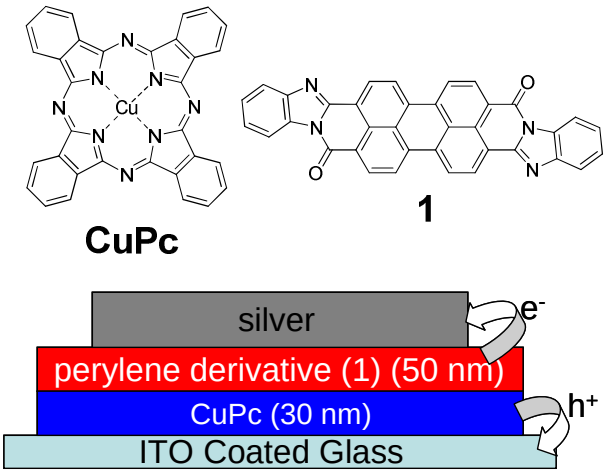

Figure 1.1. Materials used in the first organic photovoltaic cell. The perylene is the electron transporter, and the phthalocyanine transports the holes to the ITO anode.

Small molecules such as CuPc are difficult to deposit using low temperature, rapid methods at atmospheric pressure. However, soluble polymer materials readily form homogenous thin films using printing and other low cost solution deposition techniques. Recognizing this potential of conjugated polymers, the research partnership of Nobel laureate Alan Heeger & Fred Wudl began investigating conjugated polymers for use in photovoltaics. First in 1992, they found that a conjugated polymer, MEH-PPV, transferred an electron to the n-type semiconductor buckminsterfullerene when excited by light, much in the same way as the CuPc-perylene tandem in Tang's work.[2] The buckminsterfullerene (C_{60}) was poorly soluble in most organic solvents, and thus in order to develop solution processable photovoltaic cells, Wudl began investigating methods to increase the solubility of the fullerene derivative without altering its electron accepting and electron transporting properties. In 1995, Wudl reports the synthesis of [6,6]-phenyl-C61-butyric acid methyl ester ($PC_{61}BM$).[3] The addition of the phenyl-butyric methyl ester side chain

disrupts the aggregation of the $PC_{61}BM$ in solution, increasing its solubility without drastically affecting the electrochemical behavior.

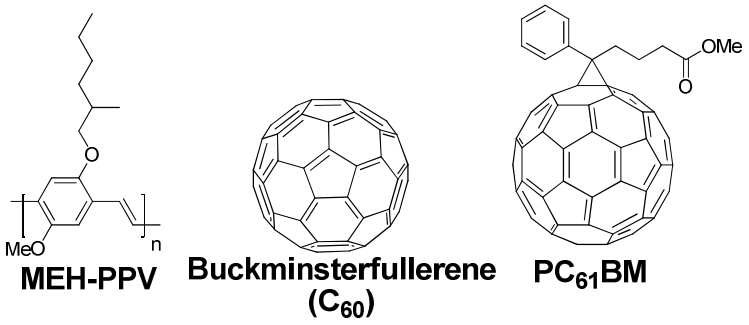

Figure 1.2. The first organic semiconducting materials developed for use in polymer photovoltaic cells.

This discovery lead to the development of the first polymer photovoltaic cells using MEH-PPV:$PC_{61}BM$ composites, which were fabricated by spin casting a blend of the two materials from solution.[4] This blend, coined a bulk-heterojunction, works especially well because the polymer and fullerene demix and phase segregate, forming a bi-continuous interpenetrating network of p-type and n-type materials. This allows for a larger interfacial area between the two semiconductors, increasing the charge separation efficiency.

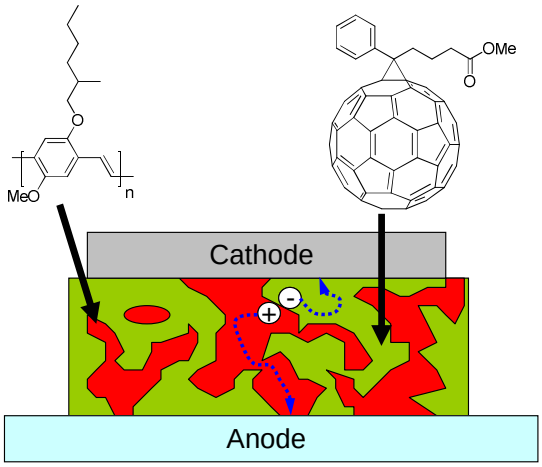

Figure 1.3. A bulk heterojunction, where charges are split at the polymer:$PC_{61}BM$ interface, and travel through either the polymer (for holes) or the $PC_{61}BM$ (for electrons) to the electrodes.

This work forms the primary basis for polymer solar cells. Advances have been accomplished, especially identifying the governing fundamental principles which affect the performance of these devices. However, the innovative idea of an organic solar cell which can be quickly and cheaply fabricated using solution processing was first explored in these four reports.

Device Mechanisms and Performance in Polymer Solar Cells

The overall power conversion efficiency (η) of any photovoltaic cell is determined from the equation:

$$\eta = \frac{J_{sc} V_{oc} FF}{P_{in}}$$

where J_{sc} is the short circuit current density (mA/cm^2), V_{oc} is the open circuit voltage (V), FF is the fill factor (%), and P_{in} is the irradiance (mW/cm^2). The values of the three variables in the numerator are determined from a current density vs. voltage plot obtained while irradiating the cell with light. The J_{sc} is a measure of how many charges are extracted from the photovoltaic cell when no opposing voltage is applied, and the V_{oc} is a measure of the voltage which must be applied in order to prohibit all charges from being extracted from the cell.

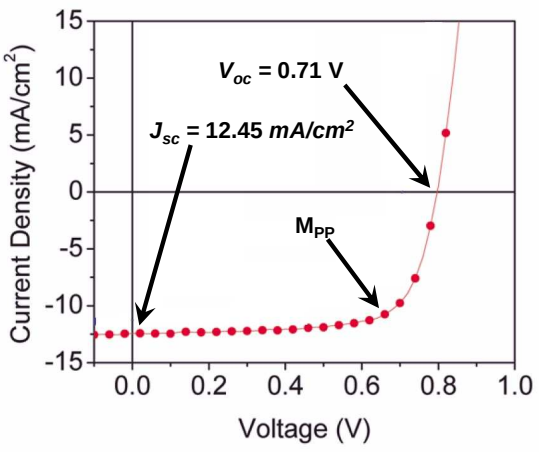

Figure 1.4. Typical current density vs. voltage plot for a conjugated polymer material, showing the J_{sc}, V_{oc}, and the maximum power point. Reprinted with permission from ref 5.

The fill factor is given by the following equation:

$$FF = \frac{V_{M_{pp}} J_{M_{pp}}}{V_{oc} J_{sc}}$$

where the V_{Mpp} and J_{Mpp} are the current and voltage at the maximum power point on the current density vs. voltage plot.

The device performance of polymer photovoltaic cells occurs in five different phases: 1) light absorption; 2) exciton diffusion and charge separation; 3) charge transfer complex dissociation into free charge carriers; 4) free charge transport through the matrix; 5) charge collection at the electrodes.

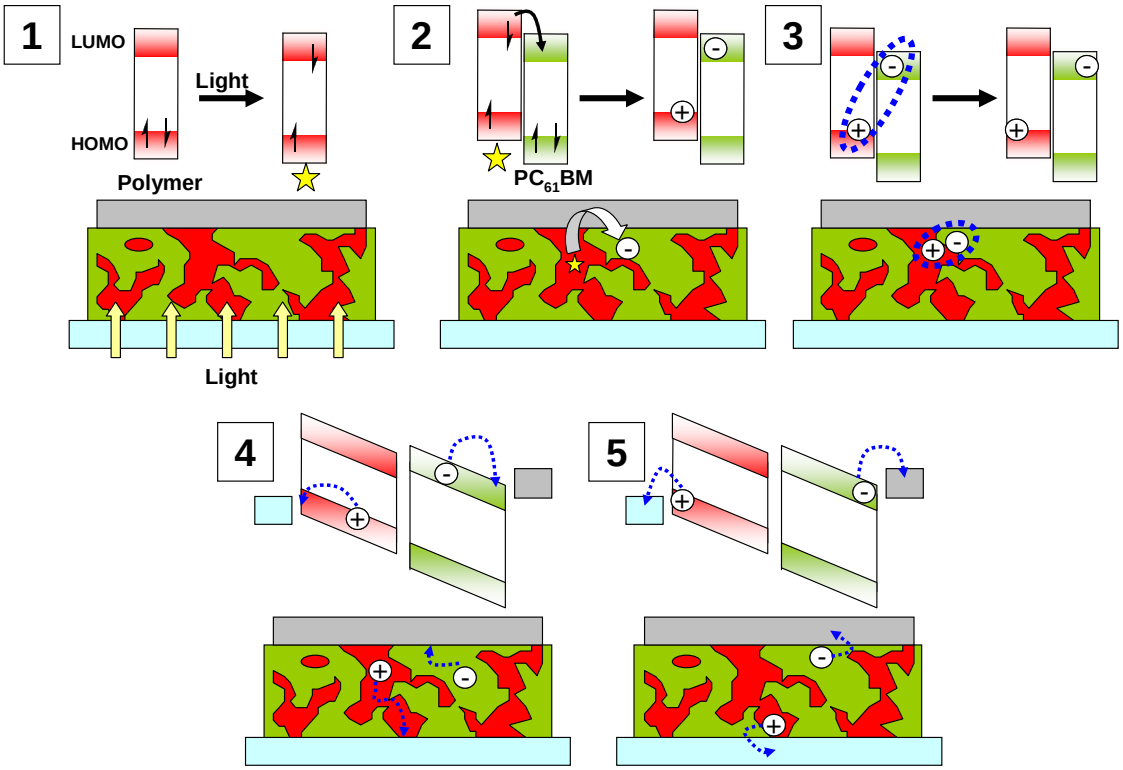

Figure 1.5. Summary of the five phases involved in power generation in polymer photovoltaic cells.

Light absorption by either the conjugated polymer or the fullerene is the first critical energy harvesting phase in the photovoltaic process. First, light passes through a transparent anode, which is typically a double layer of tin doped indium oxide (ITO) coated with poly(3,4-ethylenedioxythiophene) doped with poly(styrenesulfonate) (PEDOT:PSS). Both layers are over 80% transmissive in the visible region of the electromagnetic spectrum. Other transparent anode materials have been investigated, and

transparent cathodes used for inverted devices have also been explored.[5-7,8-10] However, for this particular study and the vast majority of research on conjugated polymer solar cells, PEDOT:PSS coated ITO is the transparent anode material employed.

The polymer material typically absorbs the majority of the light harvested by the polymer photovoltaic cell. The energy of the light absorbed must be greater than the band gap (E_g) of the polymer, or the energy difference between the HOMO and the LUMO of the polymer. Therefore, the smaller the band gap of the polymer, the amount of light absorbed will increase and the J_{sc} will increase as well. Band gaps for polymer photovoltaic materials typically range between 2.0-1.4 eV, which would allow for a maximum of 18-47% of the incident photon flux from the sun to be absorbed.[11] The amount of light absorbed is also dependent on the film thickness, and the absorption coefficient of the polymer. Thicker films will allow more photons to be absorbed, especially in regions of the absorption spectrum where the polymer absorption coefficient is low. The $PC_{61}BM$ also absorbs a non-trivial amount of light, especially in the region between 300-400 nm. Other fullerene derivatives such as [6,6]-phenyl C_{71} butyric acid methyl esters ($PC_{71}BM$) have been synthesized in order to increase the light absorption from the fullerene component, however their effect on the photovoltaic performance is modest in most cases.[12]

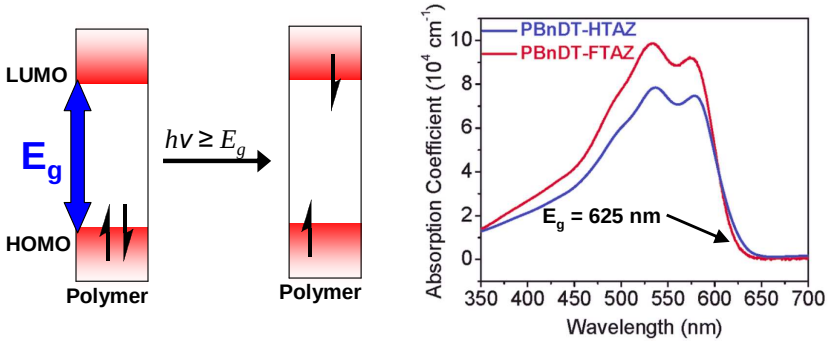

Figure 1.6. Absorption of light greater than or equal to the band gap of the polymer creates a singlet excited state. The band gap is determined from the absorption edge of the UV-Visible absorption spectrum. In the polymer absorption spectrum shown, the band gap of each polymer is roughly 625 nm or 1.98 eV. UV-Visible spectrum reprinted with permission from ref. 5.

After the light has been absorbed by the active layer, the semiconductor forms an excited state called an exciton.[13] Due to the low dielectric constant of organic materials, these excitons are bound excited

states with finite lifetimes which require anywhere from 0.1 to 0.5 eV to dissociate the exciton into charges on two separate molecules.[14-16] Excitons are dissociated at the polymer:fullerene interface, and the required distance of the exciton from the interface in order to dissociate is estimated anywhere between 5 nm for $PC_{61}BM$ excitons, to values as large as 20 nm or even 80 nm in conjugated polymer excitons.[17-19] If the charges do not reach the polymer:fullerene interface, this reduces the J_{sc}. Clearly close proximity to the polymer:fullerene interface is critical, and bulk heterojunctions currently provide the best method for exciton dissociation since the domain sizes of the polymer and fullerene are usually small and in close contact.

Exciton splitting is an exceptionally fast process once the exciton is close enough to the interface to dissociate, faster than any other exciton decay mechanisms. Therefore exciton splitting is highly efficient for materials with the required 0.1-0.4 eV $LUMO_{polymer}$-$LUMO_{PCBM}$ offset, with a yield close to unity.[2] Any energy difference greater than 0.4 eV is wasted, and therefore minimizing the LUMO-LUMO gap to the minimal value is highly important for highly efficient polymer solar cells.

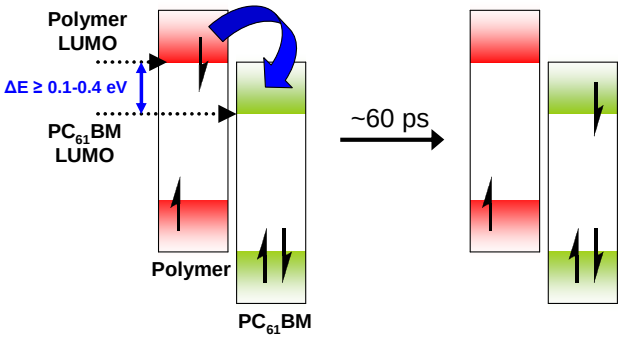

Figure 1.7. Exciton dissociation occurs if the energy offset between the LUMO of the two organic semiconductors is greater than or equal to 0.1-0.4 eV. The process is rapid, and occurs in less than 60 picoseconds.

After exciton dissociation, the two separated charges on the polymer and fullerene create a coulombically bound radical ion pair, which is called a charge transfer complex or charge transfer exciton.[20,21] These bound charge pairs at the polymer:fullerene interface determine the V_{oc} of the polymer photovoltaic cell, which is predominantly determined by the difference between the HOMO of the polymer and the LUMO of the $PC_{61}BM$ ($\Delta E_{D\text{-}A}$).[22] Additionally, the ground state interaction between the two

components, the nature of the polymer:fullerene interface, and the relative permittivity of the film also affect the V_{oc} of the photovoltaic cell. [22,23,24] The charge transfer complex may recombine to the ground state if it is not dissociated into free charge carriers.

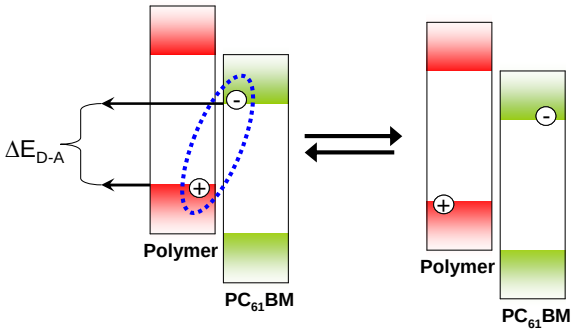

Figure 1.8. Charge transfer complex must reversibly dissociate into free charge carriers to produce current. Energy difference between the HOMO of the polymer and the LUMO of the fullerene (ΔE_{D-A}) is the primary determining factor for the V_{oc}.

Once the charge transfer complex has been dissociated into free charge carriers, the internal electric field applied by the electrodes of the photovoltaic cell cause the charges to move towards their corresponding electrodes. The rate at which these charges move for a given electric field is determined by the charge carrier mobility (μ) which has units of velocity multiplied by the inverse of the electric field ($cm^2\ V^1\ s^{-1}$). Fullerenes, being spherical, allow for π cloud overlap in any orientation relative to other fullerenes. Therefore even in a disordered system such as a bulk heterojunction, the π-π distance between fullerenes is minimal and the electron mobility is quite rapid. A balanced charge mobility between electrons and holes and an optimal phase segregated morphology will prevent free charge carriers from recombining.

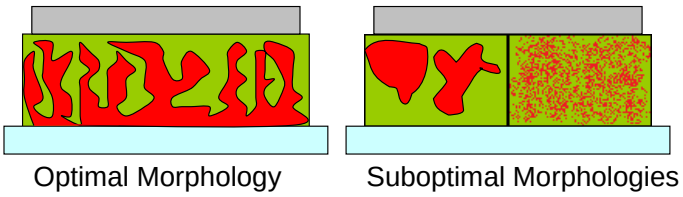

Figure 1.9. The optimal morphology is a phase segregated network, where both networks are continuous and the domain sizes are between 40-200 nm. A suboptimal morphology contains islands of material not connected to the electrodes, and either too much or too little phase segregation.

Lastly, charges must cross the interface between bulk active layer and the electrodes. The work function of the electrodes must be lower (in absolute value) than the HOMO of the polymer and the LUMO of the PCBM. Otherwise, injection barriers from non-ohmic contacts will result which limit the open circuit voltage of the photovoltaic cell.[25] Therefore low work function metals evaporated in high vacuum such as aluminum and calcium are the predominant cathode materials used for photovoltaic cells at the research scale. The PEDOT:PSS has a work function of roughly 5.0 eV, which is sufficient to inject holes into polymers with HOMO energy levels as low as -5.8 eV.

Polymer Design Strategy

The conjugated polymer in bulk heterojunction photovoltaic cells is required to do essentially three things; 1) Absorb light; 2) Split excitons efficiently with the minimum LUMO-LUMO offset required; 3) Transport holes to the anode. All three of these criteria are affected by the polymer structure, and even small changes in structure can create large effects on the properties of the material. There are two main parts to each conjugated polymer structure, the aromatic units and the aliphatic side chains.

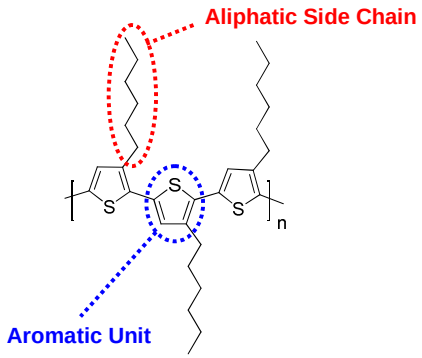

Figure 1.10. The two main parts of the conjugated polymer, region-regular P3HT.

The aromatic units should be selected with planarity, a low LUMO, and non-intrusive positions to attach the aliphatic chains as the key design parameters of the material. Control of the electronic energy levels of the conjugated polymer semiconductor is the first and easiest design parameter to be considered. Controlling the band gap of conjugated polymers is typically accomplished employing either the quinoidal stabilization approach or the intramolecular charge transfer (ICT) approach.[26]

The quinoidal stabilization approach lowers the band gap by stabilizing the quinoidal resonance form of the conjugated polymer, typically by forming stabilizing aromatic systems when the polymer is in the quinodal resonance form. This approach was pioneered by Fred Wudl in 1984 when he reported the synthesis of poly(isothianapthalene), which exhibited a band gap of 1.0 eV.[27] By stabilizing the quinodal structure, there is more double bond character between the two aromatic monomer units. This leads to an elevation of the energy level of the HOMO and a reduction of the LUMO, thus reducing the band gap. This method allows for control of the band gap, and more importantly the LUMO of the polymer so that the $LUMO_{polymer}$-$LUMO_{PCBM}$ offset may be minimized. In 2009, Luping Yu and coworkers developed a polymer which employed this method for controlling the band gap, and photovoltaic cells using this polymer obtained 6.8% efficiency.[28]

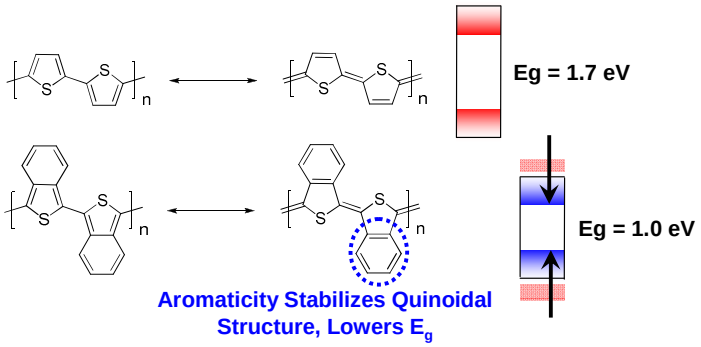

Figure 1.11. Quinoidal resonance structure is stabilized by the formation of a benzene ring in poly(isothianapthalene). This raises the HOMO and lowers the LUMO, thus reducing the band gap by 0.7 eV over unsubstituted polythiophene.

The second method for controlling the electrochemical LUMO and the band gap is the ICT approach (sometimes referred to as the Donor-Acceptor approach). Pioneered by Havinga & coworkers working for the Phillips Corporation in 1992, this approach uses alternating electron rich and electron poor heterocycles to control the HOMO and LUMO energy levels.[29] This method also functions by stabilizing the quinoidal resonance structure, except that the mechanism of the stabilization is different. The HOMO adopted by the polymer is roughly the HOMO of the electron rich unit, and the electron poor unit primarily dictates the position of the LUMO energy level. This is advantageous since the energy levels can be controlled independently from one another, rather than in tandem like the quinoidal stabilization approach.

In one particularly illustrative example, Tour & coworkers synthesized polythiophene with alternating diamino and dinitro groups at the β-positions of the thiophenes, reducing the band gap by 0.7 eV over unfucntionalized polythiophene.[30]

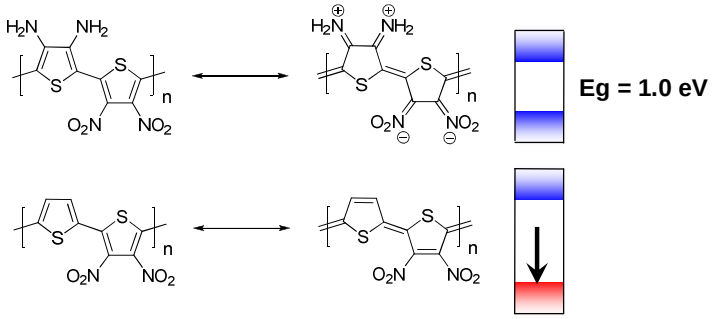

Figure 1.12. ICT approach. To affect only the LUMO, the electron rich unit can be omitted from the polymer.

The aromatic units utilized on the polymer backbone should also be selected so that they minimize any steric interactions that would cause the aromatic units to twist out of plane from one another. An illustrative example of this is the difference between poly(p-phenylene) and polythiophene. Poly(p-phenylene) has significant steric hindrance between the two hydrogens on adjacent phenyl rings. This prevents the phenyl rings from being coplanar, and thus increases the band gap significantly. Polythiophene on the other hand presents no such steric issues, and creates a coplanar polymer structure. Regio-regular poly(3-hexylthiophene) (rr-P3HT) is possibly the most notable application of this principle.[31,32] Head to head couplings in regiorandom P3HT cause undesirable steric effects, which leads to backbone twisting and red-shift in the λ_{max} by roughly 25 nm.

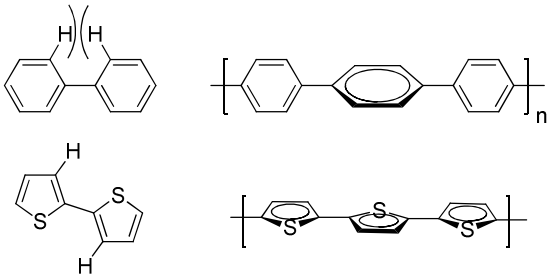

Figure 1.13. Polythiophene adopts a coplanar structure, while steric factors prohibit this planarity in the case of poly(p-phenylene).

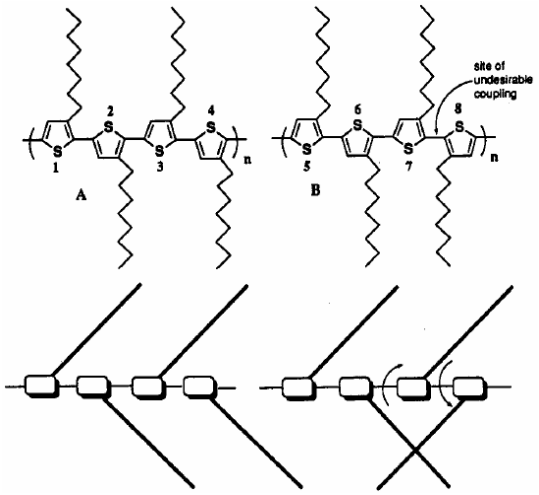

Figure 1.14. Head to head coupling in Regiorandom P3HT causes undesirable backbone twisting due to steric effects. Reprinted with permission from ref. 34.

As illustrated in the P3HT example, the regiochemical placement of the side chain is critical to the properties of the resulting polymer system, and any heterocycle employed should provide an unobtrusive location for side chain attachment. In addition to twisting of the adjacent aromatic monomer units, the side chain also needs to be placed frequently enough on the polymer backbone to prevent intimate interactions of the polymer with the $PC_{61}BM$. This is explicitly shown by the poor performance of poly(2,5-bis(3-hexadecylthiophen-2-yl)thieno[3,2-b]thiophene (pBTTT), which has wide spacing between the side chains on the aromatic backbone.[33] Intercalation of the $PC_{71}BM$ in between the side chains of the polymer requires that significantly more $PC_{71}BM$ be used to create the optimal photovoltaic performance. Additionally, intercalation causes increased recombination and a lower open circuit voltage due to increased interaction of the polymer with the fullerene in the ground state. Therefore, the aromatic units must have places to incorporate side chains frequently along the aromatic backbone.

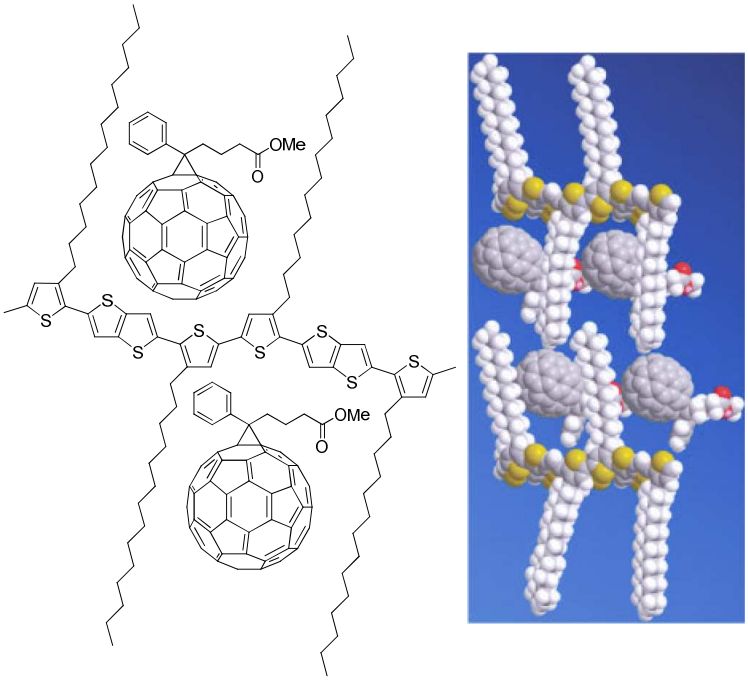

Figure 1.15. PCBM intercalates into pBTTT inhibiting phase segregation, reducing the open circuit voltage, and promoting recombination. Intercalation between the side chains of P3HT is inhibited since the space between them is significantly smaller. Reprinted with permission from ref. 35.

After correct selection and design of the aromatic units comprising the conjugated backbone, the aliphatic solubilizing chains must be selected. Selecting the correct solubilizing chains is an optimization problem between long chains which increase solubility and shorter ones which allow for more rapid hole transport. One main method to achieve both of these goals simultaneously is to branch the side chain. Side chain branching allows for an increased number of carbons to be attached while keeping the distance the side chains protrude from the polymer backbone short. Shortening this distance increases the hole mobility of the resulting polymer. In fact, since holes are transported along the polymer chain rapidly, only a few side chains must be shortened in order to increase the hole mobility of the entire film.

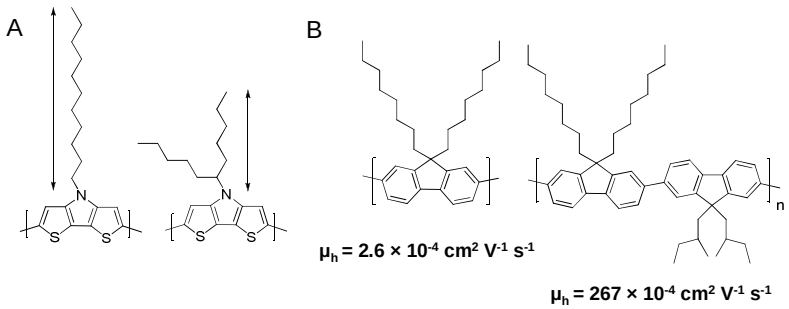

Figure 1.16. A) Both dithienopyrroles have 11 carbons in the aliphatic chain, however the branched chain allows other polymer chains to pack closer, since the in-plane distance of the alkyl chain is shorter. B) When 9,9-diisobutylfluorene is copolymerized with 9,9-dioctylfluorene, the hole mobility of the copolymer increases by two orders of magnitude over poly(9,9-dioctylfluorene).[34]

However, shorter chains only increase the hole mobility as long as the molecular weight of the polymer material remains high. Decreasing the chain length can often cause a polymer to lose solubility and precipitate during the polymerization, rather than reaching high molecular weight. The shorter polymer chains do not make homogenous films, and can form crystalline domains. And while the hole mobility in these crystalline domains is high, the grain boundaries in between each domain provide significant hole transport barriers which cause the hole mobility of the bulk film to be significantly lower.[35] This tendency to form crystalline domains causes the photovoltaic performance to suffer as well, and therefore high molecular weight polymer is critical to obtaining high photovoltaic performance.[36,37]

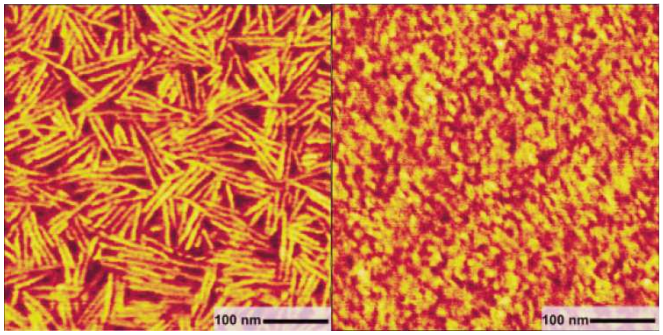

Figure 1.17. Low molecular weight P3HT (left) forms partially crystalline films, with large grain boundaries. These grain boundaries reduce the hole mobility by over three orders of magnitude. Reprinted with permission from ref. 37.

State of the Art: 2006

When this dissertation was proposed in 2006, many of the concepts discussed in this introduction were unknown or poorly understood. The polymer with the highest reported device efficiency was P3HT at 5%.[38] No polymer with a band gap lower than 1.9 eV had achieved power conversion efficiencies over 2%. The most successful low band gap conjugated polymer photovoltaic cells were reaching efficiencies of only 1%, likely due to the low molecular weight of the materials.[39,40] However, many of the performance criteria for these bulk heterojunction photovoltaic cells were just becoming understood. Therefore, this project was initiated at precisely the right time. Our efforts focused on designing polymer materials which would achieve high photovoltaic efficiencies at band gaps lower than P3HT.

Chapter 2: Polycyclic Aromatics with Flanking Thiophenes: Tuning Energy Level and Band Gap of Conjugated Polymers for Bulk Heterojunction Photovoltaics

Adapted with permission from *Macromolecules* **2009**, *43*, 797.

By Samuel C. Price, Andrew C. Stuart, and Wei You

In $PC_{61}BM$ based BHJ solar cells, the theoretical maximum V_{oc} of a device is determined by highest occupied molecular orbital (HOMO) energy level of the conjugated polymer, and the theoretical maximum J_{sc} of a device is largely dependent on the band gap of this conjugated polymer.[41] The most successful low band gap polymer design strategy to date for photovoltaic devices is the donor-acceptor alternating copolymer (or intramolecular charge transfer copolymer) strategy, which has produced several polymers with photovoltaic power conversion efficiencies larger than 4.0%.[42-51] The HOMO level of these donor-acceptor copolymers is determined almost exclusively by the donor monomer.[52,53] In order to decrease the HOMO level (and raise the V_{oc} of the resulting photovoltaic cell), donors with "weaker" electron donating ability should be applied to this strategy. However, while "weaker" donors will improve the V_{oc} by lowering the HOMO, they will also widen the band gap since the interaction between the electron rich donor and the electron poor acceptor is what lowers the band gap of these copolymers. Additionally, polymers with HOMO levels below – 5.9 eV exhibit higher rates of geminate charge recombination.[54] Thus, finding an optimal donor monomer which maximizes the photovoltaic efficiency is a complex synthetic optimization problem.

To systematically discover this optimal donor monomer, a design strategy based upon fusing aromatic rings of different oxidation potentials into bithiophene was envisioned. First, bithiophenes flanking a center aromatic ring was chosen as a template, since fused thiophenes have produced several high mobility polymers, and the flanking thiophenes would reduce steric hindrance and create smaller dihedral angles with adjacent monomers. Then pyrrole, benzene, and pyridine were inserted into the bithiophene template to create three donor monomers of decreasing electron donating ability. These three monomers were then copolymerized with 2,1,3-benzothiadiazole and with thiophene in order to study the optical, electronic, photovoltaic properties of these polymers, and to identify the most promising monomer for future study.

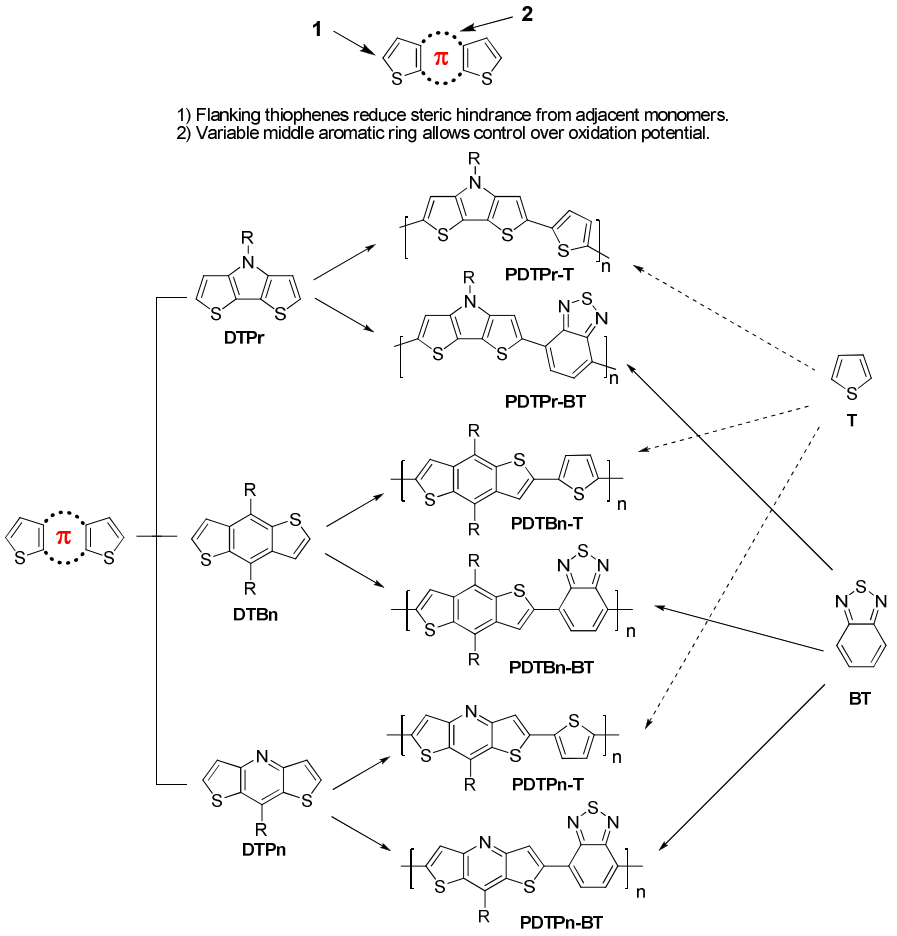

Figure 2.18. The library of structurally related polymers. "DT" stands for dithiophene. "Pr", "Bn" and "Pn" stand for fused pyrrole, benzene, and pyridine, respectively. "T" for thiophene, and "BT" for benzothiadiazole.

Monomer and Polymer Synthesis

Two structural units, dithieno[3,2-*b*:2',3'-*d*]pyrrole (DTPr)[55,56] and benzo[1,2-*b*:4,5-*b'*]dithiophene (DTBn),[57] were synthesized according to literature procedures. Long branched alkyl chains were attached in the center pyrrole or benzene unit to ensure the solubility of resulting polymers. Both units were readily converted into distannylated monomers to co-polymerize with dibrominated co-monomers via Stille coupling polymerization, offering corresponding polymers (Figure 1). The third structural unit, dithieno[3,2-*b*:2',3'-*e*]pyridine (DTPn), has also been reported in the literature.[58] However, in our efforts to synthesize dithienopyridines with long solubilizing alkyl chains, we encountered a great deal of difficulty with the established synthetic route.[58] The literature procedure employed a bromination (Figure 1A) in the final steps of the synthesis, which offered the target molecules with very low yield when long alkyl chains were involved (6% when R = *n*-dodecyl).[59] With our particular substrates which possessed a more bulky alkyl chain at the 8 position of the DTPn, the reported bromination procedure resulted in either inseparable mixtures, or exceptionally low yields.

The distannyl intermediate of the literature bromination procedure could also serve as a polymerizable monomer for Stille coupling polymerization, however, metalation of (1) with *n*-BuLi according to the literature procedure resulted in a mixture of monostannyl and distannyl compounds which could not be separated. In an attempt to optimize the stannylation procedure, (1) was lithiated with *n*-BuLi then quenched with deuterated methanol (Figure 19B). This deuterium labeling experiment reveal that even after 5 hours, the lithiation was not complete, and some starting material remained according to NMR (Figure 20). Attempts to optimize the metalation procedure using *tert*-BuLi resulted in complete deprotonation with no traces of starting material; however the deprotonation was not selective, resulting in a 57:43 mixture of α:β deprotonation. Therefore, a new synthetic route to prepare polymerizable 8-alkyldithienopyridines was required.

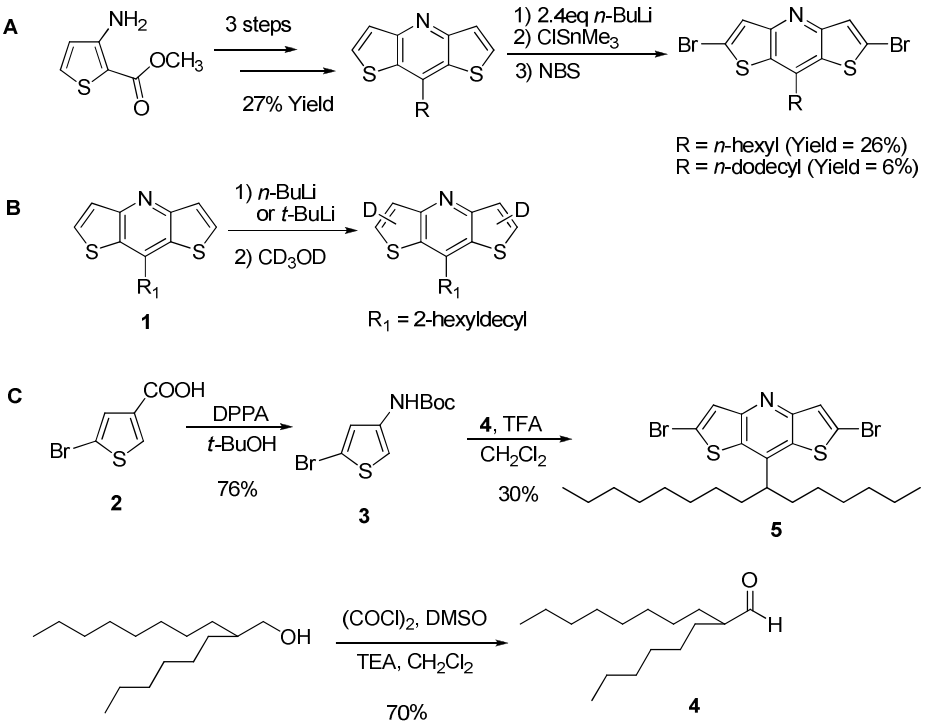

Figure 2.19. (A) Literature procedure to synthesize the dibrominated DTPn. (B) Deuterium labeling experiment. (C) Modified synthetic procedure of dibrominated DTPn.

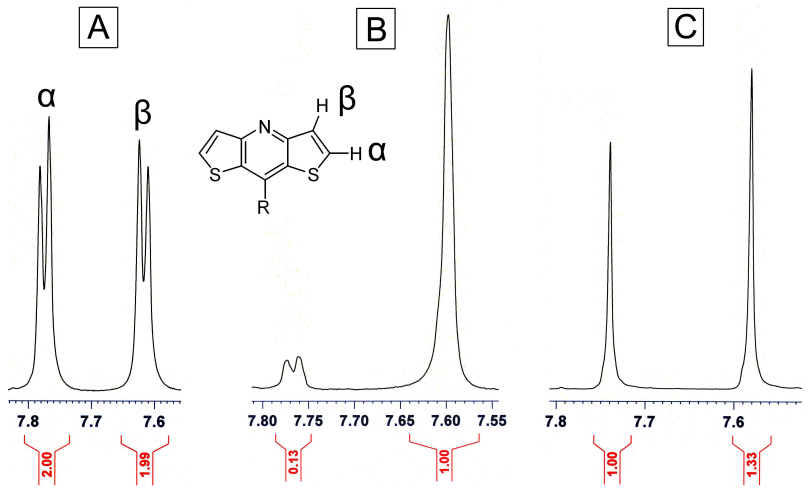

Figure 2.20. NMR results of lithiation study with deuterium labeling. (A) Starting material. (B) Product of *n*-BuLi lithiation & quench with CD_3OD. C) Product of *tert*-BuLi lithiation & quench with CD_3OD.

Due to these deficiencies with the literature preparation, a modified synthetic scheme (Figure 19C) that introduced a bromine in the α position of the thiophene before condensation to form the pyridine ring was envisioned. The bromine was introduced in the first step by bromination of the commercially available thiophene-3-carboxylic acid.[60] The acid (2) was then subjected to a Curtius rearrangement to produce the Boc protected amine (3) in good yield. The Boc protecting group stabilized the easily oxidized amine, and was readily deprotected *in situ* in the subsequent acid catalyzed condensation step. The aldehyde (4) was chosen to ensure the good solubility of the resulting polymers. The TFA catalyzed condensation then afforded the final monomer (5) as a solid, which would aid in preparing high molecular weight polymers from typical condensation polymerizations where rigorous control of stoichiometry is required. This monomer (5) was then copolymerized with 2,5-bis(trimethyltin)thiophene or 2,1,3-benzothiadiazole-4,7-bis(boronic acid pinacol ester) to offer the desired polymers, PDTPn-T and PDTPn-BT.

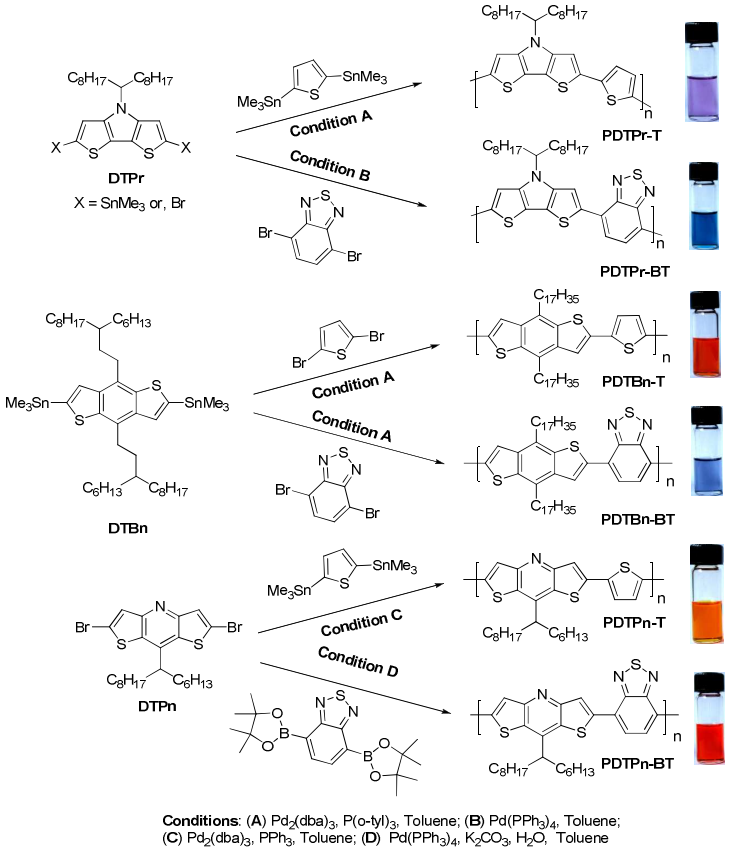

Figure 2.21. Synthesis of polymers via palladium catalyzed coupling reactions. Shown on the right are solutions of each polymer.

The crude copolymers were washed extensively with methanol, followed by the Soxhlet extraction with methanol, and ethyl acetate successively to remove byproducts and oligomers. Finally, the polymers were extracted by hexane or chloroform and re-collected by precipitating them into methanol, and dried under vacuum. The molecular structures of both polymers were confirmed by ^{1}H NMR spectroscopy. The yields, molecular weights, and degree of polymerization of polymers are listed in Figure 2.22. The low yield of PDTPr-T can be attributed to its low solubility, as large quantities of solid remained in the Soxhlet extraction thimble after chloroform extraction. The opposite problem explains the low polymer yield for PDTBn-BT, in that a large quantity of material was collected in the hexane fraction of the polymerization. However, this hexane fraction consisted of low molecular weight polymer, and only the high molecular weight chloroform fraction was used, decreasing the polymerization yield significantly. The molecular weights were determined by gel permeation chromatography (GPC) in THF or 1,2,4-trichlorobenzene by referring to polystyrene standards (Figure 22). The molecular weights of DTPn based polymers (PDTPn-T and PDTPn-BT) are noticeably low, which can be attributed to their lower solubility during the polymerization reaction.

Figure 2.22. Polymerization results for all six polymers

	Yield [%]	M_n [kg/mol]	M_w [kg/mol]	X_n	PDI
PDTPr-T	13%	12.2 [a]	50.3 [a]	24.5	4.1
PDTPr-BT	63%	8.0 [b]	17.6 [b]	14.5	2.20
PDTBn-T	93%	54.1 [b]	109.6 [b]	85.2	2.02
PDTBn-BT	8%	69.9 [b]	150.7 [b]	97.5	2.15
PDTPn-T	90%	4.3 [a]	10.7 [a]	8.9	2.47
PDTPn-BT	76%	1.5 [a]	2.6 [a]	2.8	1.68

[a] Determined by GPC in 1,2,4-trichlorobenzene using polystyrene standard at 150 °C. [b] Determined by GPC in THF using polystyrene standards.

Optical and Electrochemical Properties

This collection of structurally similar yet energetically diverse polymers allows for the interplay between the electron donating ability of the donor monomer and the optical and electronic properties to be studied in detail. The optical and electrochemical properties of these polymers are summarized in Figure 2.26.

Interestingly, the HOMO energy level of the entire conjugated polymer is dominated primarily by the most electron rich aromatic unit in the polymer, regardless of what other rings it is fused to. For example, nearly identical HOMO levels of – 4.89 eV and – 4.94 eV were observed in PDTPr-T and PDTPr-BT respectively, because the most easily oxidized ring in these two polymers is the pyrrole ring. Therefore, the monomer DTPr is polymerized with (BT or T) has little effect on the HOMO energy level, and this phenomena is common with other polymer systems.[61] However, when the pyrrole ring is substituted for a benzene or pyridine ring, a drastic reduction in the HOMO energy level is observed. Since the newly substituted benzene or pyridine ring is no longer the most electron rich ring in the system, the HOMO is relatively independent of which ring is substituted for the pyrrole ring. For example, nearly the same HOMO energy levels (– 5.55 eV vs. – 5.56 eV) are measured for PDTBn-BT and PDTPn-BT. This is because the HOMO behavior is dominated by the two flanking thiophene rings. The same trend is apparent in the case of PDTBn-T and PDTPn-T, as the HOMO behavior is dominated by the copolymerized thiophene ring and causes the HOMO position to be roughly equal for both polymers despite their structural differences.

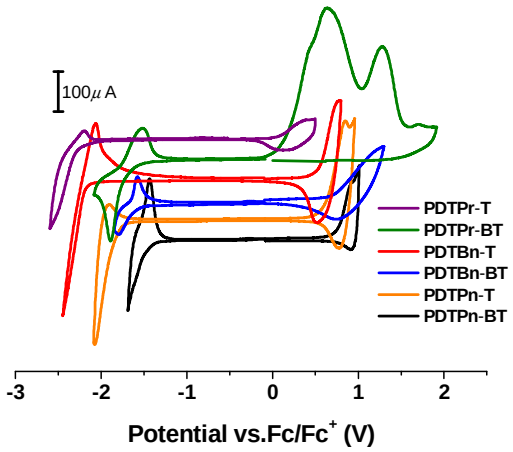

Figure 2.23. Cyclic voltammograms of all polymers.

Despite the HOMO energy level depending greatly on the most electron rich ring in the aromatic system, the optical band gap involves the entire polymeric system. Even though the HOMO energy level of the DTPn polymer series is little changed from the DTBn series, the band gaps of the DTPn series are significantly wider than these of the DTBn series. For example, the band gap of PDTPn-BT (2.1 eV) is noticeably larger than that of PDTBn-BT (1.8 eV), due to the electron deficient pyridine, which diminishes the donor-acceptor interaction in the copolymer that gives the low band gap.

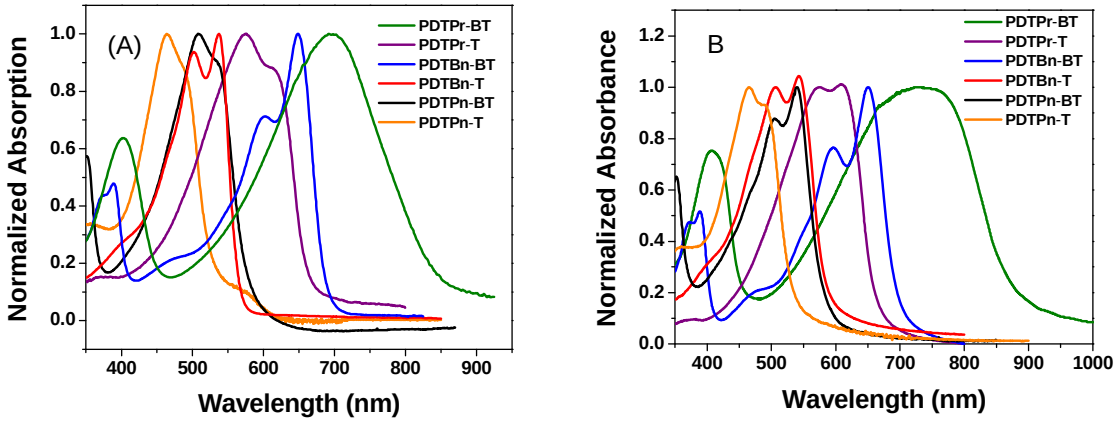

Figure 2.24. (A) Solution absorption of all polymers in chloroform. (B) Film absorption spectra.

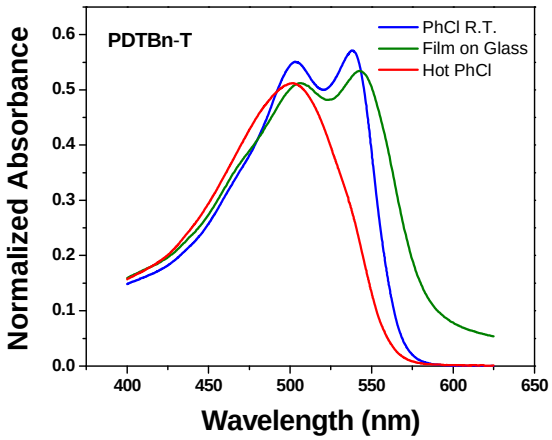

Figure 2.25. UV-Vis spectra of PDTBn-T in boiling chlorobenzene, the same solution at room temperature, and from a spun cast film on glass.

Based on electrochemical and optical considerations alone, DTBn is the most promising candidate for use in photovoltaic devices. The low measured HOMO energy levels predict high values of the V_{oc}, and the measured optical band gap remains low. Conversely, these results exhibit the DTPn and DTPr units less favorably as possible successful candidates for use in photovoltaic devices. The band gaps of polymers made from the DTPn donor unit are significantly wider than the others in this study, while the HOMO levels are almost identical to the HOMO levels of the DTBn series. While polymers based upon DTPr have large theoretical maximum currents due to their lower band gaps, the HOMO levels of this series of polymers remains too high to yield devices with high efficiencies.

Figure 2.26. Optical and electrochemical data of all polymers

	UV-Vis Absorption						Cyclic Voltammetry	
	$CHCl_3$ solution			Film			E^{ox}_{onest} (V)	E^{red}_{onest} (V)
polymer	λ_{max} [nm]	λ_{onset} [nm]	$E_g{}^a$ [eV]	λ_{max} [nm]	λ_{onset} [nm]	$E_g{}^a$ [eV]	HOMO [eV]	LUMO [eV]
PDTPr-T	575	659	1.9	609	663	1.9	0.09/– 4.89	– 2.24/– 2.56
PDTPr-BT	697	837	1.5	727	875	1.4	0.14/– 4.94	– 1.73/– 3.07
PDTBn-T	537	566	2.2	543	584	2.1	0.55/– 5.35	– 2.18/– 2.62
PDTBn-BT	648	688	1.8	650	694	1.8	0.75/– 5.55	– 1.55/– 3.25
PDTPn-T	465	535	2.3	465	534	2.3	0.63/– 5.43	– 1.83/– 2.97
PDTPn-BT	508	580	2.1	540	579	2.1	0.76/– 5.56	– 1.47/– 3.33

[a] Calculated from the intersection of the tangent on the low energetic edge of the absorption spectrum with the baseline.

Photovoltaic Properties

These structurally similar, yet optically and electrochemically very different polymers were tested in bulk heterojunction photovoltaic devices. Standard BHJ device configuration was used (ITO/PEDOT/polymer:PCBM/Ca/Al). A calibrated AM 1.5G light source (100 mW/cm^2, 1 Sun) was

employed to simulate the irradiation from the Sun. The blending ratio of polymer vs. PCBM and the thickness of the active layer were varied to achieve the best device performance under semi-optimized conditions (Figure 2.28). Representative J-V curves of these polymers under 1 Sun condition are displayed in Figure 2.27.

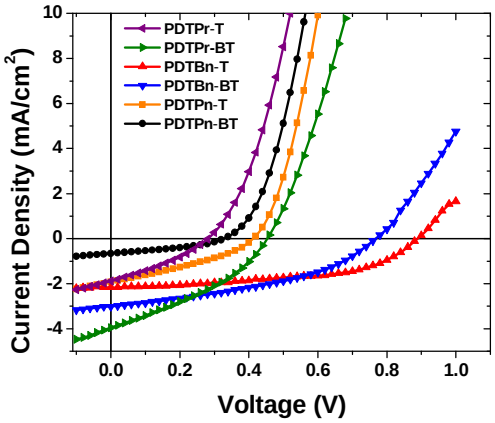

Figure 2.27. Characteristic I-V curves of the optimized devices of all polymers based BHJ solar cells under 1 Sun condition.

Figure 2.28. Photovoltaic performance of polymers

Polymer	Polymer: PCBM	Thickness (nm)	V_{oc} (V)	J_{sc} (mA/cm^2)	*FF*	η (%)	*IPCE* (%)	*Rs* (Ω)
PDTPr-T	1:1	50	0.29	1.89	0.32	0.18	0.58	117
PDTPr-BT	1:3	100	0.46	4.0	0.39	0.72	33.1	78
PDTBn-T	1:2	190	0.88	2.17	0.54	1.02	8.62	147
PDTBn-BT	1:1	155	0.77	3.02	0.41	0.94	16.1	80
PDTPn-T	1:3	50	0.41	1.93	0.34	0.27	10.1	48.7
PDTPn-BT	1:1	45	0.31	0.75	0.37	0.09	5.16	80

The PDTBn series immediately exhibits superior photovoltaic properties when compared to the rest of the polymers in this study. The theoretical predicted V_{oc} of 0.95 V and 0.75 V for PDTBn-BT and PDTBn-T,[62-64] respectively, are close to the experimentally determined values of 0.88 V and 0.77 V. Not

surprisingly, the lower HOMO of the polymers (e.g. PDTBn-BT) yields relatively higher V_{oc} values. The moderately low band gaps in the DTBn series are sufficient to produce satisfactory short circuit currents. Additionally, the symmetrical nature of the monomer combined with the alkyl chain branching being located on a carbon that is not adjacent to the polymer backbone should yield polymers films with increased π stacking. Thus despite a wider band gap, the high molecular weight causes the short circuit current of the DTBn series to be very close to that of the DTPr series of polymers.

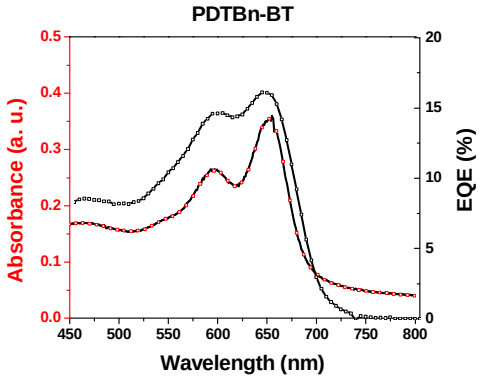

Figure 2.29. IPCE spectrum of BHJ photovoltaic device of ITO/PEDOT:PSS (45nm)/PDTBn-BT:PCBM (1:1, w/w)/Ca (30nm)/Al (100nm) and the optical absorptions for the corresponding film of the blend.

As predicted, the low V_{oc} of the polymers in the DTPr series remains the limiting factor in their solar cell performance, with both cells recording V_{oc} values lower than 0.5 V. PDTPr-BT's especially low band gap does lead to a 32% increase in the J_{sc} compared with that of PDTBn-BT, however, a significantly higher current must be obtained in order to offset its low V_{oc} (0.46 V) and Fill Factor (0.39). While these parameters can be improved by increases in molecular weight and further optimizing the polymer structure (modifying the alkyl chain length, varying the acceptor other than BT, etc.), the D-A polymers based on DTPr are intrinsically limited by their high lying HOMO energy levels. Therefore DTPr is not a particularly promising candidate for constructing new polymers as high efficiency photovoltaic materials. However, applications which require especially low band gaps (for example, infrared detectors) are still a possibility for this electron rich donor monomer.

The DTPn series does not behave as expected in terms of V_{oc}. The experimentally determined values are significantly lower than the V_{oc} expected given the low HOMO levels of the polymers in this series. The poor performance of PDTPn-BT is likely due to its low molecular weight. 1.2 kg/mol represents

a degree of polymerization of 2.25, and the effects of low molecular weight on all aspects of solar cell performance are well documented. [36,37,65,66] Additionally, the large branched alkyl chain adjacent to the polymer backbone in the DTPn (and DTPr) series could lead to polymers that do not π stack strongly, which would reduce the efficiency of charge transportation in the BHJ device. However, further optimization of the polymer structure was not warranted given the poor energetic and optical properties of this series of polymers.

Figure 2.30. Mobility measurements for pure film, and polymer:PCBM composites

Polymer	Pure Polymer	Thickness (nm)	Mobility ($cm^2 V^{-1} s^{-1}$)	Polymer: PCBM	Thickness (nm)	Mobility ($cm^2 V^{-1} s^{-1}$)
PDTPr-T		130	1.11×10^{-5}	1:1	75	8.17×10^{-6}
PDTPr-BT		120	6.41×10^{-5}	1:3	75	1.15×10^{-5}
PDTBn-T		80	2.57×10^{-5}	1:2	65	2.14×10^{-6}
PDTBn-BT		105	2.75×10^{-5}	1:1	240	3.88×10^{-7}
PDTPn-T		60	5.98×10^{-6}	1:3	45	3.55×10^{-6}
PDTPn-BT		100	5.35×10^{-6}	1:1	45	2.25×10^{-6}

The relative low efficiencies of these polymer based BHJ devices are mainly due to their low current, though low band gaps have been achieved in some of these polymers (e.g. PDTPr-BT and PDTBn-BT). In addition to a low band gap, a high hole mobility, comparable to the electron mobility of PCBM, is also required to achieve a high current. The hole mobility of these polymers in the BHJ blends was calculated via the space-charge limited current (SCLC) model by constructing hole-only devices with 40 nm of palladium (see experimental section for more details)[67]. For comparison, "polymer only" devices were also fabricated to probe the mobility of polymers in the absence of PCBM.[68] The measured hole mobilities of these polymers in the absence of PCBM are generally much lower than the electron mobility of PCBM (~10^{-4} $cm^2/V \cdot s$) (Figure 2.30), which explains the low efficiencies of these devices when compared with P3HT and other high performance polymers. Additionally, the film morphology of these devices is not optimal. For example, AFM images of PDTBn-T based devices reveal micron sized phase segregation (even though PDTBn-T based devices exhibited the highest efficiency). Thus, these devices offer a preliminary look at the potential of these polymers, and employing additional optimization

techniques beyond simple device thickness and ratio of polymer:PCBM could allow for an increase in device performance.

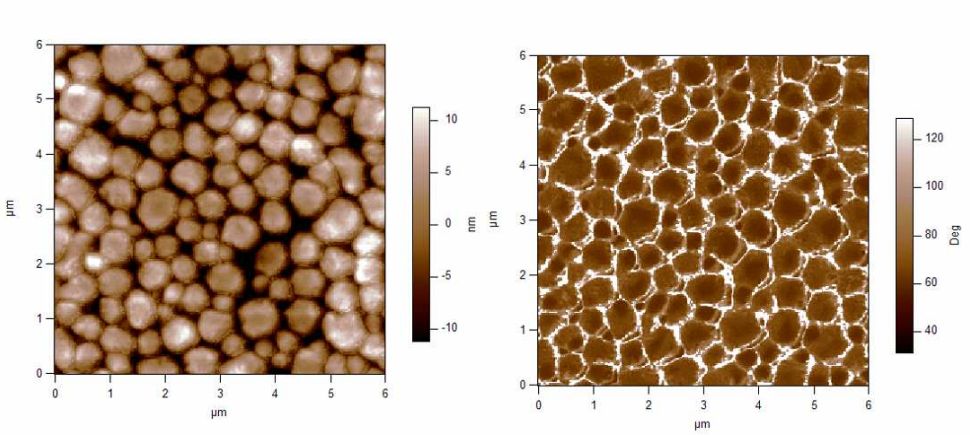

Figure 2.31. Atomic Force Microscope (AFM) images of PDTBn-T:PCBM film in a 1:2 ratio blend. Observed micron sized phase segregation is not optimal for bulk heterojunction performance (left: height image; right: phase image).

A collection of 6 electrochemically and optically unique polymers based upon three donor monomers were investigated. All three donor monomers are structurally related, featuring same flanking thiophenes, but incorporating different center aromatic units. DTBn based polymers exhibited the most potential in photovoltaic applications due to its moderately low band gap, and low HOMO energy level. The other polymers in this study either demonstrated high lying HOMO energy levels (DTPr based polymers), or unacceptably wide band gaps (DTPn based polymers).

Two key structure/property trends have also emerged. The behavior of the HOMO energy level is dominated by the most electron rich ring in the polymer backbone. Conversely, the optical band gap is a function of the electronic properties of the entire conjugated aromatic backbone. Electron deficient pyridine diminishes the donor-acceptor interaction in the copolymer that gives the low band gap. This explains the 0.3 eV change in the band gap between DTBn-BT and DTPn-BT, and the 0.3 eV change in band gap between DTBn-T and DTPr-T.

The best donor monomer candidate in this study is the DTBn monomer unit. Key advantages are the fact that it is an air stable solid, two positions to anchor alkyl chains, and a low HOMO energy level.

The photovoltaic performance of DTBn polymer series is largely inhibited by the low hole mobility of the two polymer candidates. Future study will focus on improving the hole mobility of these polymers in order to improve their photovoltaic performance.

Experimental Section

General Methods: ^{1}H nuclear magnetic resonance (NMR) spectra were obtained at 400 MHz or 300 MHz as solutions in $CDCl_3$. ^{13}C NMR spectra were obtained at 100 MHz as solutions in $CDCl_3$. Chemical shifts are reported in parts per million (ppm, δ), and referenced from tetramethylsilane. Coupling constants are reported in Hertz (Hz). Spectral splitting patterns are designated as s, singlet; d, doublet; t, triplet; m, multiplet; br, broad. Melting points are uncorrected.

UV-visible absorption spectra were obtained by a Shimadzu UV-2401PC spectrophotometer. Fluorescence spectra were recorded on a Shimadzu RF-5301PC spectrofluorophotometer. For the measurements of thin films, the polymer was spin-coated @ 600 RPM onto pre-cleaned glass slides from 10 mg/mL polymer solution in *o*-dichlorobenzene, and dried slowly in a petri dish for 3 hours.

Gel permeation chromatography (GPC) measurements were performed on two different machines, depending upon the solubility of the polymers in THF. For THF soluble polymers, a Waters 2695 Separations Module apparatus with a differential refractive index detector (at UNC Chapel Hill) was used, employing tetrahydrofuran (THF) as the eluent. For THF non-soluble polymers, a Polymer Laboratories PL-GPC 220 instrument (at University of Chicago) was used, using 1,2,4-trichlorobenzene as the eluent (stabilized with 125 ppm BHT) at 135°C. The obtained molecular weight is relative to polystyrene standards.

Cyclic voltammetry measurements were carried out using a Bioanalytical Systems (BAS) Epsilon potentiostat equipped with a standard three-electrode configuration. Typically, a three-electrode cell equipped with a glassy carbon working electrode, a $Ag/AgNO_3$ (0.01 M in anhydrous acetonitrile) reference electrode, and a Pt wire counter electrode was employed. The measurements were done in anhydrous acetonitrile with tetrabutylammonium hexafluorophosphate (0.1 M) as the supporting electrolyte under an argon atmosphere at a scan rate of 100 mV/s. Polymer films were drop-cast onto the glassy carbon working electrode from a chloroform solution and dried under house nitrogen stream prior to

measurements. The potential of Ag/AgNO3 reference electrode was internally calibrated by using the ferrocene/ferrocenium redox couple (Fc/Fc+). The electrochemical onsets were determined at the position where the current starts to differ from the baseline. The highest occupied molecular orbital (HOMO) and lowest unoccupied molecular orbital (LUMO) energy levels were calculated from the onset oxidation potential (E_{ox}) and onset reductive potential (E_{red}), respectively, according to eqs 1 and 2.

Eq 1: $HOMO = -(E^{ox} + 4.8)$ (eV)

Eq 2: $LUMO = -(E^{red} + 4.8)$ (eV)

Polymer solar cell fabrication and testing: Glass substrates coated with patterned tin-doped indium oxide (ITO) were purchased from Thin Film Devices, Inc. The 150 nm sputtered ITO pattern had a resistivity of 15Ω/□. Prior to use, the substrates were ultrasonicated for 10 minutes in acetone followed by deionized water and then 2-propanol. The substrates were dried under a stream of nitrogen and subjected to the treatment of UV-Ozone over 20 minutes. A filtered dispersion of PEDOT:PSS in water (Baytron PH500) was then spun cast onto clean ITO substrates at 4000 rpm for 60 seconds and then baked at 140 °C for 10 minutes to give a thin film with a thickness of 40 nm. A blend of polymer and PCBM (1:1, 1:2 or 1:3, w/w, depending upon the polymer, see Table 3) at 10 mg/mL (for polymer) was dissolved in dichlorobenzene (for PDTPr-BT) or chlorobenzene (for other polymers) with heating at 60 °C for 6 hours, filtered through a 0.45 μm poly(tetrafluoroethylene) (PTFE) filter, and spun cast between 800 – 1200 rpm for 60 seconds onto a PEDOT:PSS layer. The substrates were then dried at room temperature under N_2 for 12 hours. The devices were finished for measurement after thermal deposition of a 30 nm film of calcium and a 100 nm aluminum film as the cathode at a pressure of ~ 1×10^{-6} mbar. There are 8 devices per substrate, with an active area of 12 mm^2 per device. The thicknesses of films were recorded by a profilometer (Alpha-Step 200, Tencor Instruments). Device characterization was carried out under AM 1.5G irradiation with the intensity of 100 mW/cm^2 (Oriel 91160, 300 W) calibrated by a NREL certified standard silicon cell. Current versus potential (I-V) curves were recorded with a Keithley 2400 digital source meter. EQE were detected under monochromatic illumination (Oriel Cornerstone 260 ¼ m monochromator equipped with Oriel 70613NS QTH lamp) and the calibration of the incident light was performed with a monocrystalline silicon diode. All fabrication steps after adding the PEDOT:PSS layer onto ITO substrate, and characterizations were performed in gloveboxes under nitrogen atmosphere. For

mobility measurements, the hole-only devices in a configuration of ITO/PEDOT:PSS (45 nm)/polymer-PCBM/Pd (40 nm) were fabricated. The experimental dark current densities J of polymer: PCBM blends were measured when applied with voltage from 0 to 6 V. The applied voltage V was corrected from the built-in voltage V_{bi} which was taken as a compensation voltage $V_{bi}=V_{oc}$ + 0.05 V and the voltage drop V_{rs} across the indium tin oxide/poly(3,4-ethylene-dioxythiophene):poly(styrene sulfonic acid) (ITO/PEDOT:PSS) series resistance and contact resistance, which is found to be around 35 Ω from a reference device without the polymer layer. From the plots of $J^{0.5}$ vs. V (supporting information), hole mobilities of copolymers can be deduced from

$$J = \frac{9}{8}\varepsilon_r\varepsilon_0\mu_h\frac{V^2}{L^3}$$

where ε_0 is the permittivity of free space, ε_r is the dielectric constant of the polymer which is assumed to be around 3 for the conjugated polymers, μ_h is the hole mobility, V is the voltage drop across the device, and L is the film thickness of active layer.

Reagents: All solvents are ACS grade unless otherwise noted. Anhydrous THF was obtained by distillation from sodium/benzophenone prior to use. Anhydrous methylene chloride was dried over magnesium sulfate and filtered directly into the reaction flask prior to use. Anhydrous toluene was used as received. Anhydrous *tert*-butanol was obtained by treatment with sodium metal and then distillation. 2-bromothiophene-4-carboxylic acid,[60] 2,6-di(trimethyltin)-N-(1-octylnonyl)dithieno[3,2-b:2′,3′-d]pyrrole,[55] 2,5-bis(trimethyltin)thiophene,[69] 4,7-dibromo-2,1,3-benzothiadiazole, [70] and 2,1,3-benzothiadiazole-4,7-bis(boronic acid pinacol ester)[71] were prepared according to established literature procedures. 2,6-Bis(trimethyltin)-4,8-(3-hexylundecyl)benzo[1, 2-*b*:4,5-*b′*]dithiophene,[49,57] and N-(1-octylnonyl)-2,6-dibromodithieno[3,2-*b*;2',3'-*d*]pyrrole[72,73] were prepared using procedures analogous to established literature procedures and ^{1}H and ^{13}C NMR spectra are exhibited below for these monomers. All other chemicals were purchased from commercial sources (Acros, Alfa Aesar, Aldrich, Fisher Scientific, Oakwood Chemical) and used without further purification.

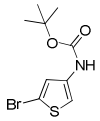

***tert*-butyl 5-bromothiophen-3-ylcarbamate (3):** 2-bromothiophene-4-carboxylic acid (11.584g, 55.95 mmol) was combined with anhydrous toluene (225 mL) in a dry flask under argon. Triethylamine (11.8 mL, 83.93 mmol) was added to the slurry, which became homogeneous after addition. Diphenylphosphoryl azide (12.1 mL, 55.95 mmol) was then added at room temperature, and the reaction mixture was stirred for 2.5 hours. The mixture was then heated to 80°C, and stirred for 1 hour. Anhydrous *tert*-butanol (16.0 mL, 167.9 mmol) was then added, and the reaction mixture was stirred for 16 hours at 80°C. The mixture was then concentrated, and purified by column chromatography using a 3:2 toluene:hexanes solution as the eluent. The fractions were concentrated, affording a beige powder of sufficient purity for the following steps. Yield: 11.807g (76%). Analytical purity was obtained by recrystallization from cyclohexanes (refluxed, then cooled to 4°C), yielding colorless prisms which were stable in atmosphere for over a week. Colorless crystalline solid; m.p. 88-91°C. ^{1}H NMR ($CDCl_3$, 300 MHz, δ): 7.04 (br s, 1H), 6.94 (br s, 1H), 6.61 (br s, 1H), 1.50 (s, 9H). ^{13}C NMR ($CDCl_3$, 100 MHz, δ): 152.5, 135.8, 123.7, 111.7, 108.7, 80.9, 28.2. ESI-TOF MS: $[M+Na]^+$ = 299.9667 (calcd $[M+Na]^+$ = 299.9670).

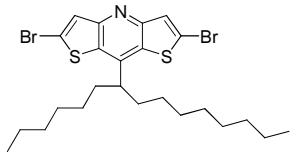

2,6-dibromo-8-(1-hexylnonyl)dithieno[3,2-*b*:2',3'-*e*]pyridine (5): 3 (2.039 g, 7.33 mmol), and 2-hexyldecanal (881 mg, 3.67 mmol) were dissolved in methylene chloride (40 mL). Trifluoracetic acid (1.8 mL) was slowly added over 3 minutes, and the resulting mixture was heated to reflux. After 18 hours, the reaction mixture was partitioned between CH_2Cl_2 and ice cold 10% NaOH solution, separated, and the organic layer was dried over Na_2SO_4. The mixture was then purified by column chromatography eluting with a 7:1 mixture of hexanes:ethyl acetate. The resulting yellow oil was then concentrated under vacuum (0.5 mmHg) for 24 hours, resulting in a pale brown solid. Yield: 615 mg (30%). Brown solid; m.p. 60-61°C. ^{1}H NMR ($CDCl_3$, 300 MHz, δ): 7.57 (s, 2H), 2.99 (m, 1H), 2.01 (m, 2H), 1.84 (m, 2H), 1.16 (m, 20H), 0.86 (m, 6H). ^{13}C NMR ($CDCl_3$, 100 MHz, δ): 154.98, 141.66, 127.66, 120.93, 47.02, 33.51, 33.47,

31.72, 31.49, 29.48, 29.19, 29.10, 27.79, 22.55, 22.48, 13.99, 13.91. ESI-TOF MS $[M+H]^+$ = 558.0506 (calcd $[M+H]^+$ = 558.0499).

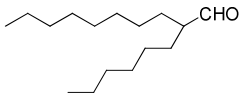

2-hexyldecanal (4): Dimethylsulfoxide (10.2 mL, 143.6 mmol) was dissolved in anhydrous methylene chloride (350 mL), and chilled to -78°C under argon. Oxalyl chloride (6.48 mL, 75.6 mmol) was then slowly added dropwise, while maintaining the temperature at -78°C. The mixture was stirred for 30 min, and then 2-hexyldecan-1-ol (20.9 mL, 71.99 mmol) was added dropwise at -78°C. The mixture was stirred for 35 minutes carefully maintaining -78°C. TEA (30 mL, 215 mmol) was added, and a thick white precipitate formed. The mixture was stirred for 10 minutes at -78°C, and then allowed to warm to room temperature. The mixture was poured into 1M HCl, and extracted with methylene chloride. The organic layer was then washed repeatedly with distilled water, and dried over $MgSO_4$. The mixture was then filtered, concentrated, and filtered through a short plug of silica gel. The silica gel was washed with hexanes, and the filtrate was concentrated and distilled under reduce pressure. The desired aldehyde was obtained at a distillate temperature of 105°C @ 0.6 mmHg. Yield: 12.087g (70%). Colorless oil; ^{1}H NMR ($CDCl_3$, 300 MHz, δ): 9.55 (d, *J* = 3.3 Hz, 1H), 2.21 (m, 1H), 1.60 (m, 2H), 1.45 (m, 2H), 1.27 (m, 20H), 0.88 (t, *J* = 6.6 Hz, 6H). ^{13}C NMR ($CDCl_3$, 100 MHz, δ): 205.45, 51.94, 31.80, 31.59, 29.66, 29.35, 29.32, 29.18, 28.88, 27.03, 26.99, 22.59, 22.52, 14.00, 13.95.

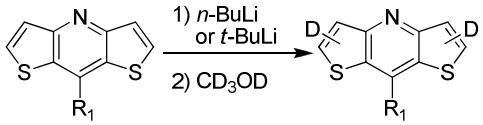

1 R_1 = 2-hexyldecyl

Deuterium Lithiation Experiments: The following lithiation conditions are reproduced from Macromolecules 2004, v. 37, p. 710. **1** (151 mg, 0.363 mmol) was dissolved in 1.5 mL of anhydrous THF in a dry flask. The solution was cooled to -78°C, and a 2.5M solution of *n*-BuLi in hexanes (0.35 mL, 0.87 mmol) was added dropwise. The solution was stirred at -78°C for 1 hour, and then at 0°C for 5 hours. The solution was then cooled back down to -78°C, and methanol-D4 (0.5 mL) was added in one portion. The solution was stirred at -78°C for 5 minutes, and then warmed to room temperature. The reaction mixture was then filtered through a silica plug (250 mg), and the plug was washed with 1 mL of CH_2Cl_2. The

resulting filtrate was then concentrated, and the residue was analyzed by NMR. The procedure was repeated using 2.05 equivalents of *t*-BuLi @ -78°C for 1 hour, and then quenching with methanol-D4.

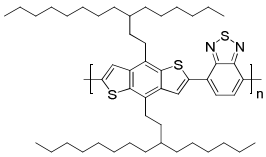

Representative Stille Coupling Polymerization Procedure: 2,6-Bis(trimethyltin)-4,8-(3-hexylundecyl)benzo[1,2-b:4,5-b]dithiophene (498 mg, 0.502 mmol), 4,7-dibromo-2,1,3-benzothiadiazole (147 mg, 0.502 mmol), tri(*o*-tolyl)phosphine (18 mg, 0.06 mmol), and 25 mL of anhydrous toluene were combined, and purged with argon for 20 minutes. Then tris(dibenzylideneacetone)dipalladium(0) (7 mg, 7.53×10^{-3} mmol) was added under a stream of argon, and the reaction mixture was purged for an additional 15 minutes. The mixture was then heated to reflux, and stirred for 72 hrs. The reaction mixture was then precipitated into methanol, and filtered into an extraction thimble. The polymer solids were then Soxhlet extracted with methanol, ethyl acetate, hexanes, and chloroform. The chloroform extracts were then concentrated, and precipitated into methanol. The resulting solids were filtered, washed with methanol, and residual solvent was removed under vacuum at 0.5 mm Hg affording polymer PDTBn-BT as a blue-black powder. Yield: 32mg (8%).

Chapter 3: Low band gap polymers based on benzo[1,2-b:4,5-b′]dithiophene: rational design of polymers leads to high photovoltaic performance

Adapted with permission from *Macromolecules* **2010**, *43*, 4609

By Samuel C. Price, Andrew C. Stuart, and Wei You

In the previous study, benzo[1,2 b:4,5 b′]dithiophene (BnDT) emerged as the most promising donor candidate for intramolecular charge transfer copolymers. In an effort to further increase the power conversion efficiency of these materials, BnDT based polymers have been designed to better fit the four key design criteria[41,74] that have emerged for the ideal candidate donor polymers to be used in BHJ devices with fullerene as the acceptor: (a) a low HOMO energy level in order to achieve a high open circuit voltage (V_{oc}); (b) a low band gap to maximize light absorption; (c) a high hole mobility, which requires a planar structure to encourage π stacking of the polymer chains; (d) a high molecular weight and good solubility, to achieve the optimal morphology, in order to maximize the short circuit current (J_{sc}), and a high fill factor (*FF*). Unfortunately, though numerous low band gap materials have been synthesized, only few polymers have closely met all these criteria and demonstrated impressive efficiencies.[43,45,51] In this study, a new intramolecular charge transfer (ICT) copolymer,[75,76] poly[4,8-dialkylbenzo[1,2-*b*:4,5-*b′*]dithiophene-alt-4,7-di(4-hexyl-2-thienyl)-2,1,3-benzothiadiazole] (PBnDT-4DTBT) was developed to fulfill these design criteria. BHJ solar cells based on the blend of this polymer and $PC_{61}BM$ demonstrated a V_{oc} of 0.81 V, a J_{sc} of 9.70 mA cm^{-2}, and a *FF* of 0.55, yielding an overall efficiency of 4.3% under 1 Sun condition (AM1.5, 100 mW cm^{-2}). To the best of our knowledge, PBnDT-4DTBT:$PC_{61}BM$ demonstrates one of the highest efficiencies achieved so far, under 1 sun conditions, by BHJ solar cells comprised of any single low band gap polymer blended with $PC_{61}BM$.[45,49,50]

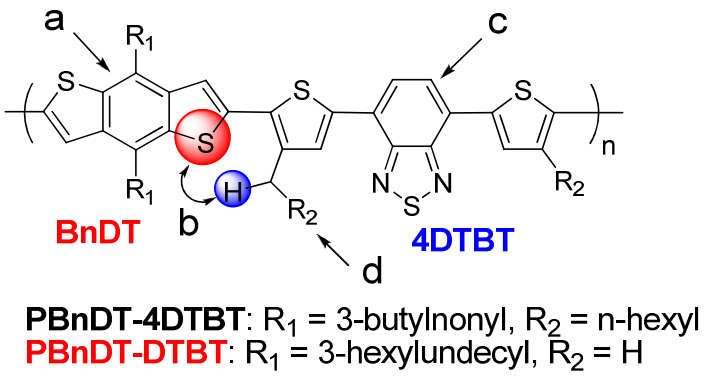

Figure 3.32. Structure of polymers. (a) Benzene center ring raises the oxidation potential, and planarity of **BnDT** unit encourages π stacking. (b) Flanking thiophenes promote planarity of the polymer backbone via reduction of steric hindrance between adjacent monomer units. (c) 2,1,3-benzothiadiazole unit lowers band gap through ICT. (d) Additional alkylated positions provide high molecular weight and soluble polymer.

Monomer and Polymer Synthesis

By fusing an electron deficient benzene with two flanking thiophene units, the co-monomer BnDT offers a high oxidation potential, thereby fulfilling criterion (a). Furthermore, BnDT has an entirely planar and symmetrical structure, an important prerequisite in order to achieve high mobility according to (c). For example, BnDT based copolymers have recently shown high hole mobility in organic field effect transistors.[77] Several ICT copolymers based upon BnDT for use in photovoltaic cells have been thoroughly investigated, but power conversion efficiencies of the resulting devices remained below 1.75%.[78,79] BnDT has also been copolymerized with thieno[3,4-*b*]thiophene by Liang et. al., and device efficiencies over 7% were obtained.[49,50] Unfortunately, the low oxidation potential of the co-monomer, thieno[3,4-*b*]thiophene, established a low V_{oc}, thereby limiting the potential of this polymer to attain 10% efficiency.[74]

The remaining two design criteria, (b) a low band gap, and (d) a high molecular weight and good solubility were satisfied by the selection of the other co-monomer, 4,7-di(4-hexyl-2-thienyl)-2,1,3-benzothiadiazole (4DTBT)[80] (Figure 3.32). The DTBT unit is a common electron deficient co-monomer, which lowers the band gap through ICT.[14,15] The two additional alkyl chains in the case of 4DTBT allow for more soluble polymers that do not precipitate during polymerization. Preventing this precipitation is critical to ensuring high molecular weight material, and the importance of molecular weight in photovoltaic

materials is well documented.[36,37,81] Monomers similar to 4DTBT and their utility in obtaining high molecular weight polymers have been previously studied, resulting in power conversion efficiencies below 3%.[80,82-85] However, BnDT is a more suitable monomer than those studied previously (e.g., fluorene) to polymerize with 4DTBT, due to the flanking thiophenes. These thiophenes eliminate steric hindrance from the alkyl chain at the 4 position of the adjacent thiophene (Figure 3.32b) that is normally exhibited in the case of benzene based monomers such as fluorenes or carbazoles that do not contain a heteroatom. This minimized steric hindrance also results in a planar conjugated backbone, leading to a small band gap and high mobility.[85]

Thus, PBnDT-4DTBT was synthesized using standard Stille coupling polymerization conditions, yielding a green-black solid. For comparison, BnDT was also polymerized with non-alkylated DTBT. Though longer branched alkyl chains were anchored on the BnDT of PBnDT-DTBT, this polymer still exhibits low molecular weight with a number average molecular weight (M_n) of 5.6 kg/mol (X_n = 5.8), likely due to precipitation of the polymer during the polymerization. Accordingly, we observed that a large quantity of solid PBnDT-DTBT remained in the Soxhlet thimble after extraction with chloroform. With additional solubilizing chains on the 4DTBT unit, PBnDT-4DTBT displayed a higher molecular weight (M_n = 21.9 kg/mol, X_n = 21.5, PDI = 4.14), ascribable to the increased solubility of this polymer.

Optical and Electrochemical Properties

Optical and electrochemical characterization of the two polymers reveals that these polymers are almost identical. The optical band gap of both polymers is 1.7 eV. PBnDT-DTBT demonstrates a more pronounced shoulder at approximately 650 nm (Figure 3.33a), which can be attributed to slightly increased π stacking and extension of the conjugation over two dimensions in the solid state.[86] CV measurements demonstrate a HOMO and LUMO energy level of – 5.33 eV and – 3.17 eV respectively for PBnDT-DTBT. In the case of PBnDT-4DTBT, these energy levels increase to a HOMO of – 5.26 eV, and a LUMO of – 2.96 eV, due to the electron releasing hexyl groups on the thiophenes of the 4DTBT unit. These small differences clearly indicate that the two hexyl chains on the 4DTBT unit were introduced into the polymer chain with minimal detrimental effect on the electrochemical and optical properties of the polymer.

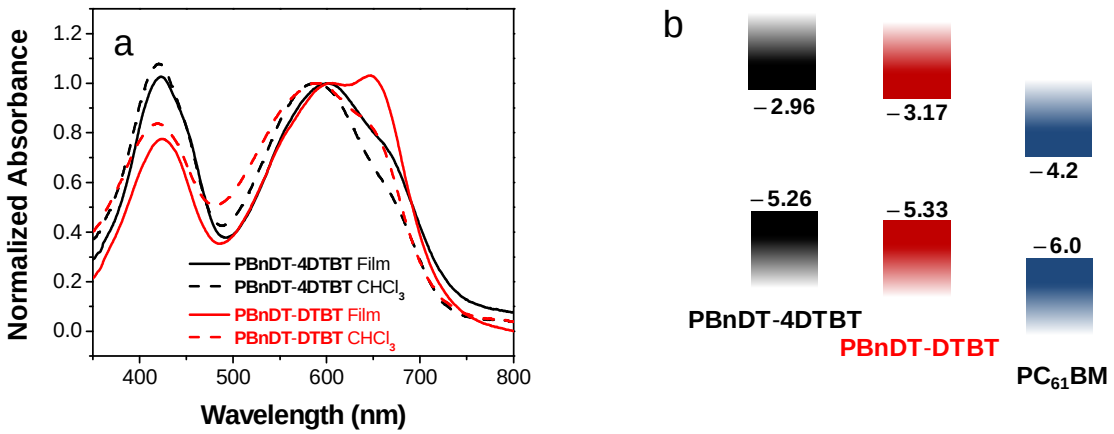

Figure 3.33. (a) UV-Vis absorption of both polymers in chloroform solutions at room temperature and as thin films. (b) Energy band diagram (eV).

Photovoltaic Properties

Preliminary photovoltaic results are exceptionally promising for each of these two materials, especially for PBnDT-4DTBT. BHJ devices of the two polymers blended with $PC_{61}BM$ yield power conversion efficiencies breaching 3.8% (Figure 3.34a). Despite exhibiting a slightly higher HOMO energy level, PBnDT-4DTBT displays a V_{oc} of 0.81 V, only 20 mV lower than that of PBnDT-DTBT (0.83 V). However, the J_{sc} increases from 7.79 mA cm^{-2} of PBnDT-DTBT to 9.70 mA cm^{-2} in the 4-hexyl version of the polymer (PBnDT-4DTBT), thus re-emphasizing the importance of a high molecular weight and solubility in BHJ polymer solar cells.[36,37,81]

Figure 3.34b shows the incident photon to current efficiency (IPCE) of two BHJ thin films, together with their individual film absorption spectra. Not surprisingly, these two thin films (~ 100 nm) have almost identical absorption spectra, since the two polymers have the same conjugated backbone and same blending ratio in regard to $PC_{61}BM$ (1:1). However, PBnDT-4DTBT:$PC_{61}BM$ film shows a much higher IPCE of 47% than that of PBnDT-DTBT based devices (30%), likely due to a high hole mobility in PBnDT-4DTBT:$PC_{61}BM$ devices. Mobility measurements via space charge limited current (SCLC) disclose a hole mobility of 3.8×10^{-5} cm^2 V^{-1} s^{-1} for the PBnDT-4DTBT:$PC_{61}BM$ device, more than double that of the PBnDT-DTBT:$PC_{61}BM$ device (1.6×10^{-5} cm^2 V^{-1} s^{-1}). Since these two polymers have an

identical conjugated backbone (BnDT-DTBT), the higher hole mobility is ascribed to the high molecular weight of PBnDT-4DTBT.

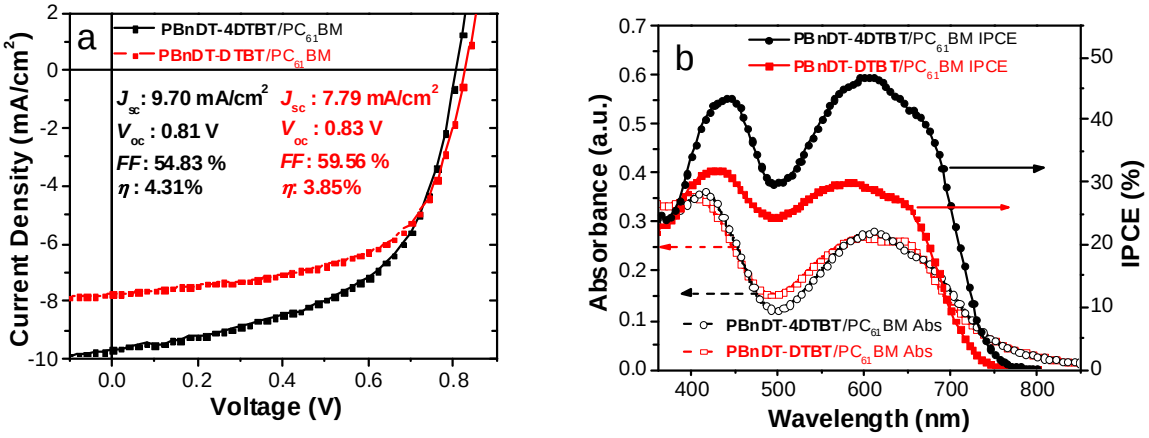

Figure 3.34. (a) Characteristic J-V curves of the devices of polymer based BHJ solar cells under 1 Sun condition (100 mW/cm2). 4.3% is one of the highest observed efficiency numbers for PBnDT-4DTBT based BHJ PV devices; the average efficiency of 8 devices was over 4%. (b) IPCE and absorption of semi-optimized devices.

We have summarized four criteria developed from the culmination of other work for the design of ideal polymers in order to achieve high efficiency BHJ solar cells.[41,74] As a close-to-ideal polymer, PBnDT-4DTBT exhibits a moderate oxidation potential, possesses an entirely planar sp^2 hybridized backbone, absorbs light as low in energy as 1.7 eV, and displays moderately high molecular weight, thus satisfying the four design criteria set forth. The additional hexyl chains at the 4 positions of DTBT do not significantly alter the optical or electrochemical properties of the resulting polymer. Furthermore, these hexyl chains increase the molecular weight and solubility of the polymer, leading to the increased power conversion efficiency of PBnDT-4DTBT over that of PBnDT-DTBT. Both of these materials exhibit exceptionally high preliminary power conversion efficiencies with $PC_{61}BM$. Finally, only optimizations to the device thickness and polymer:$PC_{61}BM$ ratio have been attempted. Switching to $PC_{71}BM$, optimizations to the spin casting and annealing conditions, and device fabrication improvements are all options to be explored. With further structural and device optimizations, increased power conversion efficiencies are possible in the near future.

Experimental Section

General Methods: ^{1}H nuclear magnetic resonance (NMR) spectra were obtained at 400 MHz or 300 MHz as solutions in $CDCl_3$ or in $C_2D_2Cl_4$ at 100°C. ^{13}C NMR spectra were obtained at 100 MHz as solutions in $CDCl_3$. Chemical shifts are reported in parts per million (ppm, δ), and referenced from tetramethylsilane. Coupling constants are reported in Hertz (Hz). Spectral splitting patterns are designated as s, singlet; d, doublet; t, triplet; m, multiplet; br, broad.

UV-visible absorption spectra were obtained by a Shimadzu UV-2401PC spectrophotometer. For the measurements of thin films, the polymer was spin-coated @ 600 RPM onto pre-cleaned glass slides from 10 mg/mL polymer solution in *o*-dichlorobenzene, and dried slowly in a petri dish for 3 hours.

Gel permeation chromatography (GPC) measurements were performed on two different machines, depending upon the solubility of the polymers in THF. For the THF soluble polymer PBnDT-4DTBT, a Waters 2695 Separations Module apparatus with a differential refractive index detector (at UNC Chapel Hill) was used, employing tetrahydrofuran (THF) as the eluent. For the THF insoluble polymer PBnDT-DTBT, a Polymer Laboratories PL-GPC 220 instrument (at University of Chicago) was used, using 1,2,4-trichlorobenzene as the eluent (stabilized with 125 ppm BHT) at 135 °C. The obtained molecular weight is relative to polystyrene standards.

Cyclic voltammetry measurements were carried out using a Bioanalytical Systems (BAS) Epsilon potentiostat equipped with a standard three-electrode configuration. Typically, a three-electrode cell equipped with a glassy carbon working electrode, a $Ag/AgNO_3$ (0.01 M in anhydrous acetonitrile) reference electrode, and a Pt wire counter electrode was employed. The measurements were done in anhydrous acetonitrile with tetrabutylammonium hexafluorophosphate (0.1 M) as the supporting electrolyte under an argon atmosphere at a scan rate of 100 mV/s. Polymer films were drop-cast onto the glassy carbon working electrode from a 2.5 mg/mL chloroform solution and dried under house nitrogen stream prior to measurements. The potential of Ag/AgNO3 reference electrode was internally calibrated by using the ferrocene/ferrocenium redox couple (Fc/Fc+). The electrochemical onsets were determined at the position where the current starts to differ from the baseline. The highest occupied molecular orbital (HOMO) and

lowest unoccupied molecular orbital (LUMO) energy levels of polymers were calculated from the onset oxidation potential (E_{ox}) and onset reductive potential (E_{red}), respectively, according to eqs 1 and 2.

Eq 1: $HOMO = -(E^{ox} + 4.8)$ (eV)

Eq 2: $LUMO = -(E^{red} + 4.8)$ (eV)

Polymer solar cell fabrication and testing: Glass substrates coated with patterned tin-doped indium oxide (ITO) were purchased from Thin Film Devices, Inc. The 150 nm sputtered ITO pattern had a sheet resistance of 15Ω/□. Prior to use, the substrates were ultrasonicated for 10 minutes in acetone followed by deionized water and then 2-propanol. The substrates were dried under a stream of nitrogen and subjected to the treatment of UV-Ozone over 20 minutes. A filtered dispersion of PEDOT:PSS in water (Baytron PH500) was then spun cast onto clean ITO substrates at 4000 rpm for 60 seconds and then baked at 140 °C for 10 minutes to give a thin film with a thickness of 40 nm. A 1:1 w/w blend of polymer and PCBM at 10 mg/mL was dissolved in trichlorobenzene with heating at 140 °C for overnight, filtered through a 0.45 μm poly(tetrafluoroethylene) (PTFE) filter, and spun cast between 500 – 1200 rpm for 60 seconds onto a PEDOT:PSS layer. The substrates were then dried at room temperature under N_2 for 12 hours. The devices were finished for measurement after thermal deposition of a 30 nm film of calcium and a 100 nm aluminum film as the cathode at a pressure of ~ 1×10^{-6} mbar. There are 8 devices per substrate, with an active area of 12 mm^2 per device. The thicknesses of films were recorded by a profilometer (Alpha-Step 200, Tencor Instruments). Device characterization was carried out under AM 1.5G irradiation with the intensity of 100 mW/cm^2 (Oriel 91160, 300 W) calibrated by a NREL certified standard silicon cell. Current versus potential (I-V) curves were recorded with a Keithley 2400 digital source meter. EQE were detected under monochromatic illumination (Oriel Cornerstone 260 ¼ m monochromator equipped with Oriel 70613NS QTH lamp) and the calibration of the incident light was performed with a monocrystalline silicon diode. All fabrication steps after adding the PEDOT:PSS layer onto ITO substrate, and characterizations were performed in gloveboxes under nitrogen atmosphere. For mobility measurements, the hole-only devices in a configuration of ITO/PEDOT:PSS (45 nm)/polymer-PCBM/Pd (40 nm) were fabricated. The experimental dark current densities *J* of polymer: PCBM blends were measured when

applied with voltage from 0 to 6 V. The applied voltage V was corrected from the built-in voltage V_{bi} which was taken as a compensation voltage $V_{bi}=V_{oc}$ + 0.05 V and the voltage drop V_{rs} across the indium tin oxide/poly(3,4-ethylene-dioxythiophene):poly(styrene sulfonic acid) (ITO/PEDOT:PSS) series resistance and contact resistance, which is found to be around 35 Ω from a reference device without the polymer layer. From the plots of $J^{0.5}$ vs. V (supporting information), hole mobilities of copolymers can be deduced from

$$J = \frac{9}{8}\varepsilon_r \varepsilon_0 \mu_h \frac{V^2}{L^3}$$

where ε_0 is the permittivity of free space, ε_r is the dielectric constant of the polymer which is assumed to be around 3 for the conjugated polymers, μ_h is the hole mobility, V is the voltage drop across the device, and L is the film thickness of active layer. AFM Images were taken using an Asylum Research MFP3D Atomic Force Microscope.

Reagents: Anhydrous toluene was purchased from EMD Chemical and used as received. Trimethyltin monomers A and B were synthesized using modified literature procedures and proton NMR spectra are provided below.[77,87] 4,7-dithien-2-yl-2,1,3-benzothiadiazole (DTBT) and 4,7-di(4-hexyl-2-thienyl)-2,1,3-benzothiadiazole (4DTBT) were synthesized according to established literature procedures.[88,89] All other chemicals were purchased from commercial sources (Acros, Alfa Aesar, Aldrich, Fisher Scientific) and used without further purification.

Polymerization of PBnDT-4DTBT: 4DTBT (212 mg, 0.338 mmol), 2,6-bis(trimethyltin)-4,8-di(3-butylnonyl)[1,2-b:4,5-b']dithiophene (304 mg, 0.345 mmol), tri-o-tolylphosphine (13 mg, 0.406 mmol), and toluene (14 mL) were combined in a dry flask, and purged with argon for 20 minutes. $Pd_2(dba)_3$ (5 mg, 0.0051 mmol) was then added, and the toluene solution was purged for an additional 15 minutes. The reaction mixture was then heated to reflux, and stirred for 60 hours, before being precipitated into rapidly stirring methanol. The resulting slurry was then filtered into a Soxhlet thimble, and extracted extensively with methanol, ethyl acetate, hexanes, and chloroform. The chloroform fraction was then concentrated under a stream of argon, and precipitated into methanol at – 55°C. The slurry was filtered, washed with methanol, and air dried. The green-black solid was then collected, and dried under vacuum at 0.7 mmHg for 24 hours. Yield = 276 mg (80%). Green-black solid; ^{1}H NMR ($C_2D_2Cl_4$, 400 MHz, δ): 8.13

(s, 2H), 7.95 (s, 2H), 7.65 (s, 2H), 3.26 (s, 4H), 3.09 (br s, 4H), 1.92 (br s, 8H), 1.48 (m, 52H), 0.99 (m, 12H). Elemental Analysis: Calculated for $C_{62}H_{86}N_2S_5$: C, 73.03; H, 8.50; N, 2.75. Found: C,72.99; H, 8.57; N, 2.71. GPC (THF @ room temp.): M_n = 21.9 kg/mol, M_w = 90.7 kg/mol, PDI = 4.14. PBnDT-DTBT was prepared in a similar fashion, using an equimolar amount of DTBT instead of 4DTBT**.**

Chapter 4: Fluorine Substituted Conjugated Polymer of Medium Band Gap Yields 7% Efficiency in Polymer−Fullerene Solar Cells

Adapted with permission from *Journal of the American Chemical Society* **2011**, *133*, 4625

By Samuel C. Price, Andrew C. Stuart, Liqiang Yang, Huaxing Zhou, and Wei You

Rapid and recent developments in the field of conjugated polymers have led to dramatic increases in polymer solar cell performance, reaching power conversion efficiencies over 6%.[28,51,90,91] Research activities on new materials development have been almost exclusively focused on creating polymers with low band gaps, in order to extend the light absorption to 900 nm and beyond for increased light harvesting.[28,92,37] However, medium (or even slightly wider) band gap polymers are still relevant to photovoltaics in their own right. Low band gap materials quite often are designed with higher than optimal HOMO energy levels in order to achieve a narrow band gap. While this provides a high short circuit current (J_{sc}) from the increased light absorption, the open circuit voltage (V_{oc}) suffers.[37] A high V_{oc} is more readily achieved through medium band gap polymers with a low HOMO energy level.[93-95] Moreover, conjugated polymers usually have a relatively narrow absorption width,[96] which significantly limits the light absorption of these materials and leads to lower than expected J_{sc}. An emerging solution is to employ a tandem cell structure, stacking two cells with active layers absorbing different parts of the solar spectrum. This would cover a much wider portion of the solar influx, significantly improving the overall device efficiency.[97,98] In this regard, medium band gap polymers with high photovoltaic efficiency would be desirable in addition to high performance low band gap polymers.

Poly(3-hexylthiophene) has long been the standard medium band gap polymer used in tandem solar cells, since single bulk heterojunction (BHJ) cells of P3HT blended with PCBM exhibit a reliably measured power conversion efficiency between 4% and 5%.[99] However, P3HT exhibits a very high lying

HOMO energy level of – 5.1 eV, which limits the V_{oc} of the resulting photovoltaic cells to a low value of 0.6 V. Second, P3HT based BHJ cell requires either thermal[99] or solvent annealing[100] to reach maximum performance, a time consuming process, which is not conducive to roll to roll high throughput manufacturing. Thus, the seemingly overlooked medium band gap polymers warrant further exploration.

Research efforts in this group have recently focused on developing low band gap intramolecular charge transfer (ICT) copolymers using the design motif outlined in Fig. 1a.[80,101-103] The motif uses a band gap reducing aromatic group (e.g. benzothiadiazole) to obtain a low band gap, and two flanking thiophenes which provide planarity and a position to anchor solubilizing alkyl chains. To apply this motif to the design of medium band gap copolymers, an acceptor unit with a higher LUMO energy level is required in order to widen the band gap. One such candidate is the 2-alkyl-benzo[*d*][1,2,3]triazoles (TAZ), which requires a higher potential to reduce due to the substitution of the sulfur atom in benzothiadiazole with a nitrogen atom. The lone pair on the nitrogen atom is more basic than the lone pairs on sulfur, and is more easily donated into the triazole ring. This causes polymers employing benzotriazoles as the acceptor unit to be more electron rich, which leads to a higher LUMO energy level. Therefore, wider band gaps are observed for TAZ based polymers than the benzothiadiazole based counterparts. TAZ based polymers also provide an additional advantage of incorporating solubilizing alkyl chains onto the acceptor unit, rather than on the thiophene rings on the backbone of the polymer. Alkyl chains anchored to the thiophene rings on the polymer backbone may cause steric repulsion between the adjacent monomer units. Therefore, placing the alkyl chain away from the polymer backbone on the TAZ unit allows the polymer backbone to adopt a more planar conformation. We hypothesize that this increased planarity would increase the hole mobility of the resulting polymer.

While a wider band gap is a disadvantage in that less light is harvested from the solar spectrum, the larger gap between the HOMO and the LUMO on the polymer provides an opportunity to increase the open circuit voltage.[104] In order to increase the V_{oc} while holding the band gap constant, the energy levels of both the HOMO and LUMO of the conjugated polymer must be decreased simultaneously. Thus, electron withdrawing groups would need to be added to the polymer. Fluorine has recently attracted attention as an electron withdrawing group used in high efficiency photovoltaic polymers.[28] Since it is only one small atom in size, it can be introduced onto the polymer backbone without any deleterious steric

effects that a larger electron withdrawing group such as a nitro or trifluoromethyl group would incur. Density functional theory calculations predicted a 0.11 eV decrease in the HOMO energy level by adding two fluorine atoms to the benzotriazole unit. Thus, the fluorinated monomer, FTAZ, was envisioned and synthesized.

Herein we report two new polymers incorporating benzodithiophene (BnDT) as the donor and either benzotriazole (HTAZ) or fluorinated analog (FTAZ) as the acceptor. Both polymers show an optical gap of 2.0 eV, which is even slightly bigger than that of P3HT (1.9 eV). However, the photovoltaic performance of PBnDT-HTAZ is on par with that of P3HT, with an overall efficiency of 4.3% at an active layer thickness of 230 nm. More impressive results come from the PBnDT-FTAZ:$PC_{61}BM$ based BHJ cells, which show a V_{oc} of 0.79 V, a J_{sc} of 12.45 mA/cm^2, and a very notable *FF* of 72.2%, leading to a highest overall efficiency of 7.1% with an active layer thickness of 250 nm. Furthermore, PBnDT-FTAZ based BHJ cells are able to achieve an efficiency of 6% at an unprecedented active layer thickness of 1 micron. All these boast the great potential of PBnDT-FTAZ in constructing low cost, high efficiency solar cells.

Synthesis of Monomers and Polymers

While HTAZ was synthesized according to literature reports, the synthesis of the fluorinated monomer FTAZ is depicted in Fig. 4.35b.[105,106] The synthesis began with a standard alkylation of 1.[107] Poor regioselectivity for the desired 2 position resulted in poor yields, which is typical for this type of reaction. In the second step, direct electrophilic bromination of the electron deficient fluorinated benzotriazole, 2, with molecular bromine resulted in low yield. Therefore, an alternative approach was explored to first activate the 4 and 7 positions of the benzotriazole by deprotonating the benzotriazole ring with LDA, and then quenching the resulting anion immediately with trimethylsilyl chloride. The resulting carbon-silicon bonds can then be brominated with excess bromine in chloroform at room temperature, affording 3 in 53% yield over two steps. A Negishi coupling followed by an NBS bromination then finished the synthesis of the fluorinated monomer FTAZ.

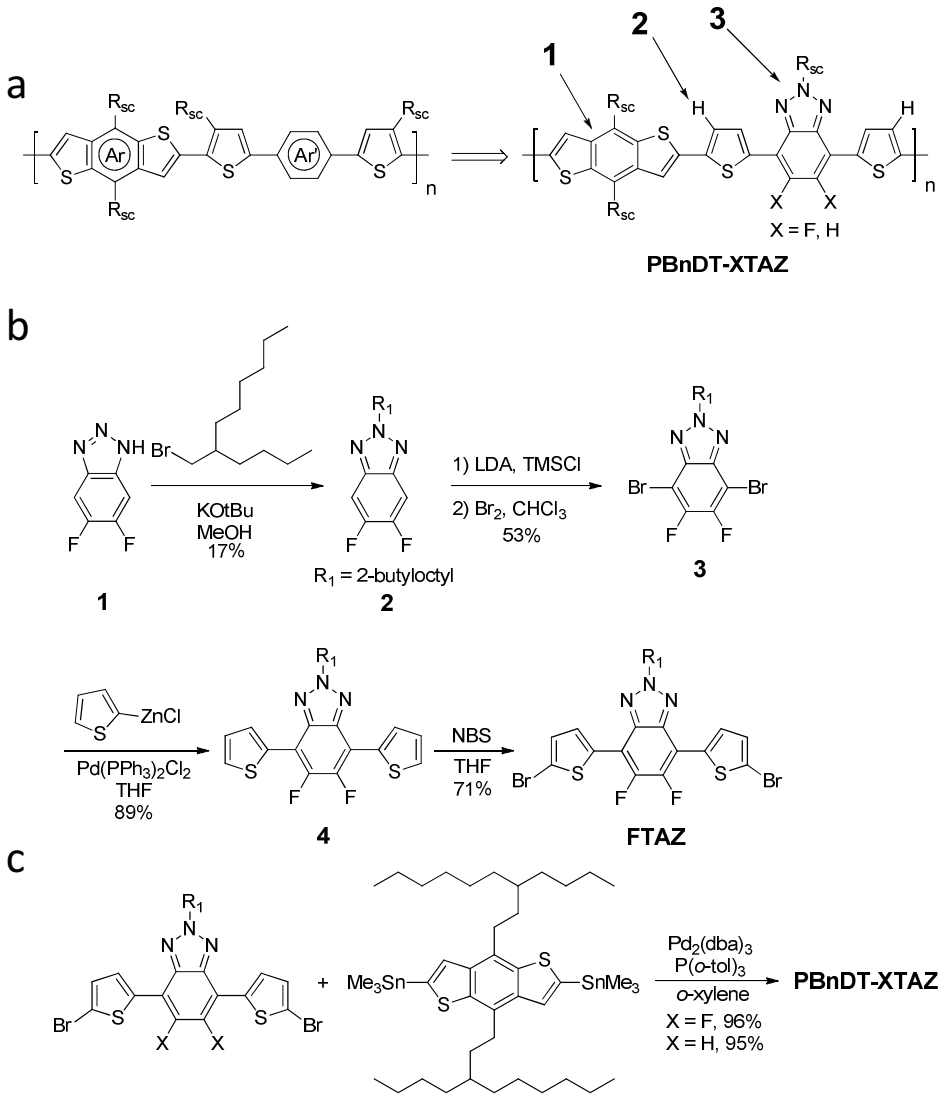

Figure 4.35. (a) Typical design motif used by our research group and others shown on the left. 1) Benzene was chosen as the Ar unit to provide a lower HOMO. 2) Movement of the solubilizing chains to the Ar' group reduces steric hindrance between the BnDT monomer and adjacent thiophenes. 3) Benzotriazole chosen as the band gap lowering aryl unit to provide a medium gap. Ar = Aryl unit used to control the HOMO energy level of the polymer. Ar'= Band gap reducing aromatic group. R_{sc} = solubilizing alkyl chain. (b) Synthesis of FTAZ monomer. (c) Synthesis of polymers PBnDT-FTAZ and PBnDT-HTAZ with a Stille polycondensation polymerization.

Polymerization of the HTAZ and FTAZ monomers using standard microwave Stille polycondensation conditions[37] with the distannyl monomer 2,6-bis(trimethyltin)-4,8-di(3-

butylnonyl)benzo[1,2-*b*:4,5-*b'*]dithiophene produced the corresponding copolymers (PBnDT-HTAZ and PBnDT-FTAZ, Fig. 4.35c) in yields greater than 95%. Both polymers were purified by Soxhlet extraction with methanol, ethyl acetate, hexanes, and chloroform. The resulting purple solids from the chloroform fraction exhibit high and nearly identical molecular weight distributions (Figure 4.36).

Figure 4.36. Key polymer properties and calculated photovoltaic performances for PBnDT-HTAZ and PBnDT-FTAZ.

Polymer	$M_n/X_n/PDI$[a] [kg/mol]	Film E_g[b] [eV]	Extinction Coefficient[c] [cm^{-1}]	HOMO (CV) [eV]	DFT Calc. HOMO [eV]	J_{so}[d] [mA/cm^2]	V_{oc}[d] Calc [V]	V_{oc} Measured [V]
PBnDT-HTAZ	47.6/47.5/2.57	1.98	7.9×10^4	– 5.29	– 5.08	33.64	0.68	0.71
PBnDT-FTAZ	42.2/40.6/2.36	2.00	9.8×10^4	– 5.36	– 5.19	18.74	0.76	0.79

a) M_n= Number-average molecular weight determined by GPC in 1,2,4-trichlorobenzene at 135°C.
b) Band gap calculated from the onset of the absorption of the solid film.
c) Measured from film absorption spectra at λ_{max} (534 nm).
d) Calculation based on HOMO measured from CV and using the saturation dark current density, according to equation $V_{oc} \approx \frac{nkT}{q} \ln\left(\frac{J_{sc}}{J_{so}}\right) + \frac{\Delta E_{DA}}{2q}$

Optical and Electrochemical Properties

The intrinsic properties of the two polymers are summarized in Figure 4.36. Both polymers exhibit nearly identical optical band gaps around 2.0 eV from the absorption edge of their thin films (Fig. 4.37c), though the fluorinated material has a slightly higher absorption coefficient. However, the fluorinated material shows a more pronounced peak at around 575 nm in solution at room temperature, which is associated with inter-chain interactions. And while both absorption spectra blue shift by about 12 nm when collected in boiling chlorobenzene, the interchain association band still remains at a higher relative intensity for the fluorinated material (PBnDT-FTAZ). This observed absorption behavior of PBnDT-FTAZ indicates that it aggregates in solution much more strongly than PBnDT-HTAZ.

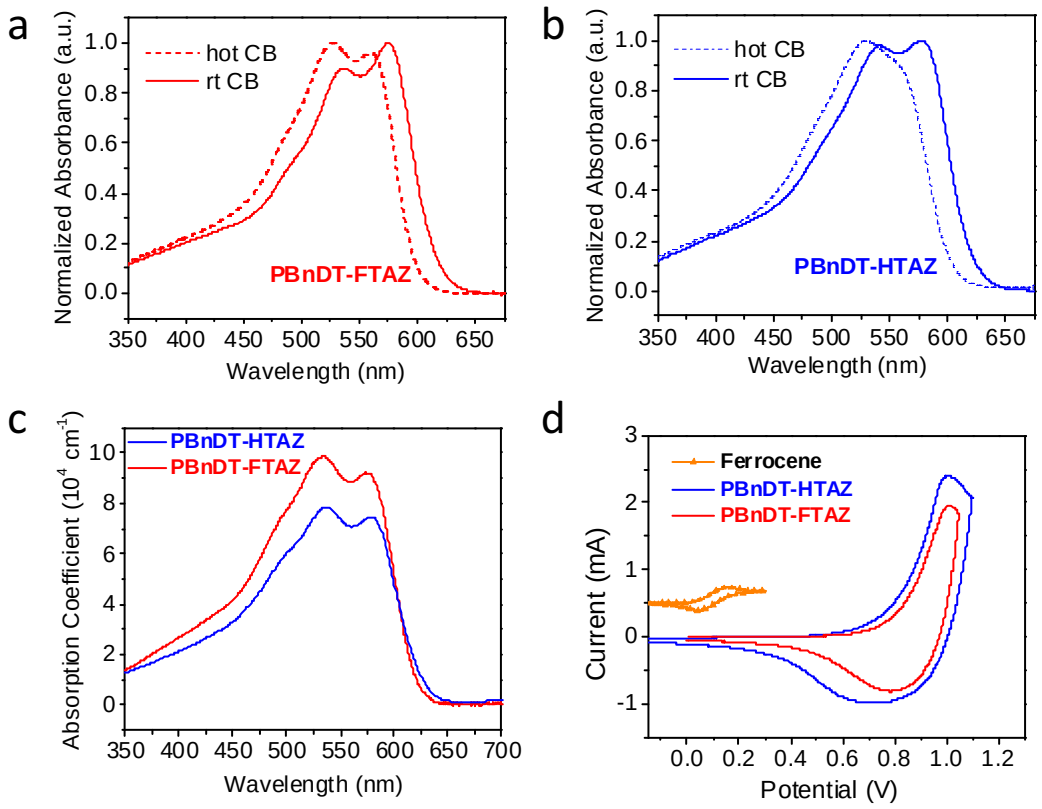

Figure 4.37. Solution UV-Visible absorption spectra for a) PBnDT-FTAZ and b) PBnDT-HTAZ; c) Film UV-Vis absorption spectra for both polymers; d) The oxidative portion of the cyclic voltammogram for PBnDT-FTAZ and PBnDT-HTAZ. The ferrocene/ferrocenium redox couple is used as a standard (-4.8 eV) and is shifted up the Y-axis by 0.5 mA for clarity.

In addition to small differences in absorption spectra, the two polymers display very similar electrochemical oxidation characteristics as well (Fig. 4.37d). Cyclic voltammetry reveals reversible oxidation behavior for both polymers, with the fluorinated polymer (PBnDT-FTAZ) being oxidized only 0.07 V after PBnDT-HTAZ. This slight difference is also predicted by DFT calculations for the HOMO energy levels of each material. Both materials display HOMO energy levels at least 0.2 eV lower than the currently favored, wide band gap polymer, P3HT (– 5.1 eV), implying that a higher V_{oc} could be obtained than that of the P3HT based devices (~ 0.6 V). The cyclic voltammetry LUMOs for PBnDT-FTAZ and PBnDT-HTAZ are -3.05 eV and -2.87 eV, respectively. In summary, despite minor differences in the

aggregation properties in solution and the oxidation behavior, these polymers possess roughly identical optical and electronic properties.

Photovoltaic Properties

Optimized photovoltaic devices were obtained by spin casting a 1:2 blend of polymer:$PC_{61}BM$ in 1,2,4-trichlorobenzene (TCB), and then allowing the trichlorobenzene to evaporate slowly in a petri dish. Solvents that evaporated faster such as dichlorobenzene and other ratios of polymer to $PC_{61}BM$ produced suboptimal results. This is likely due to the extended solvent evaporation time from the higher boiling TCB, which allows more time for polymer chains to organize into a near optimal morphology during solvent annealing. Thickness optimizations were conducted and summarized in Table 2. While the optimal thickness for PBnDT-HTAZ is easily identified as around 230 nm with the highest J_{sc} and *FF* among corresponding values associated with all thicknesses studied, the optimal thickness in the case of PBnDT-FTAZ is arguably estimated to be around 250 nm where the highest efficiency was obtained (7.1%) (Fig. 4.38a and 4.38b). In fact, one particular feature of the fluorinated material (PBnDT-FTAZ) is its insensitivity to changes in active layer thickness. The J_{sc} continuously rises as the thickness of the active layer of PBnDT-FTAZ:$PC_{61}BM$ BHJ cells increases (Fig. 4.38c and Table X). However, the fill factor peaks around 250 nm with a value of 72%, then drops off as the thickness increases. Nevertheless, an efficiency of 6% was still observed even at an unprecedented active layer thickness of 1 micron in the case of PBnDT-FTAZ (Fig. 4.38d).

It is intriguing to note that PBnDT-FTAZ performs almost twice as well as PBnDT-HTAZ, though the only difference between these two polymers is the two fluorine atoms on the benzotriazole unit. This is due to a 0.09 V increase in the V_{oc}, a 10% increase in the J_{sc}, and an increase from 55% to 72% in the *FF* of PBnDT-FTAZ based BHJ cells. The small increase in V_{oc} can be explained by two factors. First, the HOMO energy level for PBnDT-FTAZ is 0.07 eV lower than the non-fluorinated material, due to the electron withdrawing effect of the fluorine atoms. Additionally, PBnDT-FTAZ also exhibits a slightly lower J_{so} value (Figure 4.36).[23,108] This is likely due to the repulsive nature of the fluorine atoms, which repel hydrocarbon materials.[109] This hypothesis was tested with X-ray diffraction spectroscopy (Figure 4.36), and indeed a larger d-spacing was observed for the fluorinated polymer PBnDT-FTAZ than for the

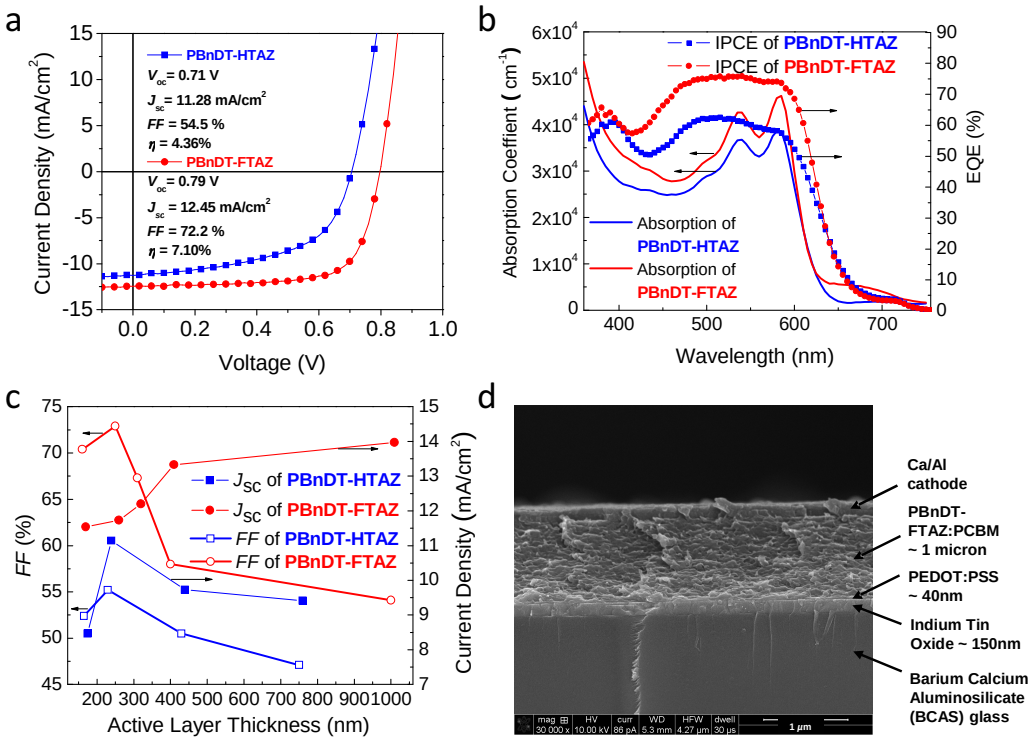

Figure 4.38. (a) J-V curves for the highest performing cells for each polymer. The fluorine atoms cause increases in every performance category. PBnDT-FTAZ overall performs 76% better than PBnDT-HTAZ. (b) Incident photon to current efficiency and solid film absorption of each blend of polymer:PC61BM. (c) Dependence of the FF and Jsc on the thickness of the active layer. (d) SEM of 1 micron active layer that showed 6% power conversion efficiency (scale bar: 1 µm).

non- fluorinated material (18.6 Å vs. 17.5 Å). It is, therefore, not unreasonable to conclude that $PC_{61}BM$ is also kept slightly farther away from the PBnDT-FTAZ chains during electron transfer reactions. This would increase the electron-hole charge transfer complex separation and slow down bimolecular recombination. This retardation of the recombination rate has also been witnessed in fluorinated dyes in dye sensitized solar cells.[110] By combining the HOMO energy level and the J_{so}, the calculated V_{oc} matches the experimental value extremely well (Figure 36), quantitatively explaining the difference in the observed V_{oc}.

Figure 4.39. Thickness optimizations for photovoltaic devices.

Polymer	Polymer: $PC_{61}BM$ (w:w)	Thickness [nm]	V_{oc} [V]	J_{sc} [mA/cm^2]	*FF* [%]	$\eta_{average}$ (η_{max}) [%]
PBnDT-HTAZ	1:2	165	0.66	8.47	52.4	2.94 (3.27)
	1:2	230	0.70	11.14	55.2	4.30 (4.36)
	1:2	430	0.66	9.73	50.5	3.25 (3.29)
	1:2	750	0.71	9.41	47.1	3.14 (3.18)
PBnDT-FTAZ	1:2	160	0.74	11.54	70.4	6.03 (6.49)
	1:2	250	0.79	11.83	72.9	6.81 (7.10)
	1:2	310	0.79	12.20	67.3	6.47 (6.76)
	1:2	400	0.74	13.33	58.0	5.83 (6.17)
	1:2	1000	0.74	13.97	54.1	5.60 (6.06)

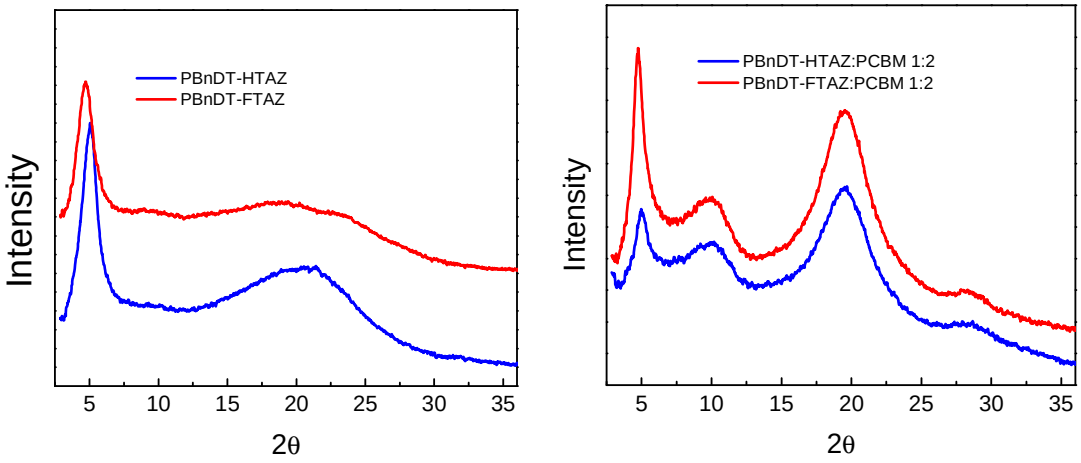

Figure 4.40. X-ray powder diffraction of both polymer films (left) and polymer:$PC_{61}BM$ blends (right).

Both polymer films show broad x-ray diffraction peaks in the π-π stacking region (~20°) of the x-ray diffraction spectrum. The PBnDT-HTAZ material exhibits an increased intensity in this region compared to PBnDT-FTAZ, which is curious given the UV-Vis and solubility data indicate that the FTAZ material aggregates much more strongly in solution. When blended with $PC_{61}BM$, the peak corresponding with the a-axis (100) direction remains much higher for the fluorinated polymer than for PBnDT-HTAZ. This may indicate that the fluorinated material maintains a morphology more similar to the neat film, and that PBnDT-HTAZ mixes more intimately with the fullerene.

Figure 4.41. X-Ray diffraction results and SCLC measured hole mobilities for PBnDT-HTAZ and PBnDT-FTAZ .

Polymer	*SCLC measurement*		*XRD measurement*	
	Thickness (nm)	*Mobility ($cm^2/V{\cdot}s$)*	*2θ [°]*	*d-spacing [Å]*
PBnDT-HTAZ Only	340	3.34×10^{-6}	5.05	17.50
PBnDT-HTAZ: PCBM (1:2)	270	2.94×10^{-4}	4.96	17.82
PBnDT-FTAZ Only	440	6.76×10^{-5}	4.73	18.68
PBnDT-FTAZ: PCBM (1:2)	170	1.03×10^{-3}	4.72	18.72

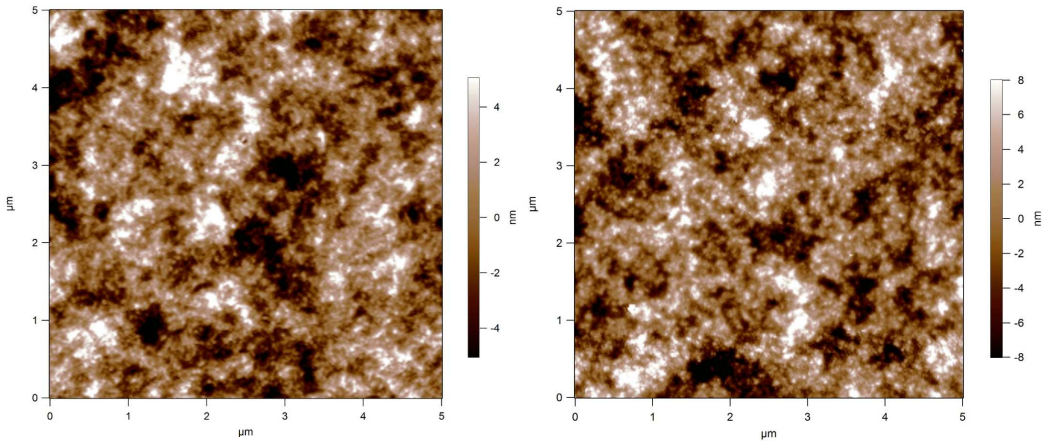

Figure 4.42. AFM images of 1:2 polymer:$PC_{61}BM$ blends. PBnDT-HTAZ (left), PBnDT-FTAZ (right). Note the wider range on the height scale for the right image.

This assertion that the fluorinated material forms films which are more phase segregated is supported by the AFM. The roughness range for blends of the fluorinated material is 16 nm, almost twice as large as the non-fluorinated material. Increased surface roughness has been shown to correspond with increased phase segregation in other conjugated polymer:fullerene composites.[42,111]

The ability of the fluorinated polymer to maintain very high *FF* even at active layer thicknesses above 200 nm, and the high J_{sc} are likely due to the high hole mobility of the polymer (Figure 4.41). The hole mobility of PBnDT-FTAZ is an order of magnitude higher than the copolymer without fluorines in

both neat polymer films, and when blended with $PC_{61}BM$. The mobility values for the PBnDT-FTAZ:$PC_{61}BM$ blend (1×10^{-3} $cm^2/V \cdot s$) are slightly larger than P3HT blends (2×10^{-4} $cm^2/V \cdot s$) in BHJ devices.[112] Hence, we attribute the large increase in J_{sc} and *FF*, at least partially, to the increased hole mobility of the fluorinated polymer.

In summary, two nearly identical polymers with a medium band gap of 2.0 eV have been designed and synthesized following our design motif. The only structural difference between the two is that PBnDT-FTAZ bears two fluorine atoms on the benzotriazole ring of the PBnDT-HTAZ. While the photovoltaic performance of PBnDT-HTAZ based BHJ solar cells is already on par with that of P3HT based devices, a pleasant surprise comes from the fluorinated material, PBnDT-FTAZ, with a peak device efficiency of 7.1% observed. Though the two fluorine atoms have a minimal effect on the optical and electrochemical properties of the polymer, they have a profound effect on the hole mobility of the polymer, and thus the photovoltaic performance. PBnDT-FTAZ based BHJ devices consistently show a higher *FF* and J_{sc} than PBnDT-HTAZ based devices at comparable thicknesses. Such a high hole mobility likely also explains that fact that PBnDT-FTAZ:$PC_{61}BM$ solar cell can still achieve over 6% efficiency even at an unprecedented active layer thickness of 1 micron. However, other factors are likely contributing to the increase in efficiency. Investigations to further understand the impact of the fluorine atoms on the morphology, self assembly behavior, and exciton related dynamics are currently underway.

Experimental Section

Reagents. All solvents are ACS grade unless otherwise noted. Anhydrous THF was obtained by distillation from sodium/benzophenone prior to use. Diisopropylamine was distilled from potassium hydroxide prior to use. 4,7-dibromo-2-(2-butyloctyl)-2H-benzo[d][1,2,3]triazole,[105,106] 2,6-Bis(trimethyltin)-4,8-(3-butylnonyl)benzo[1,2-b:4,5-b']dithiophene,[113] 2-butyloctylbromide,[114] and 5,6-difluoro-1H-benzo[d][1,2,3]triazole[107] were prepared according to modified literature procedures. All reagents were purchased from VWR, Fisher Scientific, Dynamic Absorbents, Silicycle, Accela ChemBio Inc., and were used without further purification.

4,7-bis(5-bromothiophen-2-yl)-2-(2-butyloctyl)-2H-benzo[d][1,2,3]triazole (HTAZ). Thiophene (3.01 g, 2.5 eq) was dissolved in dry THF (40 mL) in a flame dried flask under argon. The mixture was

cooled to 0°C in an ice bath, and 1.6M n-BuLi in hexanes (22.8 mL, 2.55 eq) was added dropwise over 3 minutes. The solution was stirred for 35 min maintaining the temperature at 0°C, and then anhydrous $ZnCl_2$ (5.07 g, 2.6 eq) was added as a solution in 40 mL dry THF. The reaction was stirred for 5 min at 0°C, and then $Pd(PPh_3)_2Cl_2$ (602 mg, 6 mol %) was added in one portion. 4,7-dibromo-2-(2-butyloctyl)-2H-benzo[d][1,2,3]triazole (6.39 g, 1.0 eq) was then added via cannula as a solution in 20 mL of dry THF. The reaction mixture was then heated to reflux, and stirred for 16 h. The reaction mixture was then poured into water and extracted with ethyl acetate. The organic layer was then washed with water (3x), dried ($MgSO_4$), filtered, concentrated in vacuo, and purified by column chromatography on silica gel using 4:1 hexanes:CH_2Cl_2 as the eluent. The resulting fluorescent yellow solid was then dissolved into THF (80 mL), and N-bromosuccinimide (2.89 g, 2.0 eq) was added in one portion. The reaction mixture was stirred for 3.5 h, and then poured into saturated $NaHCO_3$ solution and extracted with ethyl acetate. The organic phase was then washed with water (3x), dried ($MgSO_4$), filtered, and concentrated in vacuo. The material was then purified by column chromatography on silica gel, using 3:1 hexanes:chloroform as the eluent. The resulting yellow solid (HTAZ) was then recrystallized twice from isopropanol to yield a yellow powder. Yield (2 steps): 2.79 g (32%). Fluorescent yellow solid; mp 70°C. ^{1}H NMR ($CDCl_3$, 400 MHz, δ): 7.76 (d, $^3J_{HH}$ = 3.6 Hz, 2H), 7.46 (s, 2H), 7.10 (d, $^3J_{HH}$ = 4 Hz, 2H), 4.71 (d, $^3J_{HH}$ = 6.4 Hz, 2H), 2.27 (m, 1H), 1.26 (m, 16H), 0.90 (t, $^3J_{HH}$ = 7.2 Hz, 3H), 0.86 (t, $^3J_{HH}$ = 6 Hz, 3H). ^{13}C NMR ($CDCl_3$, 100 MHz, δ): 141.55, 141.24, 130.80, 126.81, 122.90, 122.01, 113.16, 59.88, 39.09, 31.82, 31.38, 31.15, 29.56, 28.45, 26.17, 22.96, 22.65, 14.09. Anal. Calcd for $C_{26}H_{31}Br_2N_3S_2$: C, 51.24; H, 5.13; N, 6.89. Found: C, 51.52; H, 4.95; N, 6.88.

Polymerization of PBnDT-HTAZ. 2,6-Bis(trimethyltin)-4,8-(3-butylnonyl)benzo[1,2-b:4,5-b']dithiophene (132 mg, 1.0 eq), HTAZ (91.4 mg, 1.0 eq), $Pd_2(dba)_3$ (2.8 mg, 0.02 eq), and tri(*o*-tolyl)phosphine (7.2 mg, 0.16 eq) were combined in a dry microwave vial. The vial was sealed with a septum cap, and then evacuated and refilled with argon three times. Dry, oxygen free *o*-xylene (0.75 mL) was added. The mixture was then reacted in a microwave reactor for 20 min, at 200°C (at 300W), and then cooled to room temperature. The reaction mixture was diluted with chlorobenzene (3 mL), and then the polymer solution was precipitated into methanol (100 mL) at room temperature. The resulting purple-black solid was filtered into a Soxhlet thimble, and extracted with methanol, ethyl acetate, hexanes, and

chloroform until the wash from each extraction was colorless. When there was no solid remaining in the thimble, the chloroform fraction was concentrated, and chlorobenzene was added (5 mL). The polymer solution was then precipitated into methanol at room temperature, filtered, and dried under vacuum at 0.5 mmHg. Yield: 143 mg (95%). Purple metallic solid. ^{1}H NMR @ 400K ($C_2D_2Cl_4$, 400 MHz, δ): 7.86, 7.23, 4.87, 3.14, 2.41, 1.87, 1.50, 1.08. GPC (1,2,4-trichlorobenzene at 135°C): M_n = 47.6 kg/mol, M_w = 133.4 kg/mol, PDI = 2.57.

2-(2-butyloctyl)-5,6-difluoro-2H-benzo[d][1,2,3]triazole (**2**). 5,6-difluoro-1H-benzo[d][1,2,3]triazole (8.04 g, 1.0 eq), potassium tert-butoxide (5.87 g, 1.01 eq), and 2-butyloctylbromide (13.04 g, 1.01 eq) were dissolved in 130 mL of methanol. The reaction was heated to reflux for 17 h. The reaction mixture was then poured into saturated NH_4Cl solution, and extracted with ethyl acetate. The organic layer was washed with water (2x), dried (Na_2SO_4), filtered, concentrated in vacuo, and purified by column chromatography on silica gel using 10:1 hexanes:ethyl acetate as the eluent. Yield: 2.88 g (17%). Colorless oil. ^{1}H NMR ($CDCl_3$, 400 MHz, δ): 7.59 (t, $^3J_{HF}$ = 8.4 Hz, 2H), 4.58 (d, $^3J_{HH}$ = 6.8 Hz, 2H), 2.22 (m, 1H), 1.28 (m, 16H), 0.86 (t, $^3J_{HH}$ = 5.6 Hz, 6H).

4,7-dibromo-2-(2-butyloctyl)-5,6-difluoro-2H-benzo[d][1,2,3]triazole (**3**). 1.6M n-BuLi in hexanes (12.5 mL, 2.25 eq) was added dropwise over 3 min to a solution of diisopropylamine (3.10 mL, 2.5 eq) and dry THF (90 mL) under argon at -78°C. The solution was stirred for 15 min, and then a solution of Compound 2 (2.88 g, 1.0 eq) and trimethylsilyl chloride (3.1 mL, 2.75 eq) in dry THF (35 mL) was added dropwise over 10 minutes at -78°C. -78°C was maintained while the reaction was stirred for 3 h, and then the reaction was quenched with 10 mL of saturated NH_4Cl. The reaction was warmed to room temperature and poured into saturated NH_4Cl. The mixture was extracted with ethyl acetate, washed with water (3x), dried ($MgSO_4$), and concentrated in vacuo. The residue was then dissolved into $CHCl_3$ (30 mL), and bromine (3.6 mL, 8.0 eq) was added in one portion, and the reaction was stirred for 16 h at room temperature, shielded from light. The reaction was then poured into a mixture of 10% NaOH and ice, and extracted with methylene chloride. The organic layer was washed with brine, dried ($MgSO_4$), and purified by column chromatography on silica gel using 4:1 hexanes:methylene chloride as the eluent. Yield (2 steps): 2.28 g (53%). Colorless oil. ^{1}H NMR ($CDCl_3$, 300 MHz, δ): 4.65 (d, $^3J_{HH}$ = 7.2 Hz, 2H), 2.31 (m, 1H), 1.24 (m, 16H), 0.87 (m, 6H). ^{13}C NMR ($CDCl_3$, 100 MHz, δ): 149.07 (dd, $^1J_{CF}$ = 253 Hz, $^2J_{CF}$ = 20

Hz), 138.86 (t, $^{3,4}J_{CF}$ = 2.5 Hz), 96.10 (dd, $^{2}J_{CF}$ = 15 Hz, $^{3}J_{CF}$ = 9 Hz), 61.11, 38.98, 31.64, 31.08, 30.79, 29.40, 28.18, 25.93, 22.81, 22.57, 14.05, 13.92.

2-(2-butyloctyl)-5,6-difluoro-4,7-di(thiophen-2-yl)-2H-benzo[d][1,2,3]triazole (**4**). Thiophene (0.87 g, 2.25 eq) was dissolved into dry THF (20 mL), and cooled to 0°C under argon. 1.6M n-BuLi in hexanes (6.6 mL, 2.3 eq) was added dropwise over 3 min. The reaction was allowed to stir at 0°C for 35 min, and then a solution of anhydrous $ZnCl_2$ (1.47 g, 2.35 eq) in dry THF (20mL) was added via syringe at 0°C. After 5 min, $Pd(PPh_3)_2Cl_2$ (193 mg, 6 mol %) was added in one portion at 0°C. Then compound 3 (2.21 g, 1.0 eq) was added via syringe as a solution in dry THF (15 mL). The reaction mixture was then heated to reflux, and stirred for 16 h. The reaction was then poured into water, and extracted with ethyl acetate. The organic layer was washed with water (3x), dried ($MgSO_4$), filtered, concentrated in vacuo, and purified by column chromatography on silica gel using 4:1 hexanes:methylene chloride as the eluent. Yield: 1.99 g (89%). Fluorescent yellow solid. ^{1}H NMR ($CDCl_3$, 300 MHz, δ): 8.33 (dd, $^{3}J_{HH}$ = 3.9 Hz, $^{4}J_{HH}$ = 0.9 Hz, 2H), 7.55 (dd, $^{3}J_{HH}$ = 5.1 Hz, $^{4}J_{HH}$ = 1.2 Hz, 2H), 7.24 (m, 2H), 4.73 (d, $^{3}J_{HH}$ = 6.6 Hz, 2H), 2.86 (m, 1H), 1.26 (m, 16H), 0.89 (m, 6H).

4,7-bis(5-bromothiophen-2-yl)-2-(2-butyloctyl)-5,6-difluoro-2H-benzo[d][1,2,3]triazole (**FTAZ**). Combine 4 (1.99 g, 1.0 eq), N-bromosuccinimide (1.46 g, 2.0 eq), and THF (75 mL). Stir for 20 hours at room temperature, and then pour the reaction mixture into a saturated solution of sodium bicarbonate. Extract with methylene chloride, dried ($MgSO_4$), filtered, and then silca gel was added. The slurry was concentrated in vacuo, and the resulting solid purified by column chromatography on silica gel using 10:1 hexanes:methylene chloride as the eluent. After repeating the chromatography step a second time, a fluorescent yellow solid was obtained in purity sufficient for polymerization. Yield: 1.87 g (71%). Fluorescent yellow solid; mp 76°C. ^{1}H NMR ($CDCl_3$, 400 MHz, δ): 7.97 (d, $^{3}J_{HH}$ = 4 Hz, 2H), 7.13 (d, $^{3}J_{HH}$ =4 Hz, 2H), 4.68 (d, $^{3}J_{HH}$ = 6.4 Hz, 2H), 2.23 (m, 1H), 1.40 (m, 4H), 1.27 (m, 12H), 0.91 (t, $^{3}J_{HH}$ = 7.2 Hz, 3H), 0.86 (t, $^{3}J_{HH}$ = 6.8 Hz, 3H). ^{13}C NMR ($CDCl_3$, 100 MHz, δ): 146.89 (dd, $^{1}J_{CF}$ = 252 Hz, $^{2}J_{CF}$ = 19 Hz), 137.01 (t, $^{3,4}J_{CF}$ = 4.2 Hz), 133.76, 130.26 (m), 130.19, 115.92 (m), 109.29 (dd, $^{3}J_{CF}$ = 9.5 Hz, $^{4}J_{CF}$ = 4.4 Hz), 59.84, 39.10, 31.84, 31.41, 31.17, 29.57, 28.47, 26.20, 22.97, 22.66, 14.09. Anal. Calcd for $C_{26}H_{29}Br_2F_2N_3S_2$: C, 48.38; H, 4.53; N, 6.51. Found: C, 48.20; H, 4.55; N, 6.62.

Polymerization of PBnDT-FTAZ. 2,6-Bis(trimethyltin)-4,8-(3-butylnonyl)benzo[1,2-b:4,5-b']dithiophene (132 mg, 1.0 eq), FTAZ (97 mg, 1.0 eq), $Pd_2(dba)_3$ (2.8 mg, 0.02 eq), and tri(*o*-tolyl)phosphine (7.2 mg, 0.16 eq) were combined in a dry microwave vial. The vial was then sealed with a septum cap, and then evacuated and refilled with argon three times. Dry, oxygen free *o*-xylene (0.75 mL) was added. The mixture was then reacted in a microwave reactor for 20 min, at 200°C (at 300W), and then cooled to room temperature. The reaction mixture was then diluted with chlorobenzene (3 mL), and then the polymer solution was precipitated into methanol (100 mL) at room temperature. The resulting purple-black solid was filtered into a Soxhlet thimble, and extracted with methanol, ethyl acetate, hexanes, and chloroform until the wash from each extraction was colorless. When there was no solid remaining in the Soxhlet thimble, the chloroform fraction was then concentrated, and chlorobenzene was added (5 mL). The polymer solution was then precipitated into methanol at room temperature, filtered, and dried under vacuum at 0.5 mmHg. Yield: 153 mg (98%). Purple metallic solid. ^{1}H NMR @ 400K ($C_2D_2Cl_4$, 400 MHz, δ): 8.20, 7.26, 4.84, 3.07, 2.46, 1.51, 1.14, 1.05. GPC (1,2,4-trichlorobenzene at 135°C): M_n = 42.2 kg/mol, M_w = 99.9 kg/mol, PDI = 2.36.

Chapter 5: The Synthesis of Thieno[3,4-d]imidazoles for use as a Quinoidal Structure Stabilization Monomer

Thieno[3,4-d]imidazoles were initially investigated due to the ability to stabilize the quinoidal resonance form of a conjugated polymer. The imidazole ring shows less aromatic character than benzene, and thus the HOMO energy level of the polymers resulting from thieno[3,4-d]imidazoles should remain lower than that of the materials derived from benzo[c]thiophenes. Additionally, the synthesis of thieno[3,4-d]imidazoles was expected to be simpler than other quinoidal stabilization structures which were currently being investigated in the literature that require eight or more steps to synthesize.[49,115-117] Lastly, the ability to hydrogen bond between imidazoles within the polymer chain may have provided interesting opportunities as well, possibly using hydrogen bonding to control the planarity of the polymer.

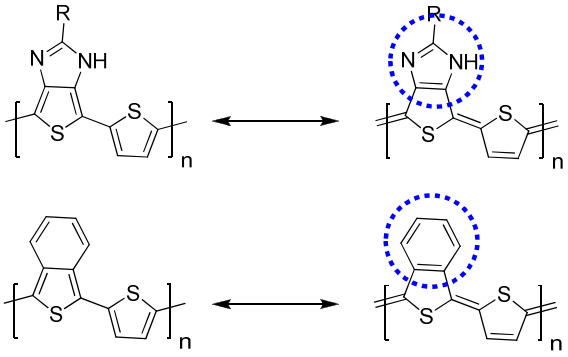

Figure 5.43. Quinoidal structure in the conjugated polymer stabilized by the formation of an imidazole ring in the thieno[3,4-d]imidazole based polymer (top), similar to polymer structures containing benzo[c]thiophenes (bottom).

The synthesis of thieno[3,4-d]imidazoles had been carried out previously in the patent literature for pharmaceutical research (US Patent #5389660).[118] Starting from 3,4-diaminothiophene which had been

prepared previously in large scale with inexpensive reagents in 3 steps, reaction with an ethyl alkylimidiate hydrogen chloride would give the desired 2-alky-1*H*-thieno[3,4-d]imidazole in just one step.[119] Therefore, the alkyl chain could be incorporated into the desired monomer during the final step, allowing simple optimization of the alkyl chain for solubility and hole mobility. Therefore 4,6-dibromo-2-undecyl-1H-thieno[3,4-d]imidazole (2) was prepared using the synthetic route in figure 5.44.

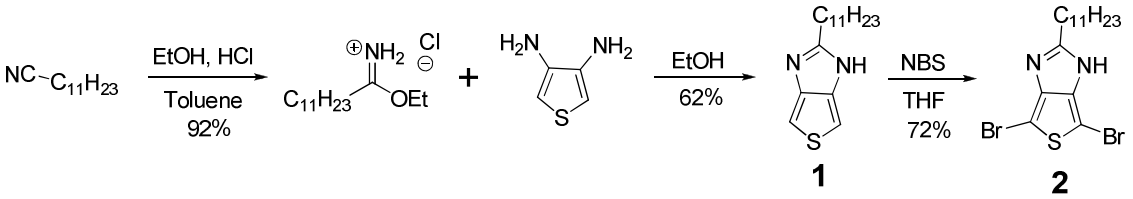

Figure 5.44. The synthesis of 4,6-dibromo-2-undecyl-1H-thieno[3,4-d]imidazole. Reaction of dodecanonitrile with anhydrous HCl and ethanol in toluene yields the desired imidate in high yield, which is then reacted with diaminothiophene to yield the desired heterocycle (1).

Following monomer synthesis, polymerization with 2,6-bis(trimethyltin)-4,8-di(dodecyl)benzo[1,2-b:4,5-b']dithiophene (3) using standard Stille coupling polymerization conditions was attempted. However after 41 hours stirring at reflux in toluene the TLC showed the major product as unreacted tin monomer, and no appreciable solid appeared when the reaction was precipitated into methanol. The polymerization reaction mixture was also a dark blue color, the same dark blue color of highly polar side products formed in the bromination with NBS. Additionally, attempts to deprotonate the imidazole nitrogen of 2 with a methyl group using sodium hydroxide or sodium hydride yielded the same dark blue color and complete consumption of the starting material. Therefore we hypothesized that due to the electron rich nature of the thieno[3,4-d]imidazole heterocycle, rapid oxidation was occurring, especially when deprotonated. Therefore, even if conjugated polymers could be synthesized, their electron rich nature would limit their success in photovoltaic cells. The high lying HOMO energy level, the success of other projects, and dwindling material ultimately caused us to pursue other avenues. Future work addressing the electron rich nature of the thieno[3,4-d]imidazole heterocycle would be merited, given the potential of low band gap polymers made from this material.

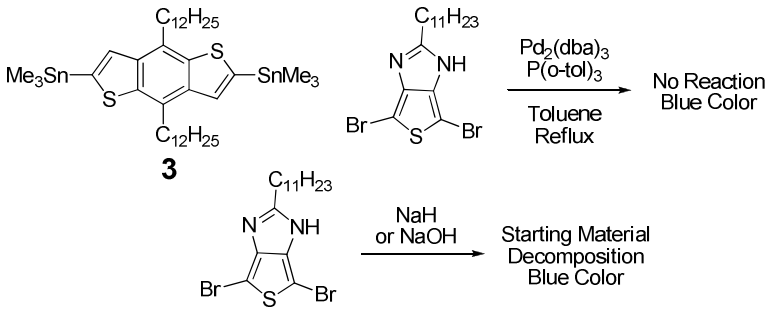

Figure 5.45. Both the Stille coupling polymerization (top) and deprotonation (bottom) caused decomposition of the starting materials into blue decomposition products.

With previous quinoidal stabilization monomers such as thieno[3,4-b]thiophene, electron withdrawing groups such as ketones or esters have been employed to reduce the HOMO energy level of the resulting conjugated polymer.[28] A similar strategy may be employed in this case as well, and other stronger electron withdrawing groups may be utilized. Additionally, rings which are more electron deficient than imidazole may be used for the quinoidal stabilization approach. Either of these approaches will likely lower the HOMO of the resulting polymer, however they both add significant synthetic complexity.

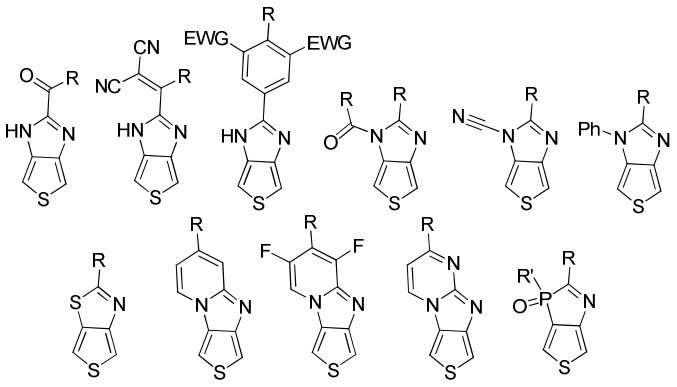

Figure 5.46. Thienoimidazoles employing electron withdrawing groups to lower the HOMO energy level (top row). Other possible quinoidal stabilization monomers using a ring which is less electron rich than imidazole (bottom row). All monomer candidates offer possible solutions to the exceptionally electron rich thienoimidazoles.

Experimental Section

All solvents are ACS grade unless otherwise noted. Anhydrous THF was obtained by distillation from sodium/benzophenone prior to use. Absolute ethanol and anhydrous toluene were purchased from commercial sources and used as received. Gaseous, dry HCl was made via dropwise addition of concentrated HCl into a cooled (10°C) solution of concentrated sulfuric acid (1 part HCl to 1.5 parts H_2SO_4). Sodium hydride was purchased as a dispersion in mineral oil, which was diluted with hexanes and decanted (3×), dried on hivac, and stored in a glove box as a white powder. Brine was used as necessary during extractions to break emulsions. 3,4-diaminothiophene and ethyldodecanimidate hydrogen chloride were prepared according to literature procedures.[119,120] All reagents were purchased from VWR, Fisher Scientific, Silicycle, and were used without further purification. ^{1}H nuclear magnetic resonance (NMR) spectra were obtained at 400 or 300 MHz as solutions in $CDCl_3$ or DMSO-d_6. ^{13}C NMR proton decoupled spectra were obtained at 100 MHz as solutions in $CDCl_3$. Chemical shifts are reported in parts per million (ppm, δ) and referenced from tetramethylsilane. Coupling constants are reported in hertz (Hz). Spectral splitting patterns are designated as s, singlet; d, doublet; dd, doublet of doublets; t, triplet; quin, quintet; m, multiplet; and br, broad. Melting points are uncorrected.

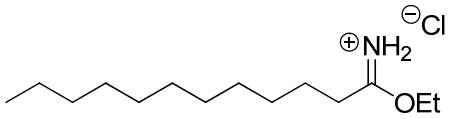

ethyldodecanimidate hydrogen chloride. Prepared following a procedure similar to reference 7. Dodecanonitrile (5.46 mL, 25 mmol), absolute ethanol (2.19 mL, 37.5 mmol), and anhydrous toluene (33 mL, 0.75 M in dodecanonitrile) were combined in a sealed flask under argon. The solution was then chilled to 0°C. The argon needle was then removed, and dry HCl gas was purged through the solution for 20 min while maintaining a temperature of 0°C. The reaction mixture was then warmed to rt and allowed to stir in the sealed vessel for 16.5 h. The solvent was then removed via rotary evaporation, and diethyl ether (250 mL) was added to the remaining residue. A white solid immediately precipitated, which was then filtered and washed with diethyl ether (100 mL). The slightly hygroscopic solid was air dried briefly and then collected and stored in a dessicator until use. Yields white solid. Yield: 6.407 g (92%). No characterization performed, compound immediately used in the following step.

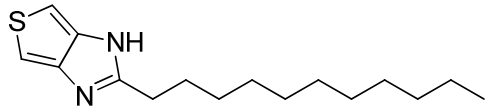

2-undecyl-1H-thieno[3,4-d]imidazole. Prepared following a procedure similar to reference 5. 3,4-diaminothiophene (415 mg, 3.63 mmol), ethyldodecanimidate hydrogen chloride (3.026 g, 10.89 mmol), and absolute ethanol were combined in a flask and purged with argon for 15 minutes. The reaction was then heated to reflux under argon for 1 hour. The reaction was then placed in a room temperature water bath and stirred for 17 hours. The ethanol was then removed via rotary evaporation, and then remaining residue was purified by column chromatography on silica gel using 2:1 hexanes:ethyl acetate. Yield: 622 mg (62%). White solid; mp 78°C. ^{1}H NMR ($CDCl_3$, 300 MHz, δ): 6.74 (s, 2H), 2.78 (t, $^{3}J_{HH}$ = 7.8 Hz, 2H), 1.82 (quin, $^{3}J_{HH}$ = 7.8 Hz, 2H), 1.25 (m, 16H), 0.88 (t, $^{3}J_{HH}$ = 6.9 Hz, 3H). ^{13}C NMR ($CDCl_3$, 100 MHz, δ): 165.47, 97.22, 31.87, 30.12, 29.58, 29.57, 29.46, 29.34, 29.31, 29.30, 27.87, 22.65, 14.09.

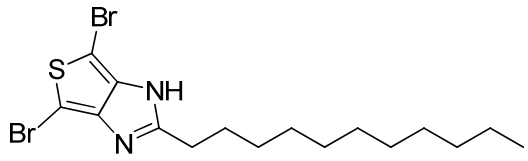

4,6-dibromo-2-undecyl-1H-thieno[3,4-d]imidazole. 2-undecyl-1H-thieno[3,4-d]imidazole (622 mg, 2.23 mmol) was dissolved into THF (25 mL) in an open flask. *N*-Bromosuccinimide (794 mg, 4.46 mmol) was added in one portion at rt. The resulting blue-black solution was stirred at room temperature for 2.5 h, and then poured into water. The organic phase was diluted with diethyl ether, and washed with water (2×). The organic solvent was then removed via rotary evaporation, and the remaining blue-white solid was recrystallized from boiling chloroform. The resulting white solid was then filtered, washed with cold hexanes, and collected. Yield: 699 mg (72%). White solid; decomposition point 114°C. ^{1}H NMR (DMSO-d_6, 400 MHz, δ): 12.05 (br s, 1H), 2.65 (t, $^{3}J_{HH}$ = 7.6 Hz, 2H), 1.71 (m, 2H), 1.24 (m, 16H), 0.86 (t, $^{3}J_{HH}$ = 6.8 Hz, 3H). ^{13}C NMR (DMSO-d_6, 100 MHz, δ): 167.92, 31.22, 29.21, 28.93, 28.91, 28.77, 28.63, 28.55, 28.50, 26.77, 22.02, 13.87. ESI-TOF MS $[M+H]^+$ = 435.0105 (calcd $[M+H]^+$ = 435.0027).

Chapter 6: Future Research Directions

The primary accomplishment of this dissertation is identifying the aggregating effects of a planar conjugated backbone and fluorine atoms on the electron deficient ring of the conjugated polymer. These discoveries highlighted the importance of phase segregation and the hole mobility of the conjugated polymer. Therefore, the clear method for optimizing these polymer cells is to lower the LUMO energy level of the conjugated polymer while keeping these other considerations (hole mobility, phase segregation ability, ect.) constant.

The polymer with the highest power conversion efficiency on record was measured to have a LUMO energy level of -3.45 eV.[28] The lowest conjugated polymer LUMO measured in this work was -3.3 eV, and the fluorinated benzotriazole monomer which reached efficiencies of 7% has an electrochemical LUMO of -3.05 eV. Clearly there is sufficient room for optimization in conjugated polymer materials, since the ideal LUMO for a conjugated material is estimated to be between 3.8 – 4.0 eV.[22] Therefore stronger, more electron deficient acceptors which have positions for alkyl chains and fluorine atoms should be the primary focus of new research on conjugated polymers.

The fluorinated benzotriazole monomer is limited in how far the LUMO can be decreased in energy since it is already heavily substituted. The only available modifications to the monomer without altering the fluorinated benzotriazole core would be to attach electron withdrawing groups to the alkyl chain of the benzotriazole. The lone pair of the nitrogen at the 2 position on the benzotriazole is very basic, and is the primary reason the LUMO is raised in energy compared to polymers synthesized with 2,1,3-benzothiadiazole. Therefore electron withdrawing groups that limit the electron donating ability of the nitrogen may possibly decrease the LUMO of the resulting conjugated polymers.

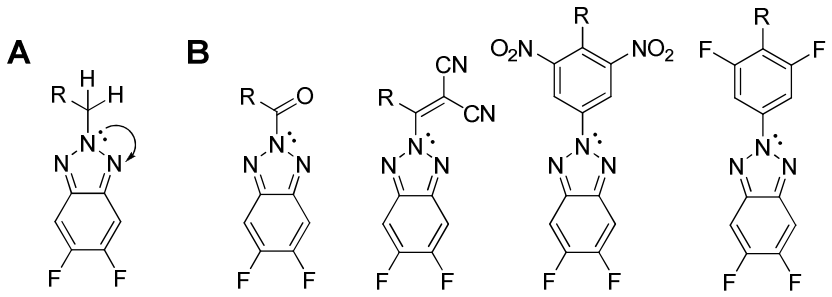

Figure 6.47. A) the lone pair on the 2 nitrogen is quite basic, donating more electron density onto the preferably electron deficient benzotriazole. B) Electron withdrawing groups which may limit the electron donating ability of the 2 nitrogen, lowering the LUMO.

In order for the LUMO to be decreased further beyond the ability of the fluorinated benzotriazole, new aromatic moieties must be developed which contain a low LUMO energy level, positions to affix solubilizing alkyl chains, and fluorine atoms to promote cofacial π-stacking. Monomers 1 and 2 proposed below employ the quinoidal stabilization approach to lower the LUMO of the resulting polymer, while possessing the two fluorine atoms and alkyl chains required. Density functional theory calculations on the LUMO of a similar conjugated polymer predicts a LUMO of -3.8 eV, which would narrow the LUMO-LUMO gap to unprecedented levels.

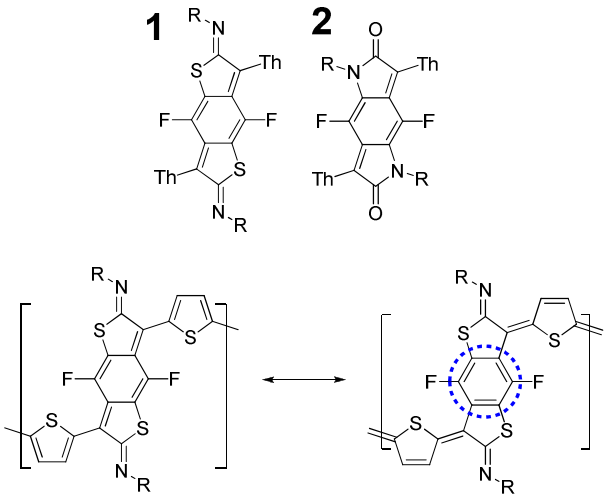

Figure 6.48. Proposed low LUMO quinoidal stabilization monomers, which form a benzene ring to stabilize the quinoidal structure. Monomers also contain fluorine atoms, and solubilizing alkyl chains to meet the remaining design criteria.

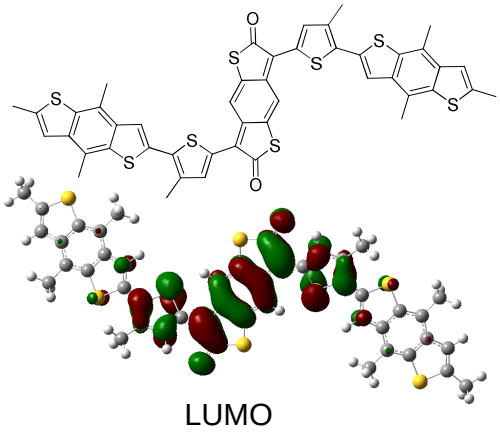

HOMO = -5.2 eV
LUMO = -3.8 eV
Eg = 1.4 eV

Figure 6.49. DFT calculated LUMO for a conjugated polymer containing a structurally similar core to monomer 1.

In addition to optimizing the LUMO of the conjugated polymer, a more thorough understanding of the fluorine induced polymer aggregation (and subsequent hole mobility increase) is required. The conventional explanation for the aggregation of fluorinated heterocycles with non-fluorinated aromatic hydrocarbons is due to the opposite quadrapole moments.[121] The typical example is the case of hexafluorobenzene packing in a co-facial fashion with benzene when frozen in a single crystal. Similar crystalline packing has been observed in short oligomers.[122] This explanation must be verified in the case of a complex conjugated polymer system, and the extent of fluorination required to achieve this aggregation effect must be measured. Therefore, crystal structures of oligomers of BnDT-FTAZ should be studied to determine what the likely nature of the crystalline packing in the solid polymer film is. Additionally, polymers with varying degrees of fluorination should be studied to determine exactly how often fluorine atoms are required on the polymer backbone to see a performance increase.

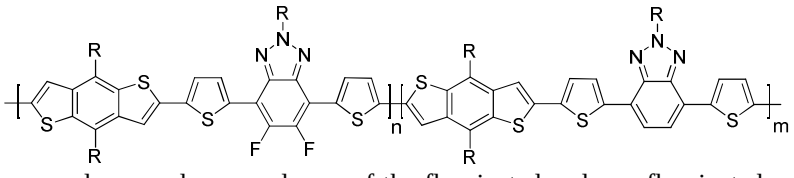

Figure 6.50. For example, a random copolymer of the fluorinated and non-fluorinated material should be synthesized. Often, only a small portion of the polymer chain must possess strong electronic coupling with other polymer chains in order to increase the mobility for the bulk film.

Appendix 1: Benzodithiophene Synthesis

The synthesis of 2,6-Bis(trimethyltin)-4,8-(alkyl)benzo[1,2-*b*:4,5-*b'*]dithiophenes have been reported in a number of publications.[49,57,123] However, after synthesizing this compound on numerous occasions I have made some minor modifications to the synthetic procedures used. This appendix will give a highly detailed experimental on the synthesis of this key monomer unit.

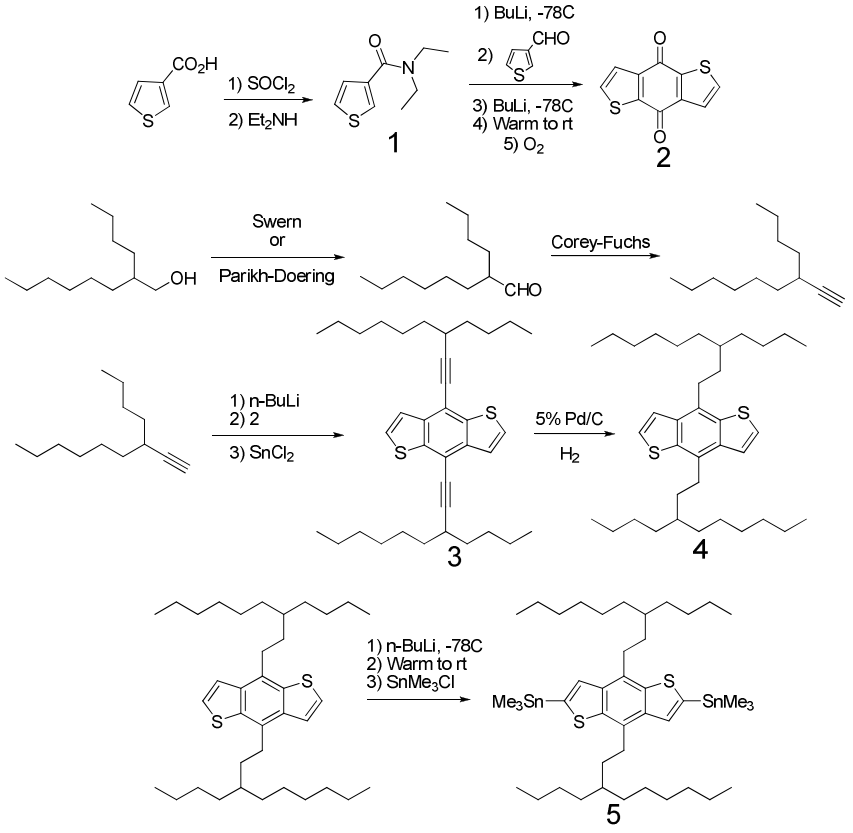

Figure A1.51. Synthesis of 2,6-Bis(trimethyltin)-4,8-(3-butylnonyl)benzo[1, 2-*b*:4,5-*b'*]dithiophene.

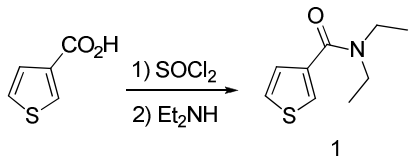

1

N,N-diethylthiophene-3-carboxamide (1). Thiophene-3-carboxylic acid (15.0 g, 117.05 mmol) was suspended in methylene chloride (200 mL) in a flask fitted with a reflux condenser and an acid vapor trap. Thionyl chloride (55.7 g, 468.2 mmol) was then added slowly over 5 min. The reaction was heated to reflux for three hours, and then the volatiles were removed by rotary evaporation. Methylene chloride was then added, and the mixture was cooled in an ice bath. While swirling the contents of the flask by hand, diethyl amine (36 mL, 351 mmol) was then added SLOWLY until gas evolution ceases (Caution: HCl gas evolution! Exothermic!). The resulting highly viscous slurry was then poured into 150 mL of 1M HCl (to remove excess amine), and extracted with methylene chloride. The organic phase was then washed with 1M HCl (twice), 10% NaOH solution (twice), water, and then dried over sodium sulfate. The organic phase was filtered through a silica plug and concentrated on a rotary evaporator affording a pale yellow oil. Yield: 17.39 g (81%). ^{1}H NMR ($CDCl_3$, 300 MHz, δ): 7.48 (dd, $^{4}J_{HH}$ = 3 Hz, $^{4}J_{HH}$ = 0.9 Hz, 1H), 7.32 (dd, $^{3}J_{HH}$ = 4.8 Hz, $^{4}J_{HH}$ = 3 Hz, 1H), 7.19 (dd, $^{3}J_{HH}$ = 4.8 Hz, $^{4}J_{HH}$ = 0.9 Hz, 1H), 3.39 (m, 4H), 1.20 (m, 6H).

Notes: The acid vapor trap is tygon tubing fitted to the top of the reflux condenser, which runs through an Erlenmeyer filter flask (to prevent suck-backs), and then to a funnel which is submerged in 10% NaOH solution. During the addition of the diethyl amine, the solution releases large quantities of HCl gas and becomes highly exothermic, and very viscous. Typically a stir bar isn't sufficient to stir the viscous mixture, and therefore I usually swirl the contents by hand on an ice bath while slowly adding diethyl amine.

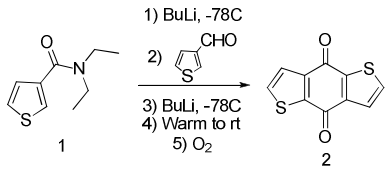

1 2

Dithienoquinone (2). Compound 1 (18.19 g, 99.3 mmol) was weighed into a dry 500 mL flask, which was the evacuated and refilled with argon (3x). Anhydrous THF (200 mL) was then added via cannula, and the reaction was chilled to -78°C in a dry ice/acetone bath. A 1.6 M solution of n-BuLi in hexanes (63 mL,

100.8 mmol) was added dropwise at -78°C and the reaction mixture was stirred for 25 min. Thiophene-3-carbaldehyde (8.7 mL, 99.3 mmol) was added, and the reaction was stirred for 20 min while maintaining -78°C. An additional portion of 1.6 M n-BuLi in hexanes (63 mL, 100.8 mmol) was then added at -78°C and the reaction was stirred for 25 minutes. The reaction was warmed to rt on an ambient water bath and stirred for 2 h. The reaction was then poured into water and air was bubbled through the mixture overnight, while stirring rapidly. A yellow-green precipitate then formed out of the brown solution, and the solid was filtered. The filter cake was washed with water, chilled methanol, and hexanes until the washes were colorless. The resulting yellow solid was air dried. Yield: 17.28 g (79%). ^{1}H NMR ($CDCl_3$, 300 MHz, δ): 7.69 (d, $^3J_{HH}$ = 4.8 Hz, 2H), 7.65 (d, $^3J_{HH}$ = 4.8 Hz, 1H).

Notes: Reaction can be done with only compound 1, however, the aldehyde allows for a more convergent synthesis. Distill the aldehyde prior to this reaction, and use within 1-2 days.

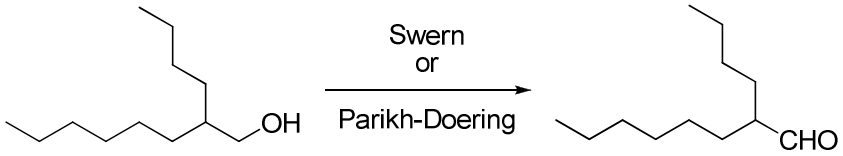

For a swern oxidation, follows the same synthetic procedure used in chapter 2, for 2-hexyldecanal. This is the procedure used for the Parikh-Doering oxidation method.

2-butyloctanal. Pyridine·SO_3 complex (31.8 g, 200 mmol) was added to a solution of anhydrous dimethylsulfoxide (36 mL, 500 mmol) and methylene chloride (200 mL) in an open flask. The mixture was stirred for 5 minutes, and then chilled on an ice bath to 0°C. 2-butyloctanol (22.4 mL, 100 mmol) and triethylamine were added in one portion as a solution in methylene chloride (50 mL). The reaction rapidly turned homogenous, and was stirred for 1 hour. The reaction mixture was then poured into 1M HCl and ice (Caution exothermic). The organic phase was then washed with saturated ammonium chloride, and then dried over magnesium sulfate. The organic phase was then filtered, concentrated, and then dissolved into 50 mL of hexanes. The hexanes solution was filtered through a silica plug, and then concentrated via rotary evaporation. Affords a pale yellow oil of sufficient purity, and was immediately used in the following steps. Yield: 15.68 g (85%). ^{1}H NMR ($CDCl_3$, 300 MHz, δ): 9.55 (d, $^3J_{HH}$ = 3.3 Hz, 1H), 2.22 (m, 1H), 1.61 (m, 2H) 1.43 (m, 2H), 1.27 (m, 12H), 0.89 (m, 6H).

Note: The yield is slightly reduced if you don't add the alcohol at 0°C.

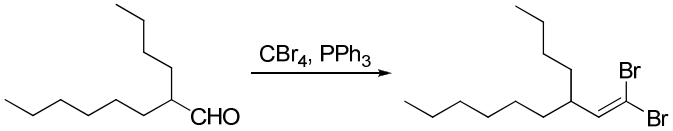

5-(2,2-dibromovinyl)undecane. Carbon tetrabromide (89.54 g, 270 mmol), zinc dust (17.66 g, 270 mmol), and methylene chloride (775 mL) were combined in an open flask and cooled to 0°C. Triphenylphosphine (70.82 g, 270 mmol) was added in 5-6 portions and the reaction was stirred for 25 min. 2-butyloctanal (24.855 g, 135 mmol) was added in one portion, using a small portion of methylene chloride to rinse all of the aldehyde into the reaction. The reaction was then stirred for 18 h at rt. The reaction was then vacuum filtered through a short plug of silica gel, and then concentrated via rotary evaporation. The resulting viscous brown sludge was then dissolved into a small portion of methylene chloride, and the organic solution was added dropwise to 600 mL of hexanes with rapid stirring. The resulting hexanes solution was then filtered through silica until no trace of triphenylphosphine oxide was detectable by TLC. The hexane solution was then concentrated, yielding a colorless oil which turned yellow-brown upon standing for 1-2 weeks. Yield: 38.38 g (84%). ^{1}H NMR ($CDCl_3$, 300 MHz, δ): 6.38 (t, $^{3}J_{HH}$ = 7.2 Hz, 1H), 2.07 (m, 2H), 1.48 (m, 1H), 1.26 (m, 16H), 0.89 (m, 6H).

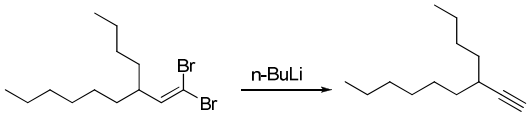

5-ethynylundecane. 5-(2,2-dibromovinyl)undecane (38.38 g, 112.8 mmol) was added to a dry flask, and then the flask was evacuated and refilled with argon (3x). Anhydrous THF (225 mL) was then added, and the reaction mixture was cooled to to -78°C in a dry ice/acetone bath. A 2.5 M solution of n-BuLi in hexanes (92.5 mL, 231.24 mmol) was added dropwise and the solution was stirred for 1 h at -78°C. Water (20 mL) was then added at -78°C, and then the reaction was allowed to slowly warm to rt. The reaction was poured into water, and extracted with hexanes. The organic phase was washed with water (3x), dried over sodium sulfate, filtered, and concentrated in vacuo. The resulting oil was distilled, and the desired alkyne was collected at 60°C @ 0.8 mm Hg. Yield: 14.699 g (72%). ^{1}H NMR ($CDCl_3$, 400 MHz, δ): 2.30 (m, 1H), 2.04 (d, $^{3}J_{HH}$ = 2.4 Hz, 1H), 1.46 (m, 6H), 1.29 (m, 10H), 0.90 (m, 6H).

Note: Higher yield can be obtained simply by filtering the reaction through a silica plug instead of distillation, but the purity is slightly lower.

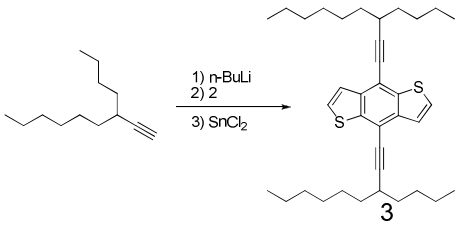

3

Compound 3. 5-ethynylundecane (6.068 g, 33.65 mmol) was placed in a dry flask and the flask was evacuated and refilled with argon (3x). Anhydrous THF (100 mL) was then added, and the reaction was cooled to 0°C. A 2.5 M solution of n-BuLi in hexanes (13.6 mL, 34 mmol) was added dropwise at 0°C, and the reaction mixture was allowed to stir for 1 h. Compound 2 (2.95 g, 13.39 mmol) was added under a stream of argon at 0°C, and then solution immediately turned green-black in color. The reaction was stirred for 3 h at rt, then water (5 mL) was added in one portion and the argon line was removed. The dark green color disappeared, leaving a yellow heterogeneous solution. A solution of $SnCl_2 \cdot 2H_2O$ (15.10 g, 66.95 mmol) in 1 M HCl (75 mL) was added in one portion, and the reaction was allowed to stir overnight at rt. The reaction was then poured into 10% HCl and extracted with toluene. The organic phase was then filtered through a silica plug, and then concentrated on a rotary evaporator. The resulting oil was then distilled to remove unreacted 5-ethynylundecane. The resulting residue was then redissolved in a small volume of hexanes and purified by column chromatography on silica gel using hexanes as the eluent. Yield: 3.14 g (43%). ^{1}H NMR ($CDCl_3$, 400 MHz, δ): 7.56 (d, $^3J_{HH}$ = 5.4 Hz, 2H), 7.50 (d, $^3J_{HH}$ = 5.7 Hz, 2H), 2.73 (m, 2H), 1.56 (m, 14H), 1.36 (m, 18H), 0.97 (t, $^3J_{HH}$ = 7.2 Hz, 6H), 0.91 (t, $^3J_{HH}$ = 6.3 Hz, 6H).

Note: This reaction has two problem areas. First, removing the tin salts after the reduction is tricky. If you wash the organic layer with base, all the tin salts will precipitate, forming a nasty emulsion. However, aqueous extraction with 10% HCl does not remove the tin salts from the organic layer. Therefore, filter the organic phase through silica with a non-polar solvent like toluene. These tin salts need to be removed before distillation. Secondly, the distillation to recover the unreacted 5-ethynylundecane is critical, since it is very difficult to separate the alkyne from compound 3 using chromatography. The yield may possibly be improved with the use of a Grignard reagent instead of n-BuLi.

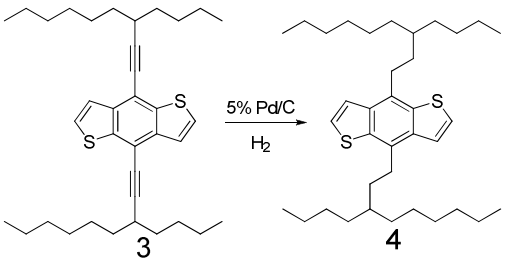

Compound 4. Compound 3 (4.99 g, 9.1 mmol) was dissolved into ethyl acetate (90 mL), and the flask was purged with argon for 5 min. 5% Pd/C (455 mg) was added, and the reaction mixture was purged with hydrogen gas from a balloon for 30 minutes. A fresh, full balloon was then fixed to the flask, and the mixture was stirred overnight under a hydrogen atmosphere. The reaction mixture was then filtered through medium porosity filter paper and then concentrated via rotary evaporation. The residue was then purified by column chromatography in hexanes, affording a colorless oil. Yield: 4.25 g (84%). ^{1}H NMR ($CDCl_3$, 400 MHz, δ): 7.45 (s, 4H), 3.13 (m, 4H), 1.72 (m, 4H), 1.50 (m, 2H), 1.37 (m, 8H), 1.30 (m, 24H), 0.91 (m, 12H).

Note: The purity of the compound out of the reaction varies a lot by how much catalyst is used, and how new it is. Using too little, old catalyst will cause partial reduction byproducts to occur, and they can often be somewhat difficult to column out. However, if you give the reaction enough hydrogen and enough catalyst, you can sometimes get it to go spot to spot on the TLC plate.

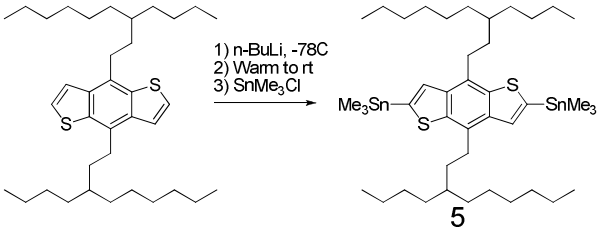

Compound 5, BnDT Monomer. Compound 4 (1.301 g, 2.34 mmol) was placed in a dry flask, which was then evacuated and refilled with argon (3x). Anhydrous THF (50 mL) was then added, and the reaction mixture was cooled to -78°C in a dry ice/acetone bath. A 2.5 M solution of n-BuLi in hexanes (2.25 mL, 5.64 mmol) was added, and the reaction was stirred for 30 min. The reaction was then placed in an ambient water bath and the reaction mixture was stirred at rt for 30 min. A white precipitate formed. Then the reaction was placed back in the -78°C in a dry ice/acetone bath, and stirred for 10 min. A 1.0 M solution of trimethyltin chloride in hexanes (6.1 mL, 6.1 mmol) was then added in one portion, and the reaction was

allowed to stir for 1 h. The reaction was then poured into water and extracted with ethyl acetate. The organic phase was washed with water (3x), dried over sodium sulfated, filtered, and concentrated in vacuo. The resulting pale yellow solid was then recrystallized from boiling methanol. Yield: 1.544 g (75%). White crystalline solid. ^{1}H NMR ($CDCl_3$, 400 MHz, δ): 7.49 (s, 2H), 3.15 (m, 4H), 1.75 (m, 4H), 1.52 (m, 2H), 1.33 (m, 32H), 0.9 (m, 12H), 0.45 (s, 18H). ^{13}C NMR ($CDCl_3$, 100 MHz, δ): 141.39, 140.12, 136.66, 129.64, 127.76, 37.79, 33.61, 33.31, 33.03, 32.07, 30.57, 29.88, 29.08, 26.78, 23.22, 22.76, 14.27, 14.18, -8.39.

Notes: You must warm up the reaction to rt before you quench with the $SnMe_3Cl$, otherwise you will not get complete lithiation. Methanol has always worked best for me as a recrystalization solvent, but the compound is fairly insoluble in methanol, so it takes ~350 mL to recrystalize 1.5 g of product. The white solid is stable if stored at rt in the dark for at least several months, however the container must be capped & sealed. Long term exposure to atmospheric oxygen will cause the monomer to degrade. If there are traces of byproducts in the NMR, you can recover the starting material by treating the tin monomer with H_2SO_4. Spectra for this compound can be seen in appendix 3.

Appendix 2: Supporting Information for Chapter 2

NMR Spectra

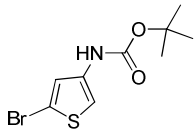

^{1}H NMR

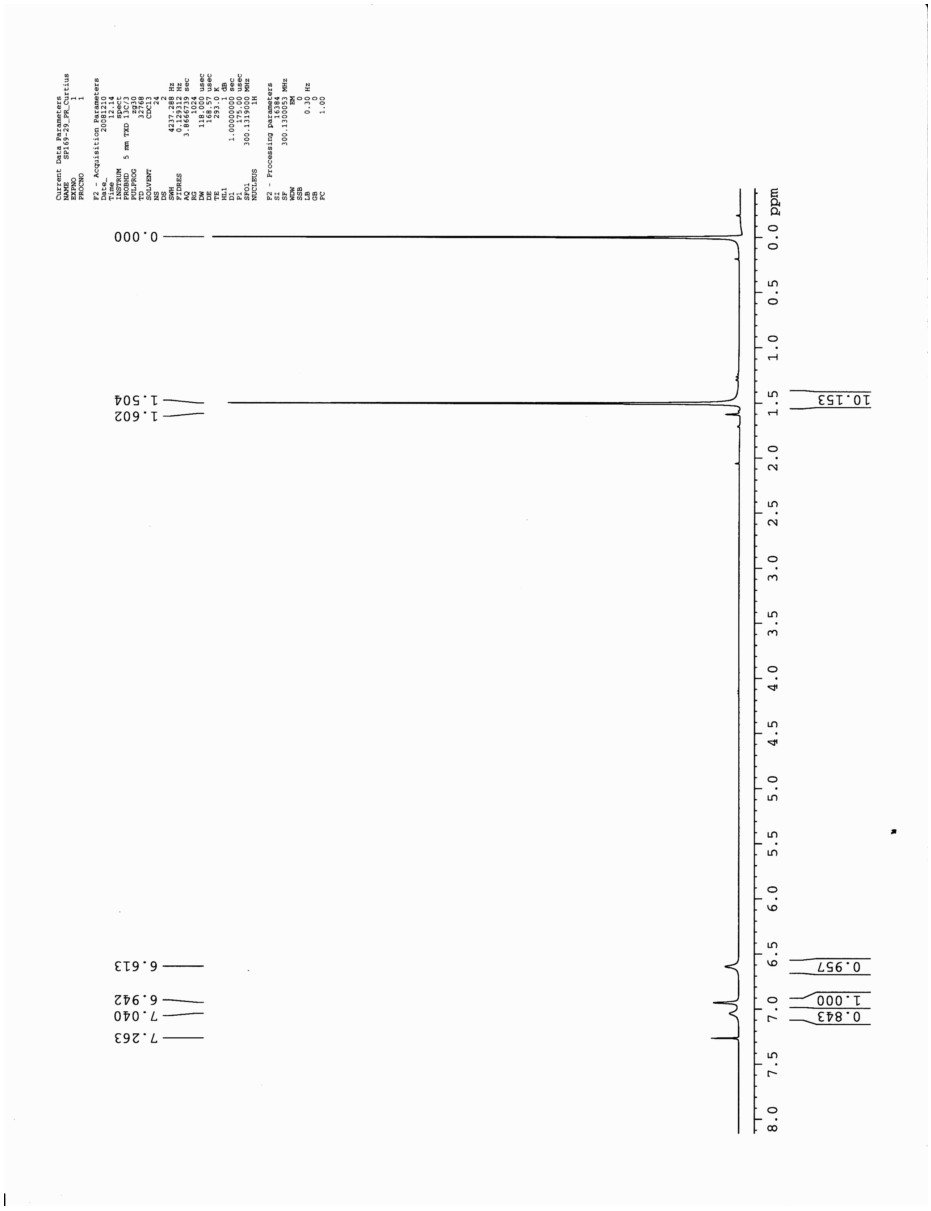

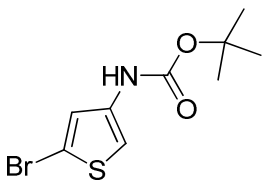
HN
O
O
Br
S

^{13}C NMR

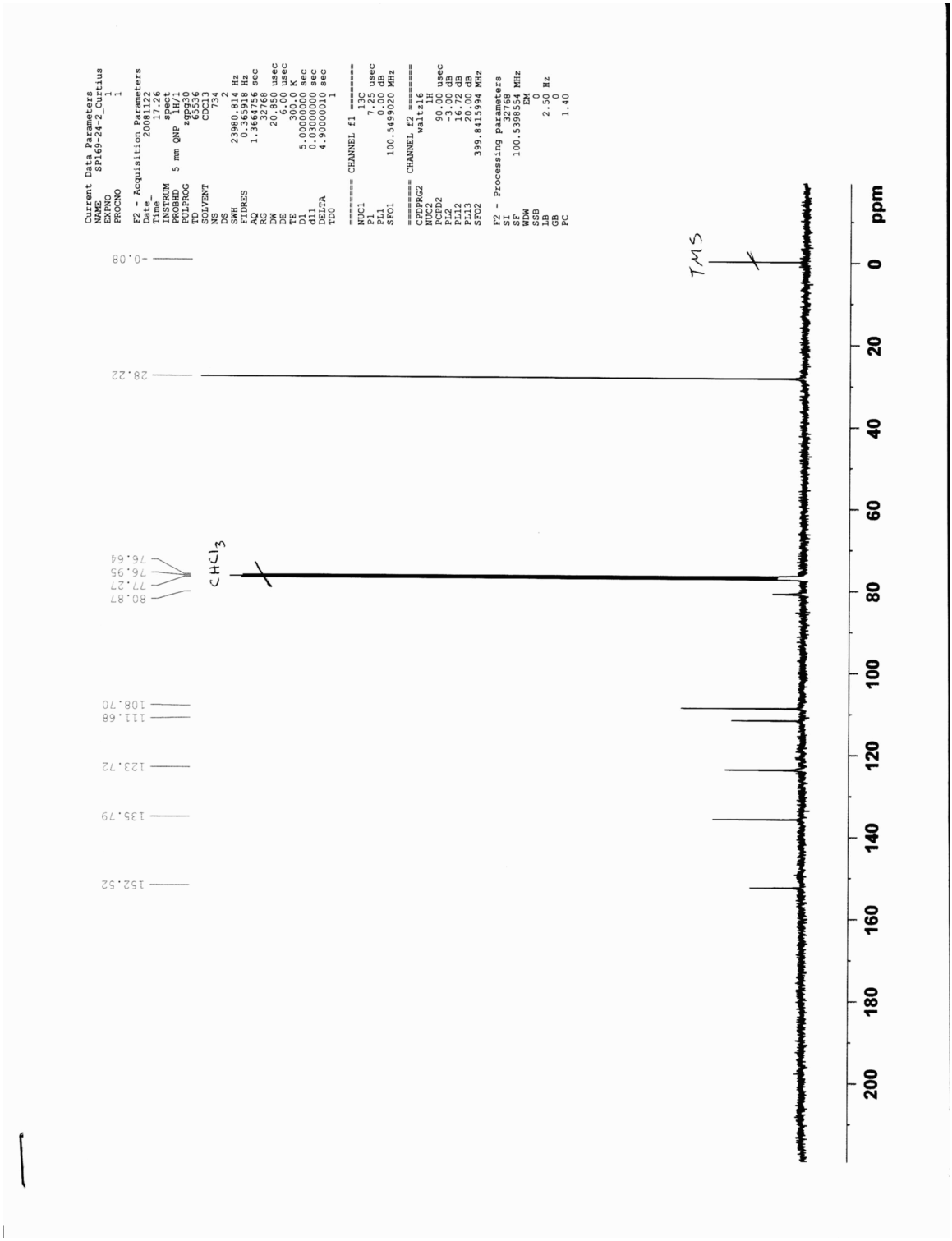
Current Data Parameters
NAME SP169-24-2_Curtius
EXPNO 1
PROCNO 1
F2 - Acquisition Parameters
Date_ 20081122
Time 17.26
INSTRUM spect
PROBHD 5 mm QNP 1H/1
PULPROG zgpg30
TD 65536
SOLVENT CDCl3
NS 734
DS 2
SWH 23980.814 Hz
FIDRES 0.365918 Hz
AQ 1.3647456 sec
RG 32768
DW 20.850 usec
DE 6.00 usec
TE 300.0 K
D1 5.00000000 sec
d11 0.03000000 sec
DELTA 4.90000010 sec
TD0 1
======== CHANNEL f1 ========
NUC1 13C
P1 7.25 usec
PL1 0.00 dB
SFO1 100.5499020 MHz
======== CHANNEL f2 ========
CPDPRG2 waltz16
NUC2 1H
PCPD2 90.00 usec
PL2 -3.00 dB
PL12 16.72 dB
PL13 20.00 dB
SFO2 399.8415994 MHz
F2 - Processing parameters
SI 32768
SF 100.5398554 MHz
WDW EM
SSB 0
LB 2.50 Hz
GB 0
PC 1.40
-0.08
28.22
76.64
76.95
77.27
80.87
108.70
111.68
123.72
135.79
152.52
CHCl3
TMS
200
180
160
140
120
100
80
60
40
20
0
ppm

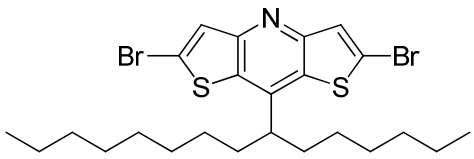

^{1}H NMR

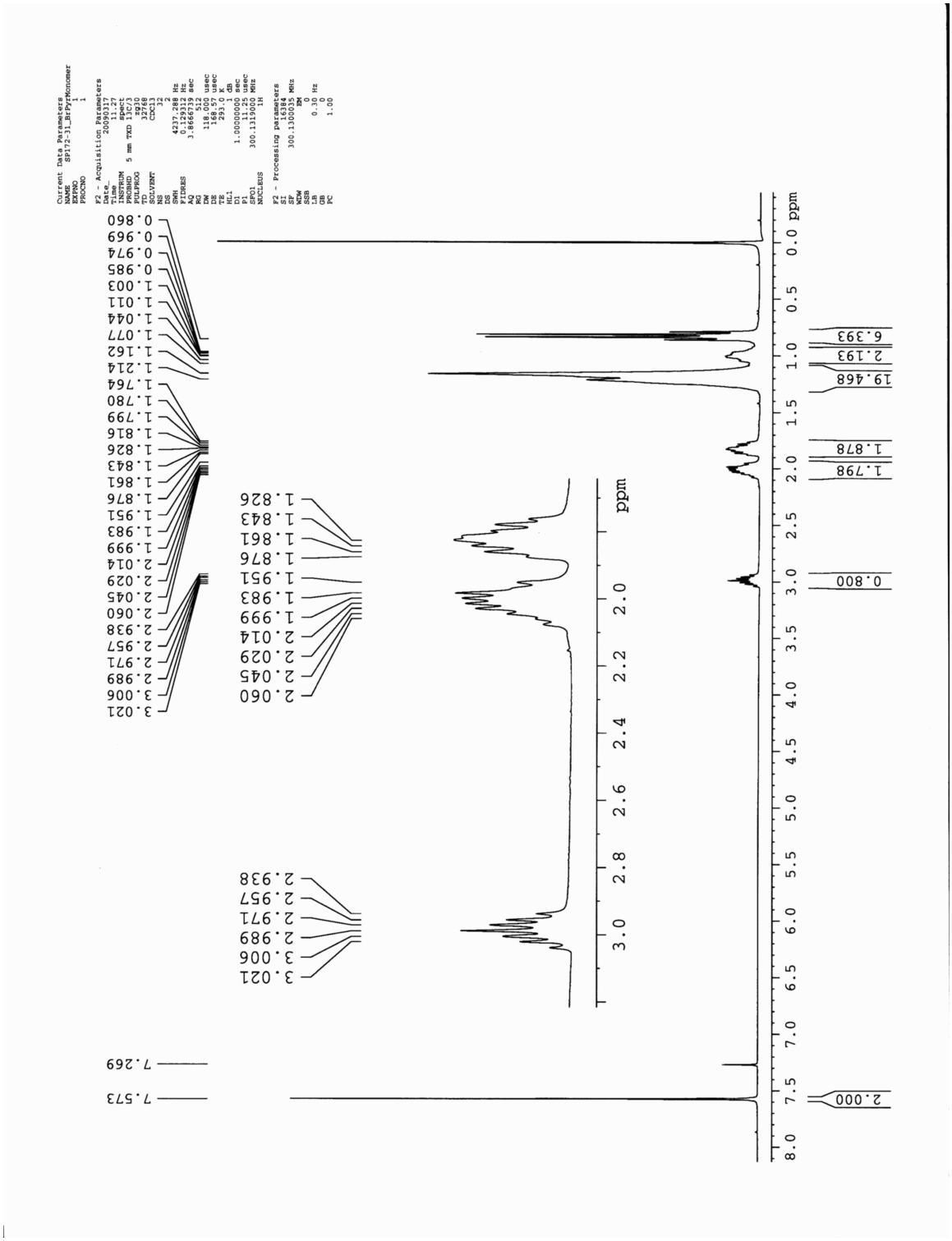

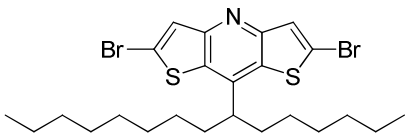
N
Br
Br
S
S

^{13}C NMR

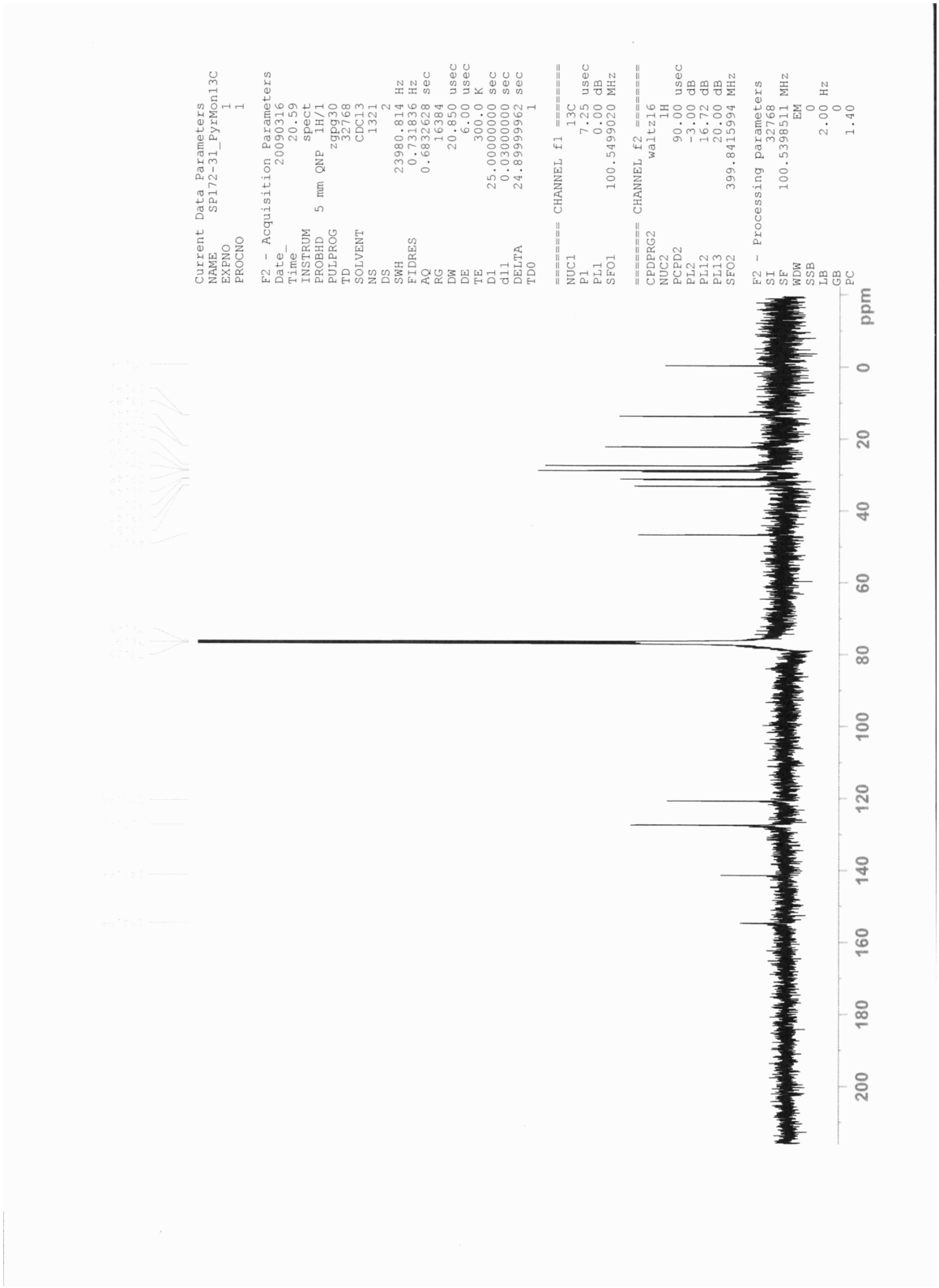
Current Data Parameters
NAME SP172-31_PyrMon13C
EXPNO 1
PROCNO 1
F2 - Acquisition Parameters
Date_ 20090316
Time_ 20.59
INSTRUM spect
PROBHD 5 mm QNP 1H/1
PULPROG zgpg30
TD 32768
SOLVENT CDCl3
NS 1321
DS 2
SWH 23980.814 Hz
FIDRES 0.731836 Hz
AQ 0.6832628 sec
RG 16384
DW 20.850 usec
DE 6.00 usec
TE 300.0 K
D1 25.00000000 sec
d11 0.03000000 sec
DELTA 24.89999962 sec
TD0 1
======== CHANNEL f1 ========
NUC1 13C
P1 7.25 usec
PL1 0.00 dB
SFO1 100.5499020 MHz
======== CHANNEL f2 ========
CPDPRG2 waltz16
NUC2 1H
PCPD2 90.00 usec
PL2 -3.00 dB
PL12 16.72 dB
PL13 20.00 dB
SFO2 399.8415994 MHz
F2 - Processing parameters
SI 32768
SF 100.5398511 MHz
WDW EM
SSB 0
LB 2.00 Hz
GB 0
PC 1.40
200
180
160
140
120
100
80
60
40
20
0
ppm

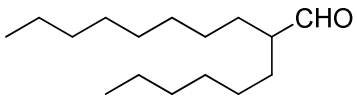

^{1}H NMR

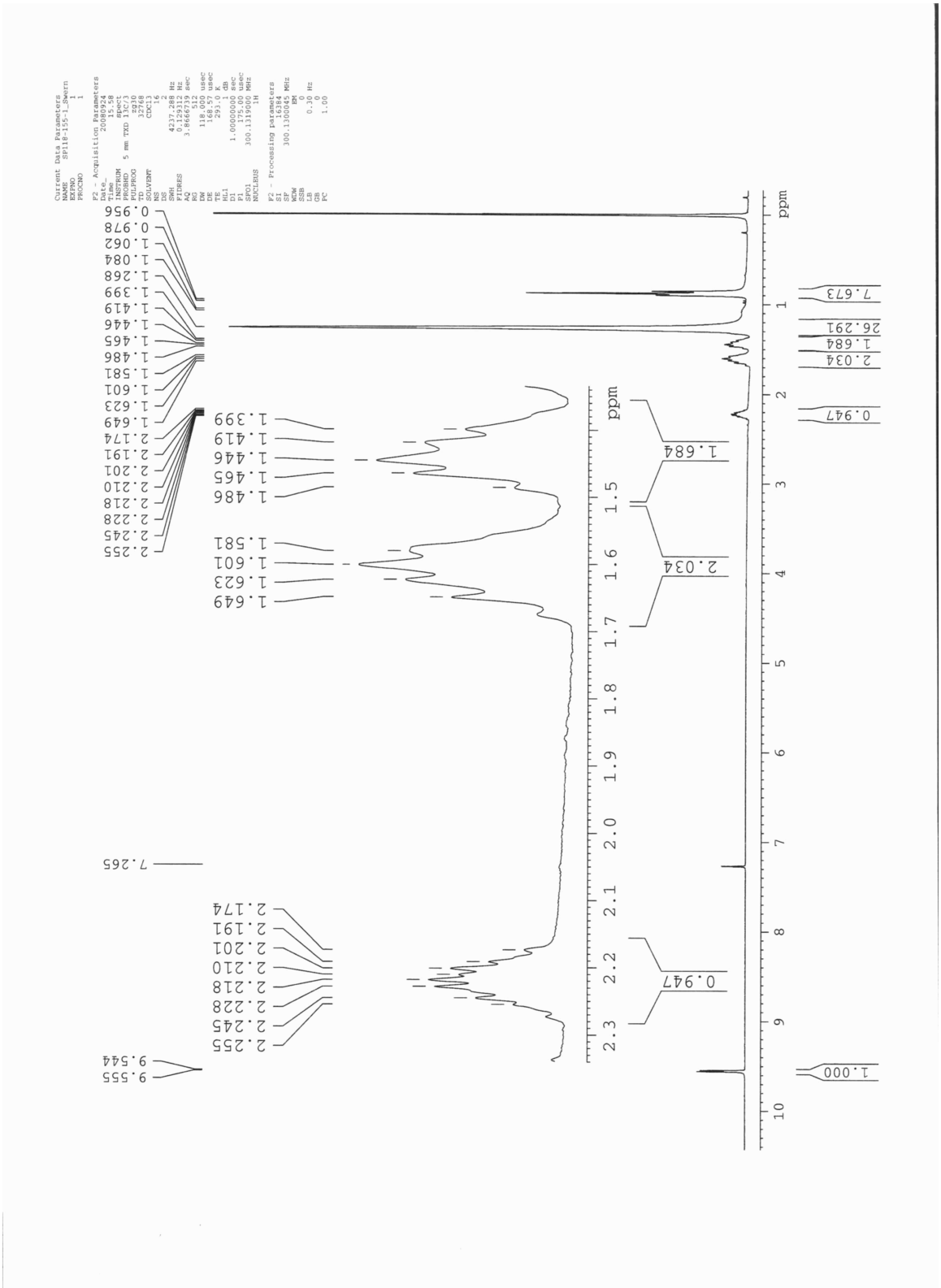

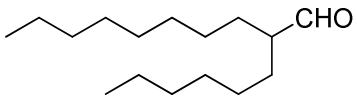
CHO

^{13}C NMR

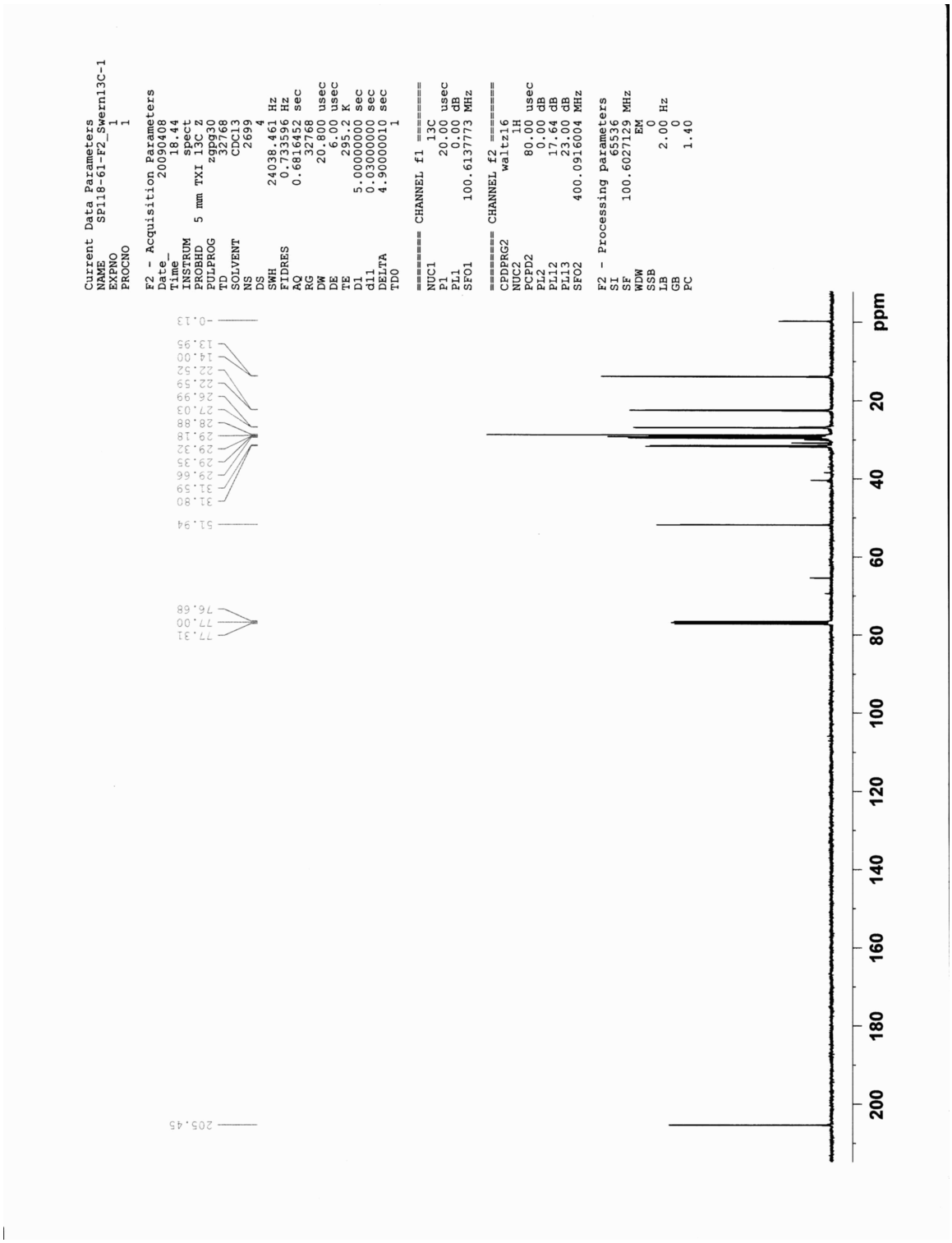
Current Data Parameters
NAME SP118-61-F2_Swern13C-1
EXPNO 1
PROCNO 1
F2 - Acquisition Parameters
Date_ 20090408
Time 18.44
INSTRUM spect
PROBHD 5 mm TXI 13C Z
PULPROG zgpg30
TD 32768
SOLVENT CDCl3
NS 2699
DS 4
SWH 24038.461 Hz
FIDRES 0.733596 Hz
AQ 0.6816452 sec
RG 32768
DW 20.800 usec
DE 6.00 usec
TE 295.2 K
D1 5.00000000 sec
d11 0.03000000 sec
DELTA 4.90000010 sec
TD0 1
======== CHANNEL f1 ========
NUC1 13C
P1 20.00 usec
PL1 0.00 dB
SFO1 100.6137773 MHz
======== CHANNEL f2 ========
CPDPRG2 waltz16
NUC2 1H
PCPD2 80.00 usec
PL2 0.00 dB
PL12 17.64 dB
PL13 23.00 dB
SFO2 400.0916004 MHz
F2 - Processing parameters
SI 65536
SF 100.6027129 MHz
WDW EM
SSB 0
LB 2.00 Hz
GB 0
PC 1.40
205.45
77.31
77.00
76.68
51.94
31.80
31.59
29.66
29.35
29.32
29.18
28.88
27.03
26.99
22.59
22.52
14.00
13.95
-0.13
ppm
200
180
160
140
120
100
80
60
40
20

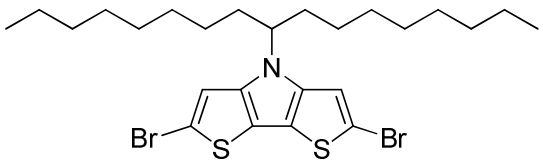

^{1}H NMR

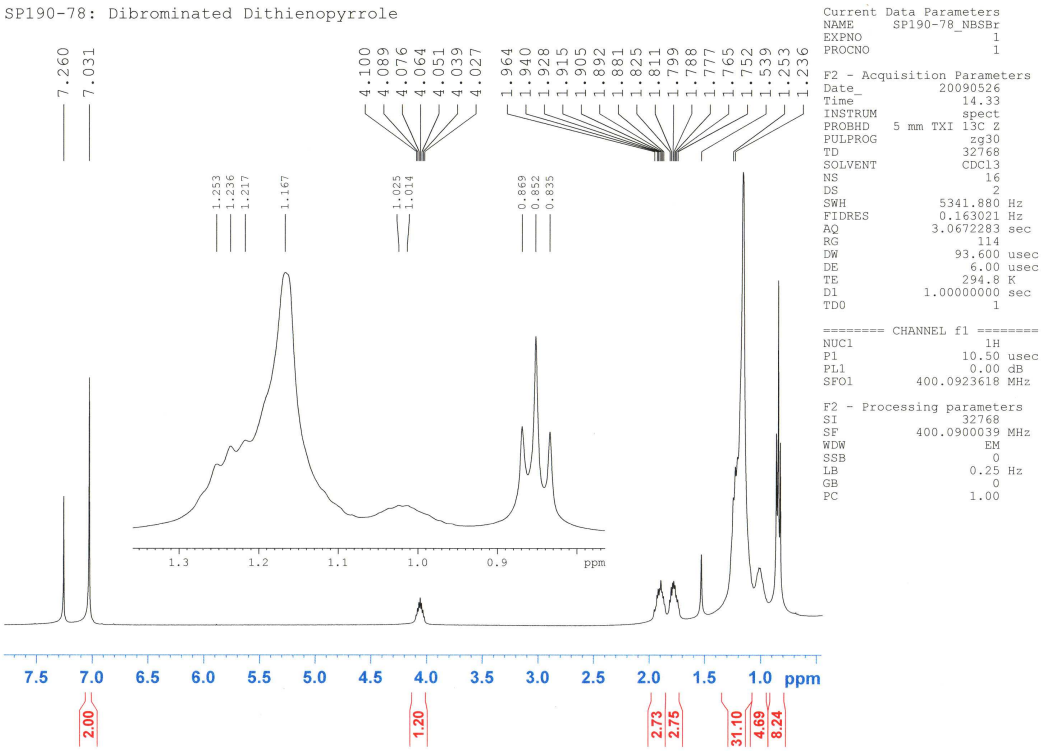

^{1}H NMR ($CDCl_3$, 400 MHz, δ): 7.03 (s, 2H), 4.06 (m, 1H), 1.92 (m, 2H), 1.79 (m, 2H), 1.17 (m, 24H), 0.85 (t, J = 6.8 Hz, 6H).

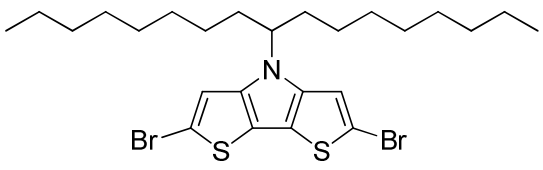

^{13}C NMR

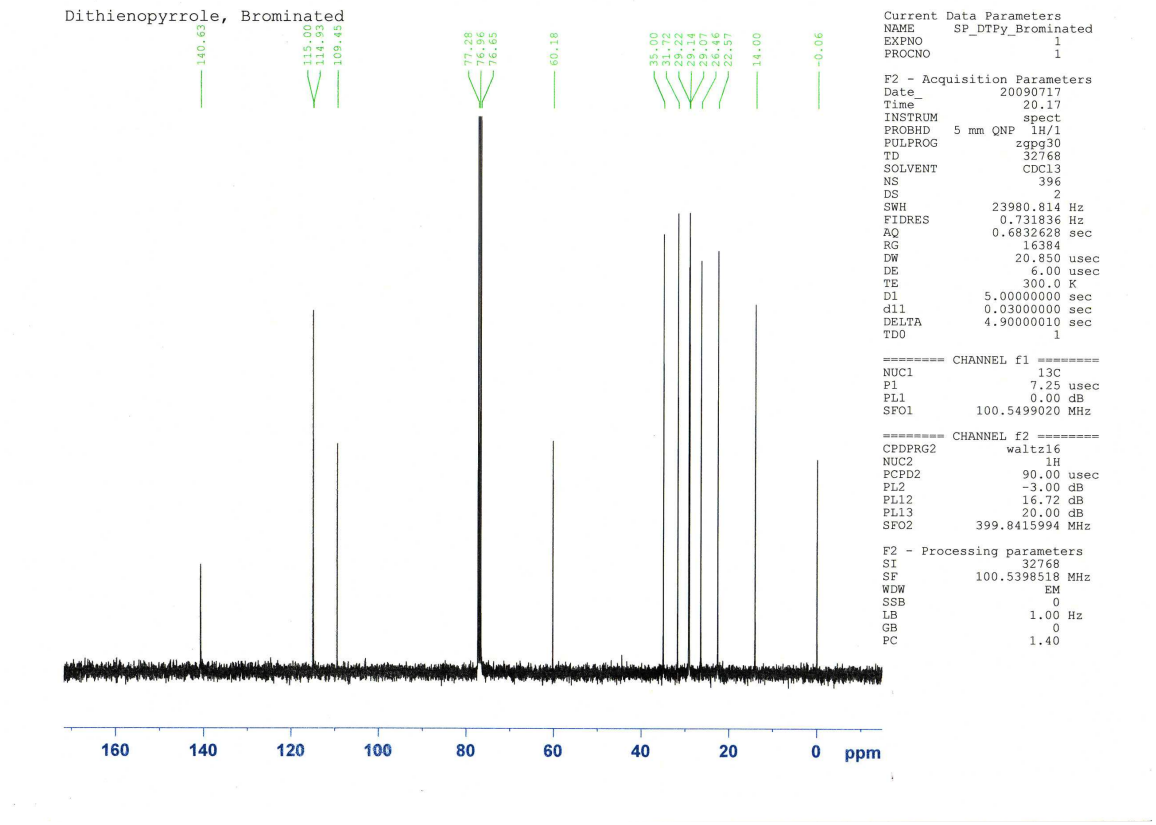

^{13}C NMR ($CDCl_3$, 100 MHz, δ): 140.63, 115.00, 114.93, 109.45, 60.18, 35.00, 31.72, 29.22, 29.14, 29.07, 26.46, 22.57, 14.00.

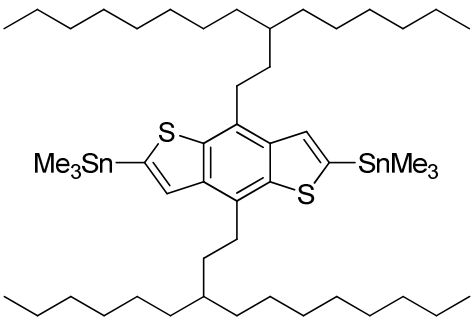

^{1}H NMR

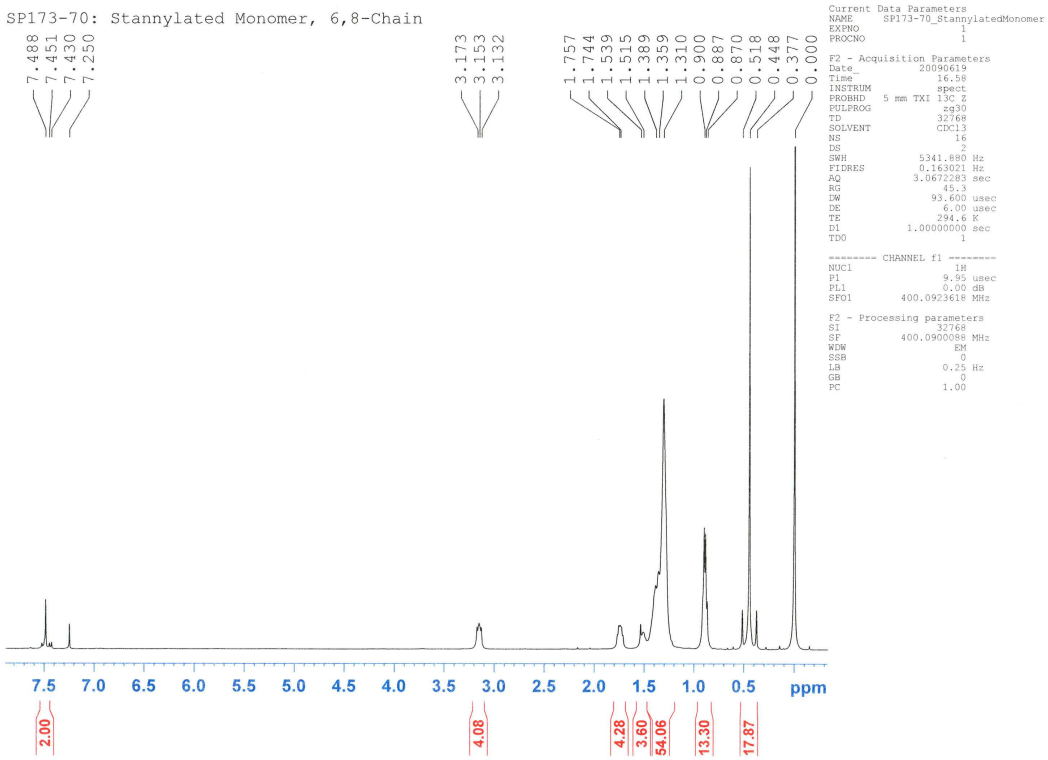

^{1}H NMR ($CDCl_3$, 400 MHz, δ): 7.45 (s, $J_{Sn\text{-}H}$ = 14.8 Hz, 2H), 3.15 (t, J = 8.4 Hz, 4H), 1.74 (m, 4H), 1.31 (m, 50H), 0.89 (m, 12H), 0.45 (s, $J_{Sn\text{-}H}$ = 28.4 Hz, 18H).

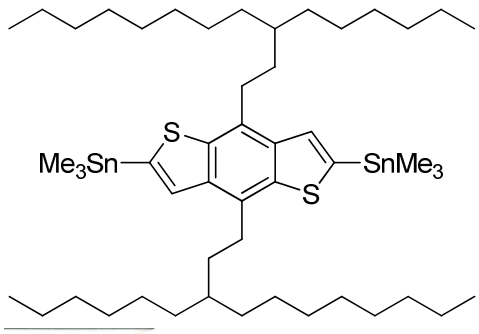

^{13}C NMR

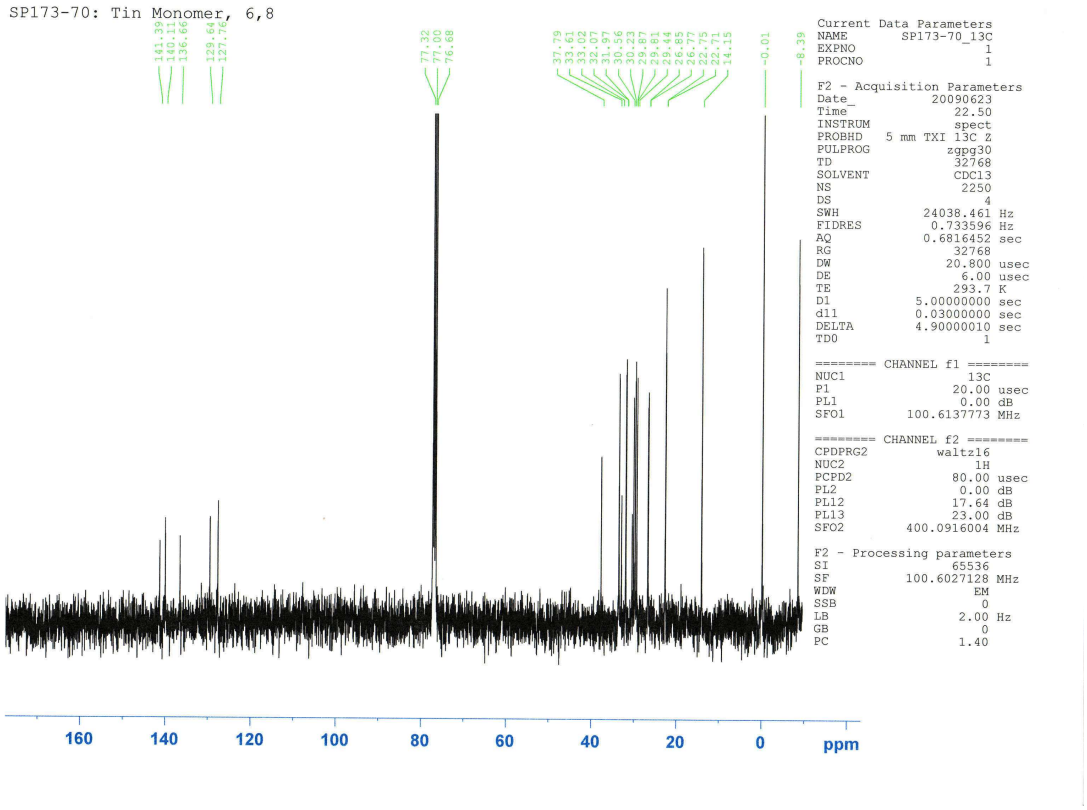

^{13}C NMR ($CDCl_3$, 100 MHz, δ): 141.39, 140.11, 136.66, 129.64, 127.76, 37.79, 33.61, 33.02, 32.07, 31.97, 30.56, 30.23, 29.87, 29.81, 29.44, 26.85, 26.77, 22.75, 22.71, 14.15, -8.39.

SCLC Measurement

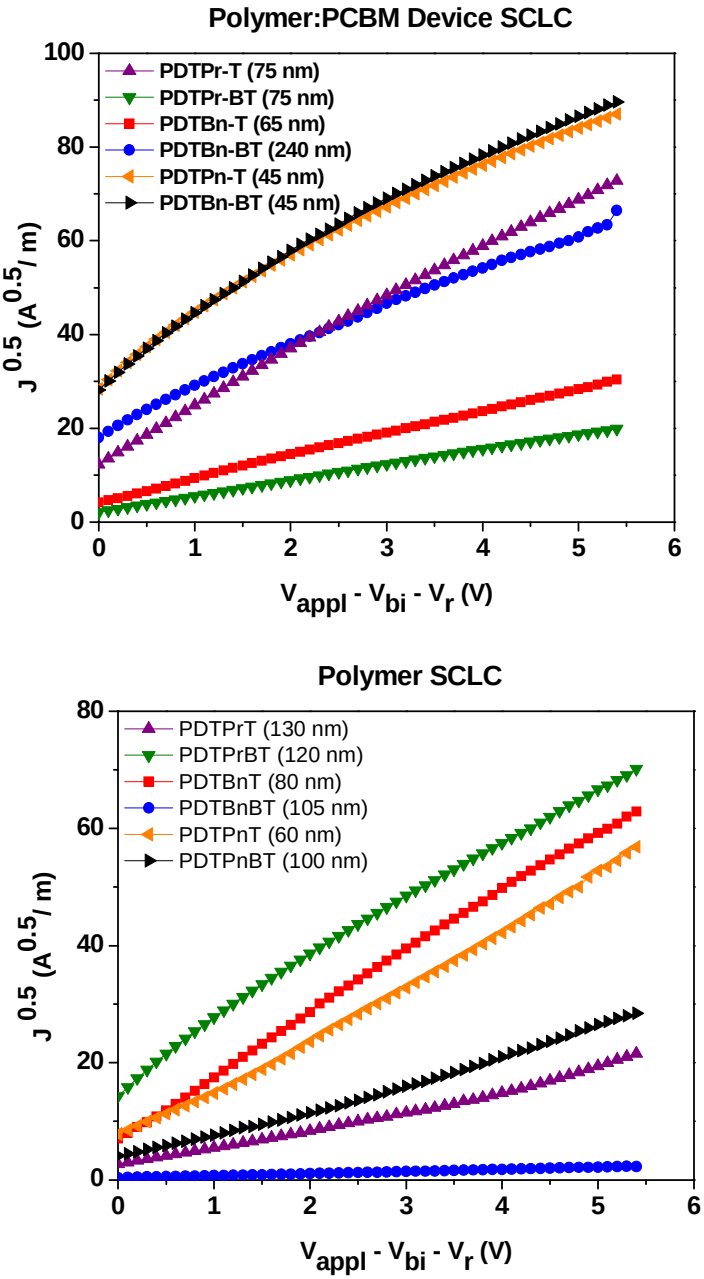

Figure A2.52. *Top:* $J^{0.5}$ vs V plots for the polymer films at room temperature from a hole-only BHJ device of ITO/PEDOT:PSS (45nm)/polymer:PCBM/Pd (40nm). *Bottom:* $J^{0.5}$ vs V plots for the polymer films at room temperature from a polymer-only device of ITO/PEDOT:PSS (45nm)/polymer /Al (100nm). In both Figures, the thickness of the films is indicated, and the solid lines are fits to the data points using $J = \frac{9}{8}\varepsilon_r \varepsilon_0 \mu_h \frac{V^2}{L^3}$.

Additional Optical Data for PDTBn-T

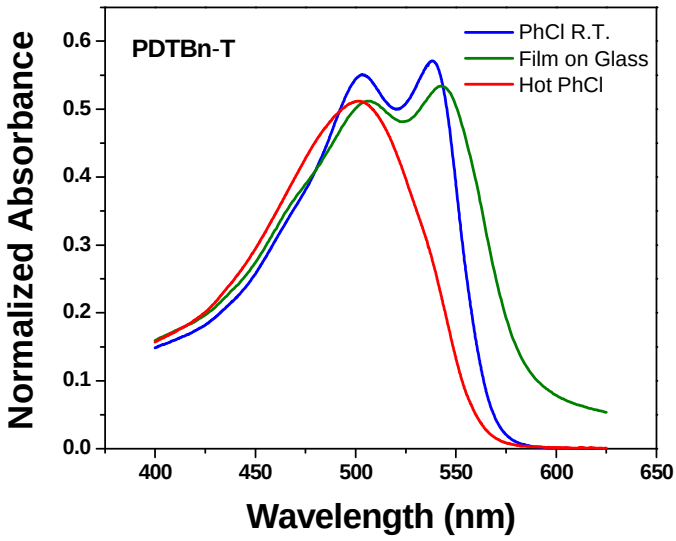

Figure A2.53. UV-Vis spectra of PDTBn-T in boiling chlorobenzene solution, the same solution at room temperature, and from a spun cast film on glass. The bathochromic shift from hot solvent to room temperature solvent and from cold solvent to solid film is typical for planar conjugated polymers. The second red shifted absorption peak is attributed to extension of the conjugation over two dimensions, and aggregation of the polymer backbones.

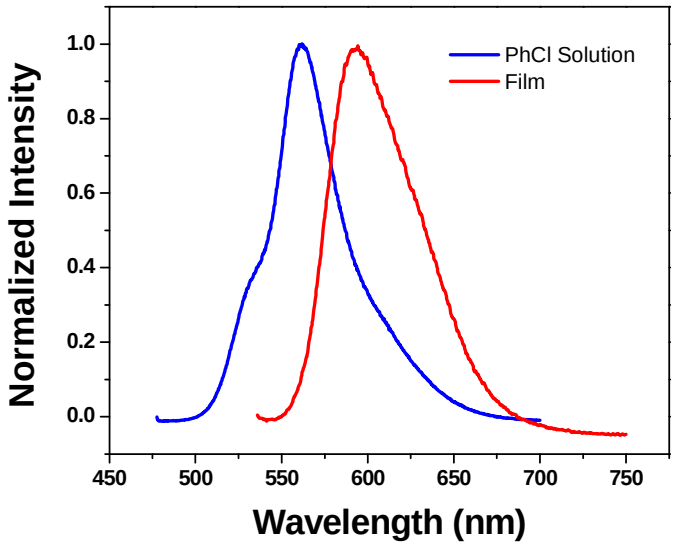

Figure A2.54. Fluorescence spectra for PDTBn-T. The solution spectra was excited at 475 nm, the film spectra was excited at 525 nm. The resulting red shift in the solid film is typical for conjugated polymers, due to increased inter-chain interaction.

XRD Measurement for PDTBn-T

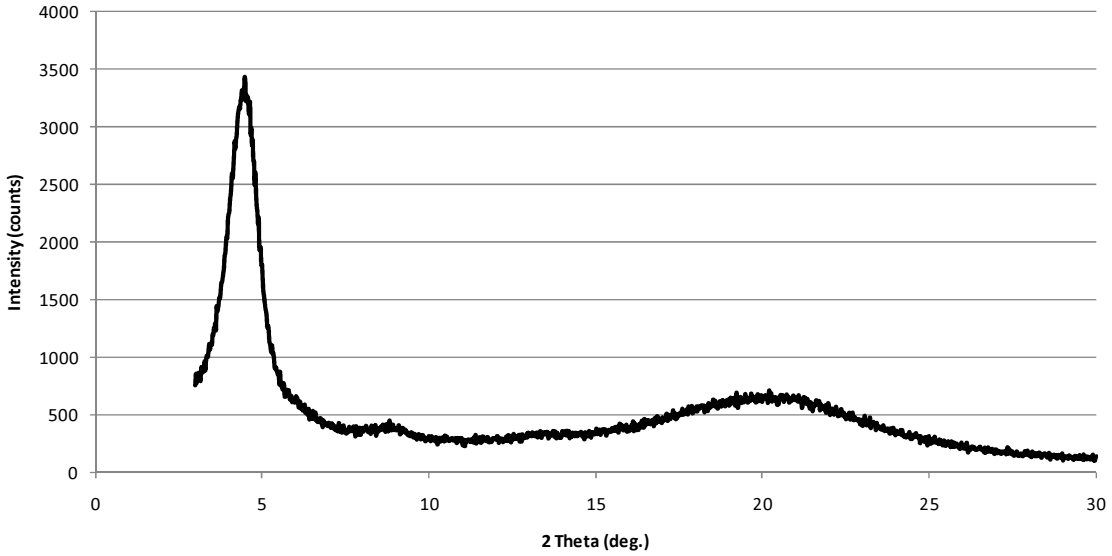

Figure A2.55. Powder X-Ray Diffraction of pure PDTBn-T. $2\theta \approx 4.55°$ corresponds to an inter-chain spacing of 19.4 Å or 1.94 nm (100 direction); $2\theta \approx 19.45°$ corresponds to an face to face stacking distance of 4.55 Å or 0.46 nm (010 direction).

Appendix 3: Supporting Information for Chapter 3

NMR Spectra

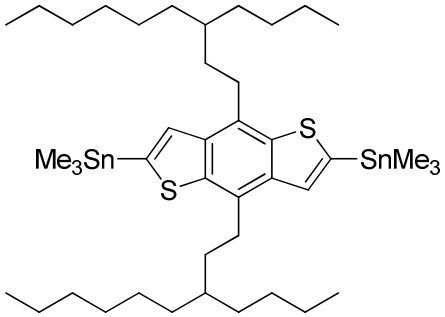

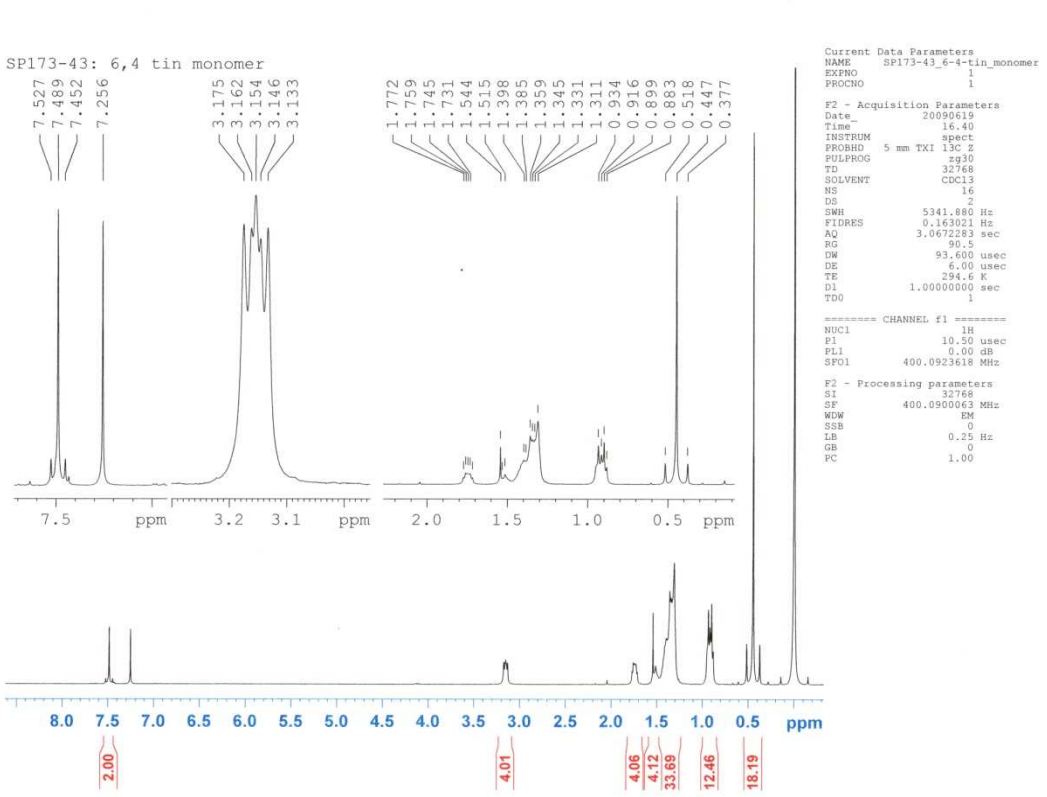

^{1}H NMR ($CDCl_3$, 400 MHz, δ): 7.49 (s, 2H), 3.15 (m, 4H), 1.75 (m, 4H), 1.52 (m, 2H), 1.35 (m, 32H), 0.92 (m, 12H), 0.45 (s, 18H).

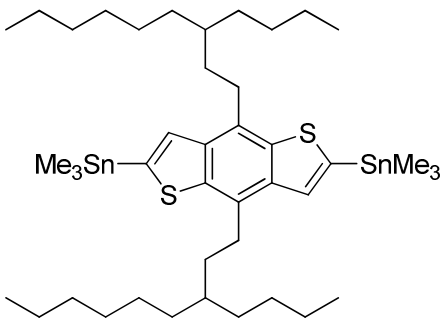

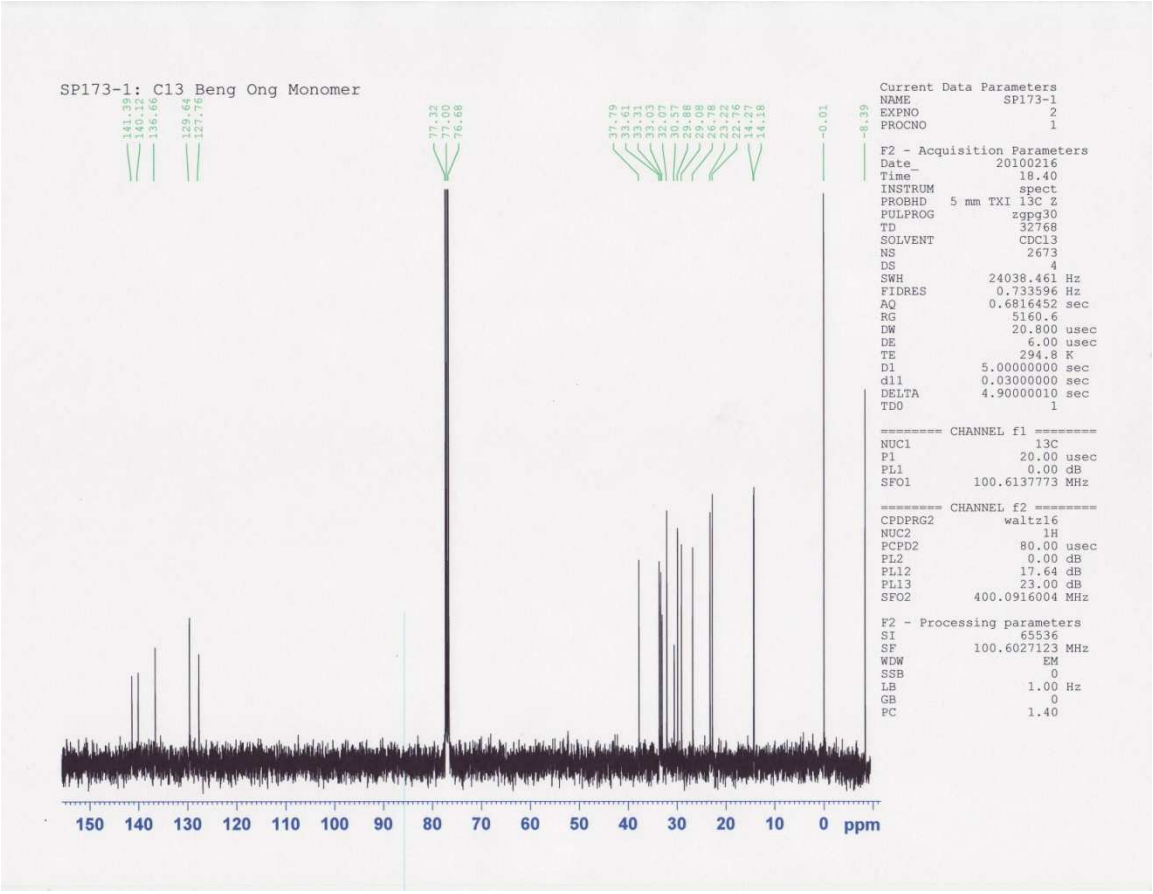

^{13}C NMR ($CDCl_3$, 100 MHz, δ): 141.39, 140.12, 136.66, 129.64, 127.76, 37.79, 33.61, 33.31, 33.03, 32.07, 30.57, 29.88, 29.08, 26.78, 23.22, 22.76, 14.27, 14.18, -8.39

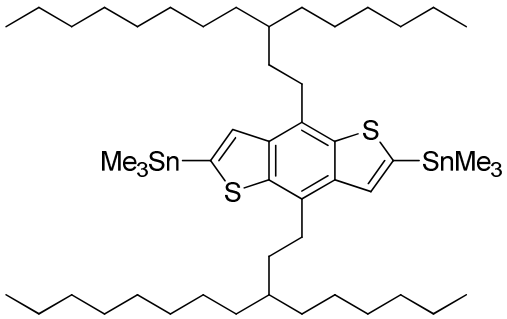

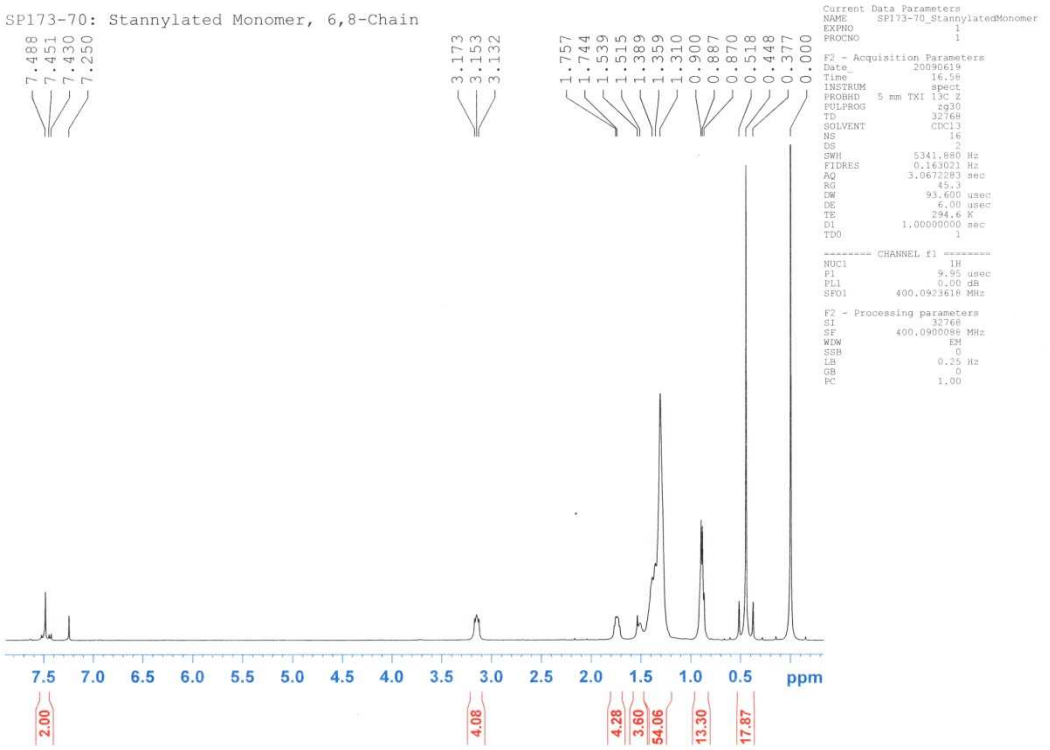

^{1}H NMR ($CDCl_3$, 400 MHz, δ): 7.45 (s, 2H), 3.15 (m, 4H), 1.74 (m, 4H), 1.52 (m, 2H), 1.35 (m, 48H), 0.92 (m, 12H), 0.45 (s, 18H).

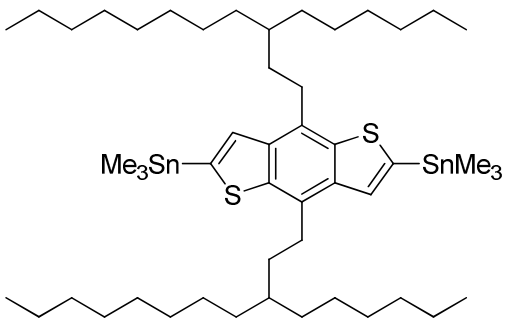

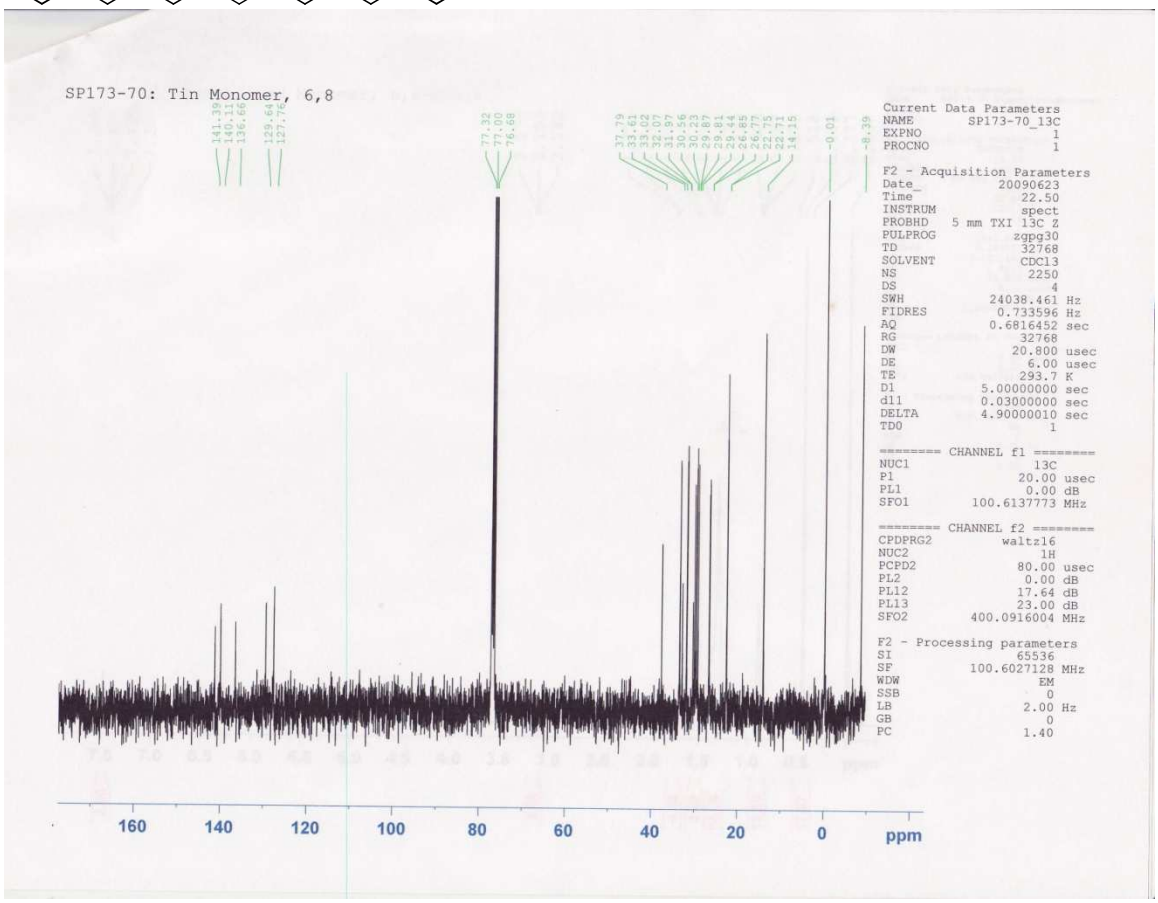

^{13}C NMR ($CDCl_3$, 100 MHz, δ): 141.39, 140.11, 136.66, 129.64, 127.76, 37.79, 33.61, 33.02, 32.07, 31.97, 30.56, 30.23, 29.87, 29.81, 29.44, 26.85, 26.77, 22.75, 22.71, 14.15, -8.39.

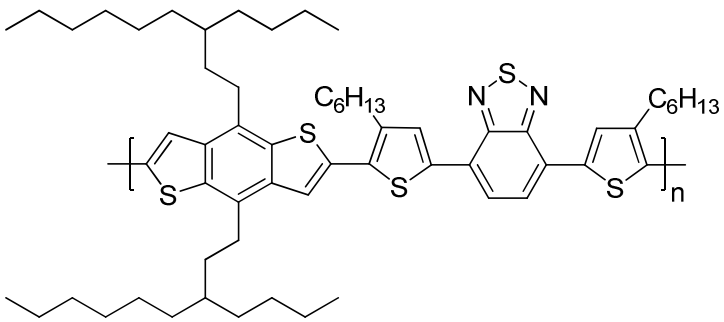

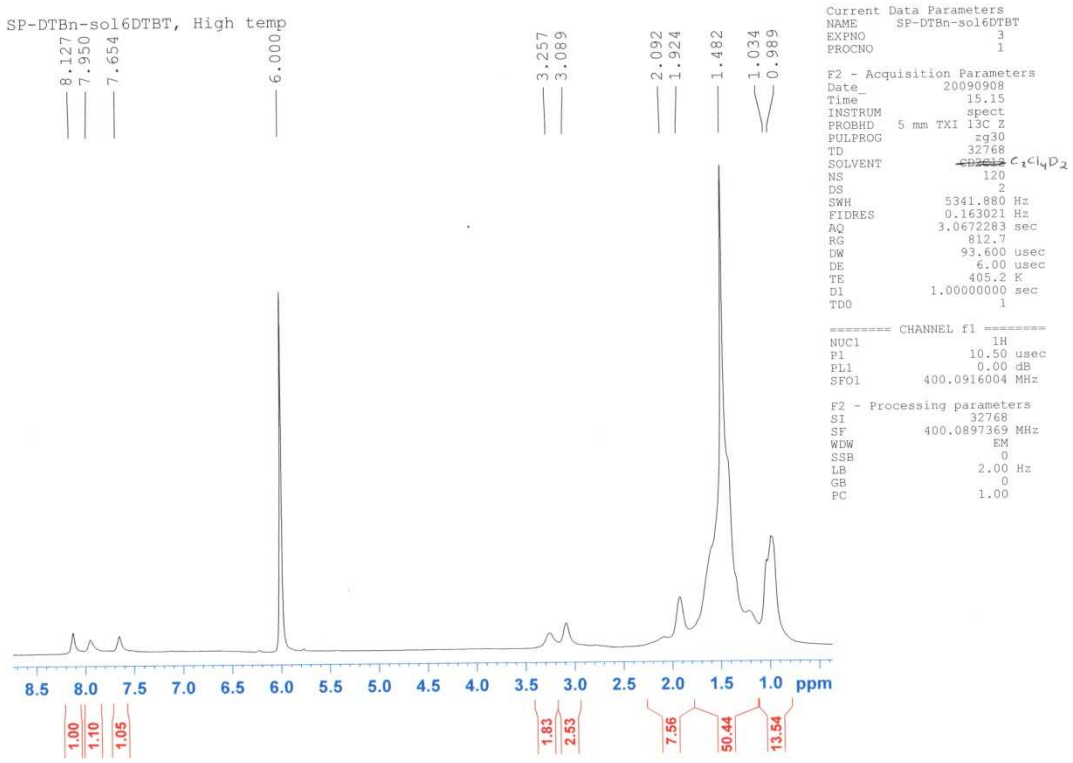

^{1}H NMR ($C_2D_2Cl_4$, 400 MHz, δ): 8.13 (s, 2H), 7.95 (s, 2H), 7.65 (s, 2H), 3.26 (s, 4H), 3.09 (br s, 4H), 1.92 (br s, 8H), 1.48 (m, 52H), 0.99 (m, 12H).

SCLC Measurement

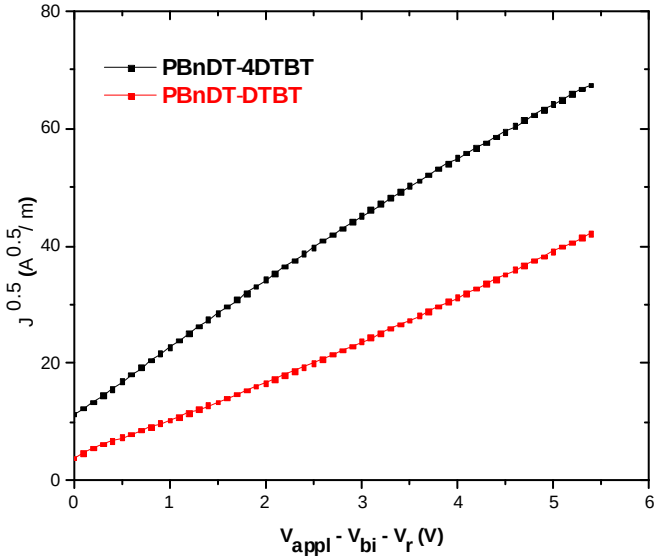

Figure A3.56. $J^{0.5}$ vs V plots for the polymer films at room temperature from a hole-only BHJ device of ITO/PEDOT:PSS (45nm)/polymer:PCBM/Pd (40nm). Thickness: ~ 100 nm. The solid lines are fits to the data points using $J = \frac{9}{8}\varepsilon_r \varepsilon_0 \mu_h \frac{V^2}{L^3}$.

Appendix 4: Supporting Information for Chapter 4

NMR Spectra

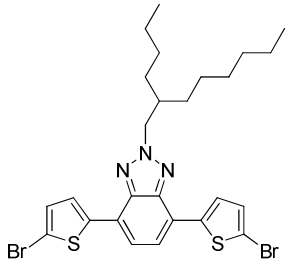

(HTAZ)

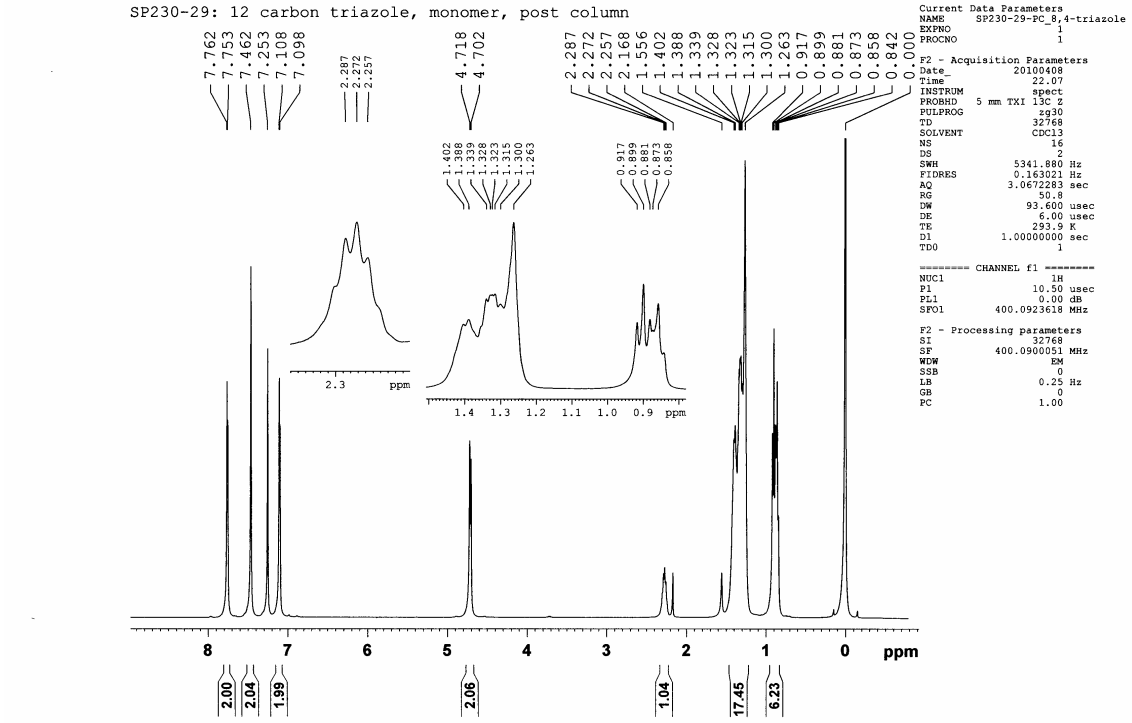

^{1}H NMR ($CDCl_3$, 400 MHz, δ): 7.76 (d, $^{3}J_{HH}$ = 3.6 Hz, 2H), 7.46 (s, 2H), 7.10 (d, $^{3}J_{HH}$ = 4 Hz, 2H), 4.71 (d, $^{3}J_{HH}$ = 6.4 Hz, 2H), 2.27 (m, 1H), 1.26 (m, 16H), 0.90 (t, $^{3}J_{HH}$ = 7.2 Hz, 3H), 0.86 (t, $^{3}J_{HH}$ = 6 Hz, 3H).

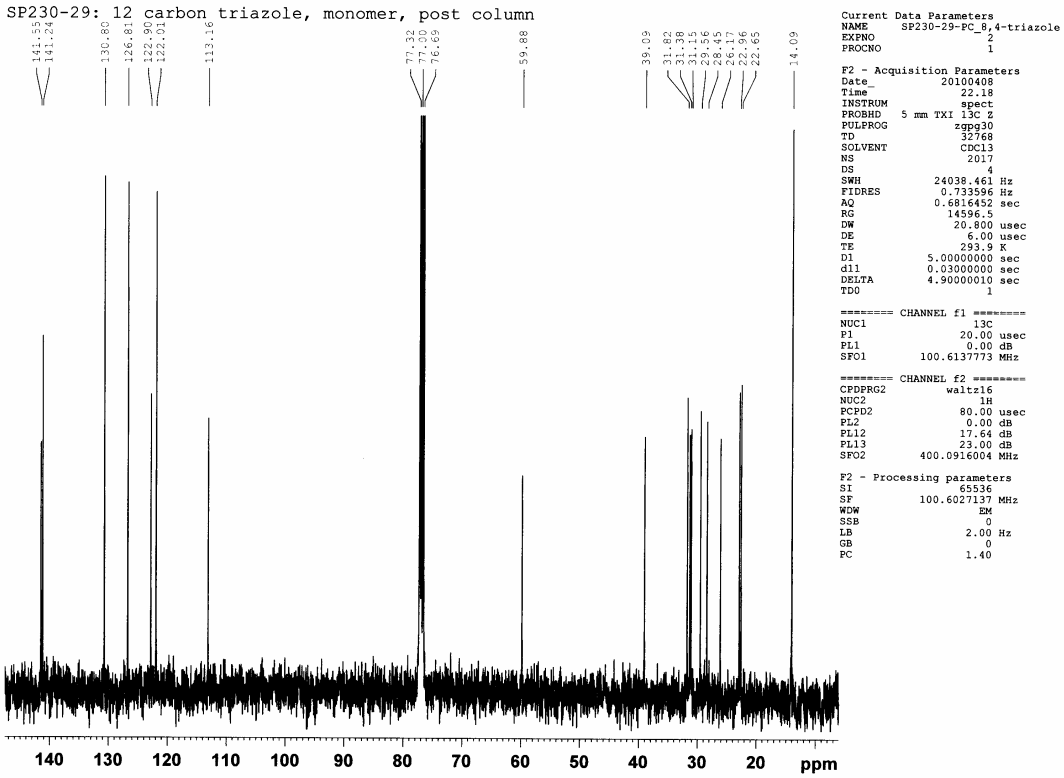

^{13}C NMR ($CDCl_3$, 100 MHz, δ): 141.55, 141.24, 130.80, 126.81, 122.90, 122.01, 113.16, 59.88, 39.09, 31.82, 31.38, 31.15, 29.56, 28.45, 26.17, 22.96, 22.65, 14.09.

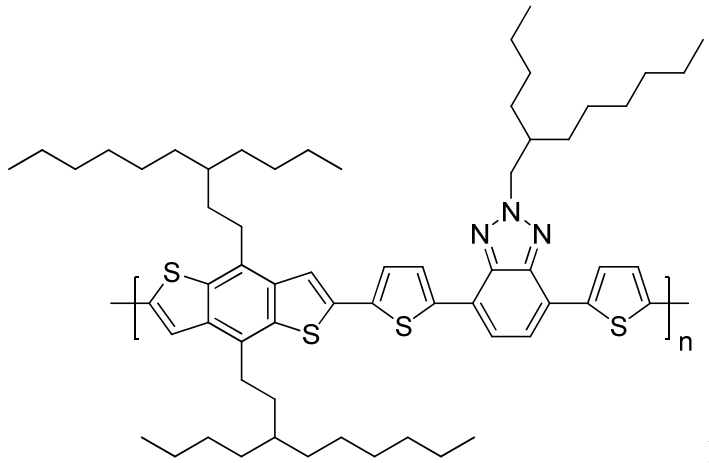

PBnDT-HTAZ

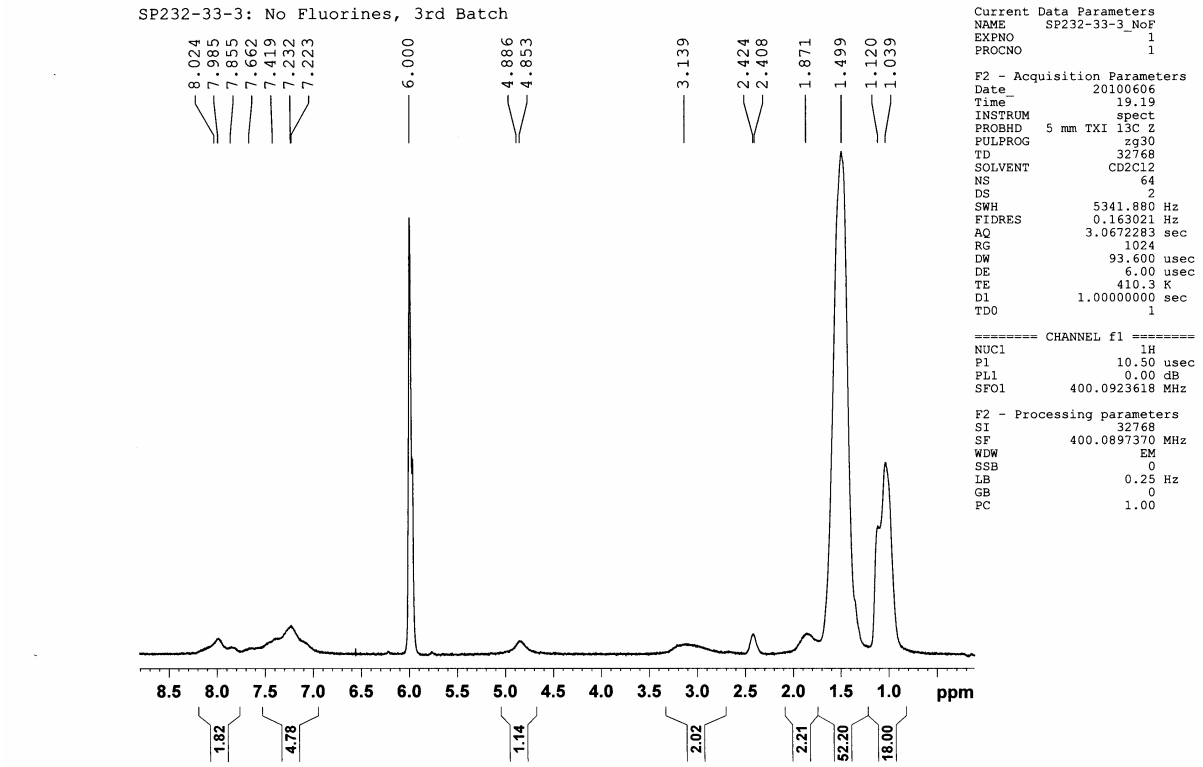

^{1}H NMR @ 400K ($C_2D_2Cl_4$, 400 MHz, δ): 7.86, 7.23, 4.87, 3.14, 2.41, 1.87, 1.50, 1.08.

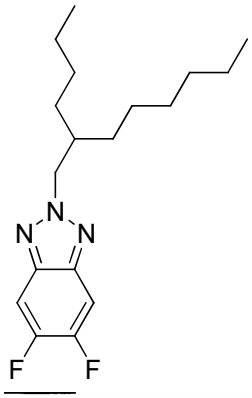

Compound 2

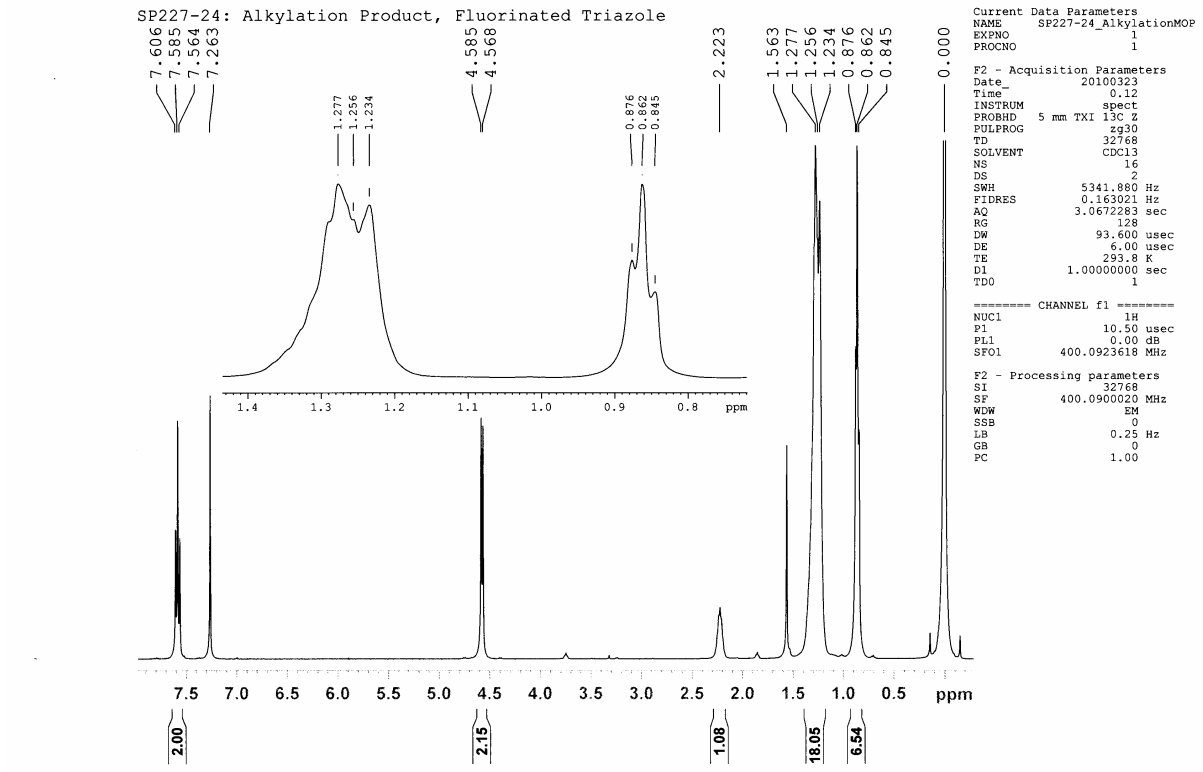

^{1}H NMR ($CDCl_3$, 400 MHz, δ): 7.59 (t, $^{3}J_{HF}$ = 8.4 Hz, 2H), 4.58 (d, $^{3}J_{HH}$ = 6.8 Hz, 2H), 2.22 (m, 1H), 1.28 (m, 16H), 0.86 (t, $^{3}J_{HH}$ = 5.6 Hz, 6H).

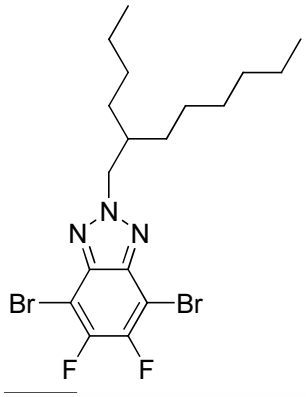

Compound 3

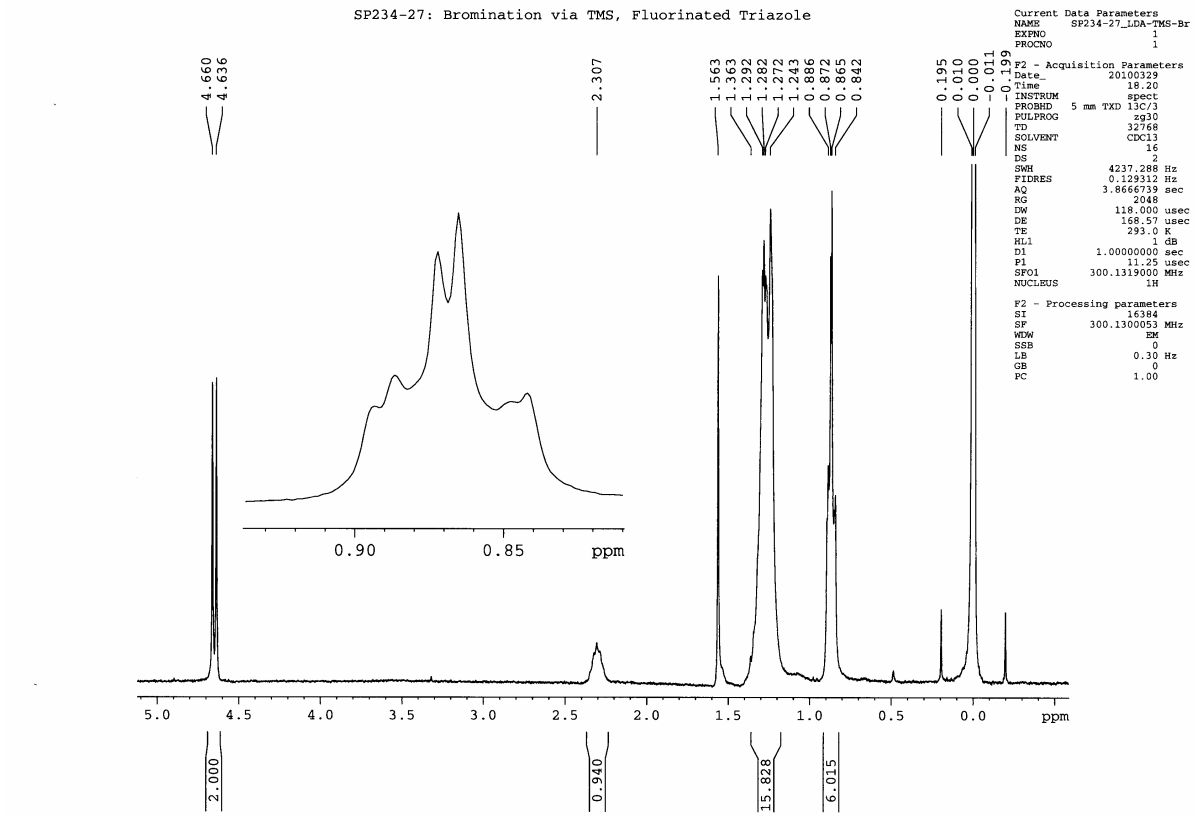

^{1}H NMR ($CDCl_3$, 300 MHz, δ): 4.65 (d, $^{3}J_{HH}$ = 7.2 Hz, 2H), 2.31 (m, 1H), 1.24 (m, 16H), 0.87 (m, 6H).

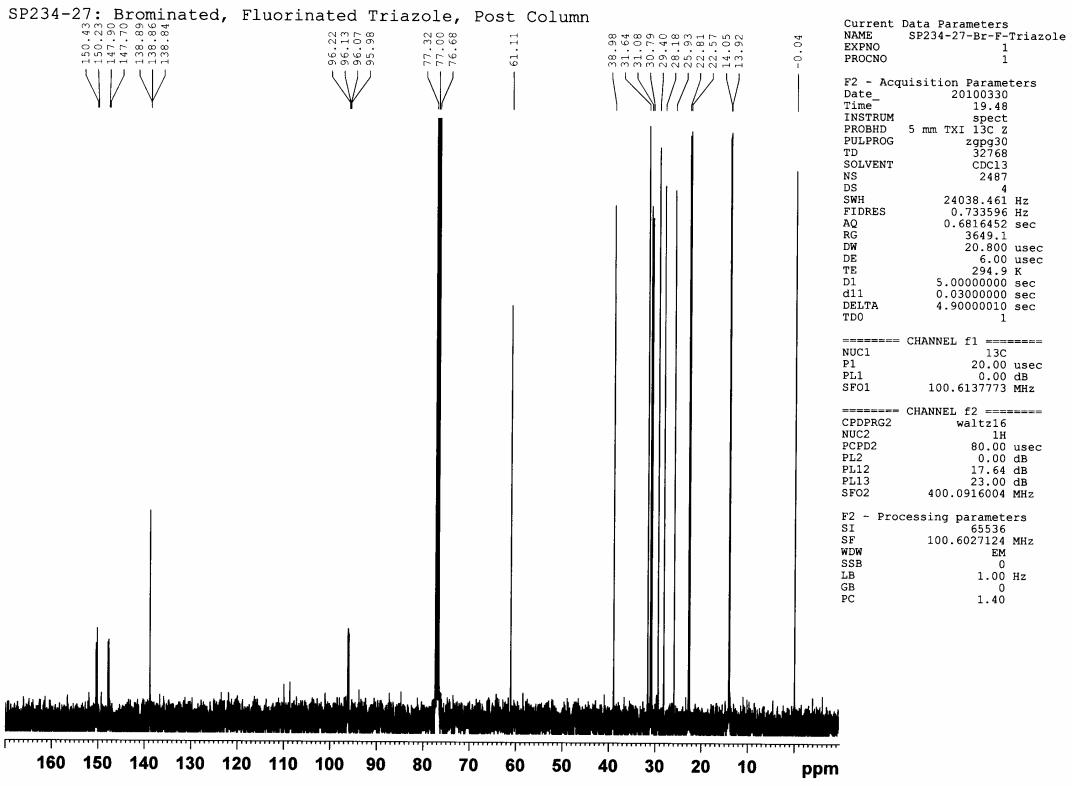

^{13}C NMR ($CDCl_3$, 100 MHz, δ): 149.07 (dd, $^{1}J_{CF}$ = 253 Hz, $^{2}J_{CF}$ = 20 Hz), 138.86 (t, $^{3,4}J_{CF}$ = 2.5 Hz), 96.10 (dd, $^{2}J_{CF}$ = 15 Hz, $^{3}J_{CF}$ = 9 Hz), 61.11, 38.98, 31.64, 31.08, 30.79, 29.40, 28.18, 25.93, 22.81, 22.57, 14.05, 13.92.

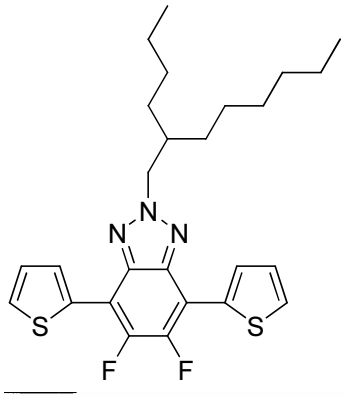

Compound 4

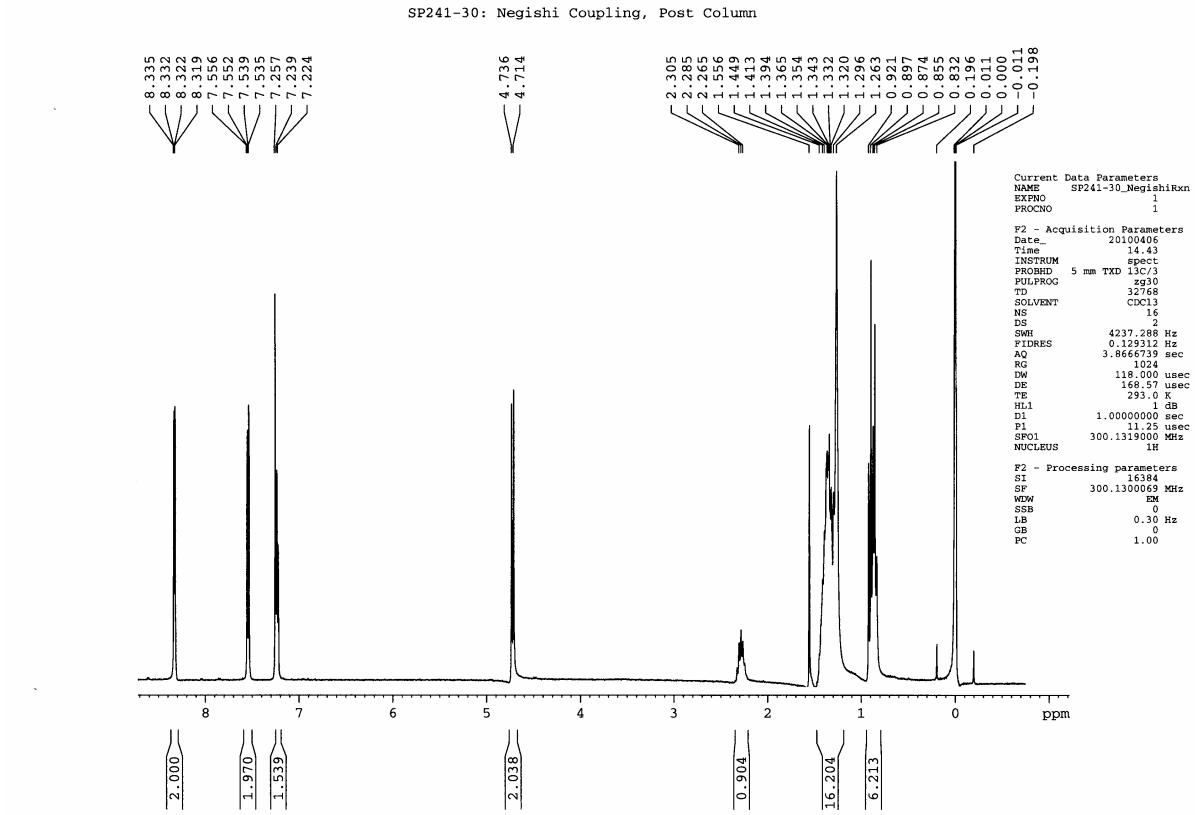

^{1}H NMR ($CDCl_3$, 300 MHz, δ): 8.33 (dd, $^{3}J_{HH}$ = 3.9 Hz, $^{4}J_{HH}$ = 0.9 Hz, 2H), 7.55 (dd, $^{3}J_{HH}$ = 5.1 Hz, $^{4}J_{HH}$ = 1.2 Hz, 2H), 7.24 (m, 2H), 4.73 (d, $^{3}J_{HH}$ = 6.6 Hz, 2H), 2.86 (m, 1H), 1.26 (m, 16H), 0.89 (m, 6H).

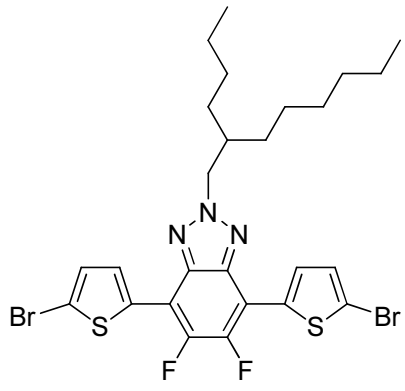

FTAZ

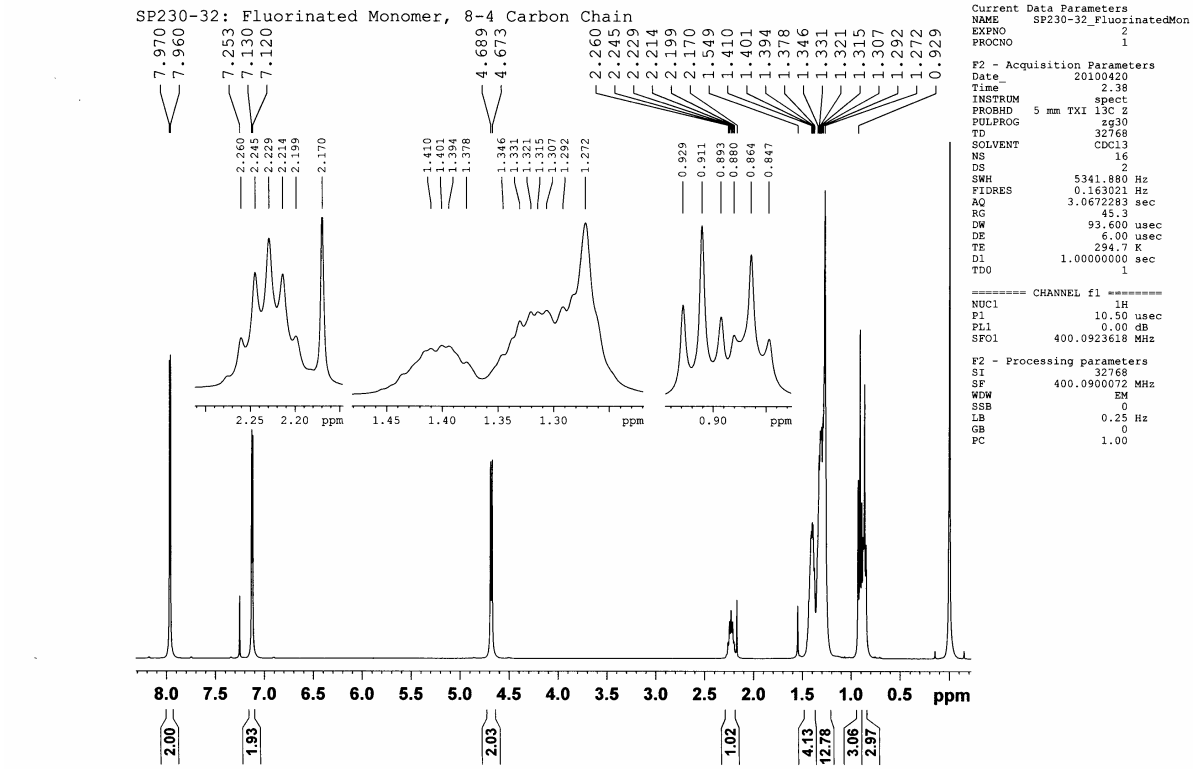

^{1}H NMR ($CDCl_3$, 400 MHz, δ): 7.97 (d, $^{3}J_{HH}$ = 4 Hz, 2H), 7.13 (d, $^{3}J_{HH}$ =4 Hz, 2H), 4.68 (d, $^{3}J_{HH}$ = 6.4 Hz, 2H), 2.23 (m, 1H), 1.40 (m, 4H), 1.27 (m, 12H), 0.91 (t, $^{3}J_{HH}$ = 7.2 Hz, 3H), 0.86 (t, $^{3}J_{HH}$ = 6.8 Hz, 3H).

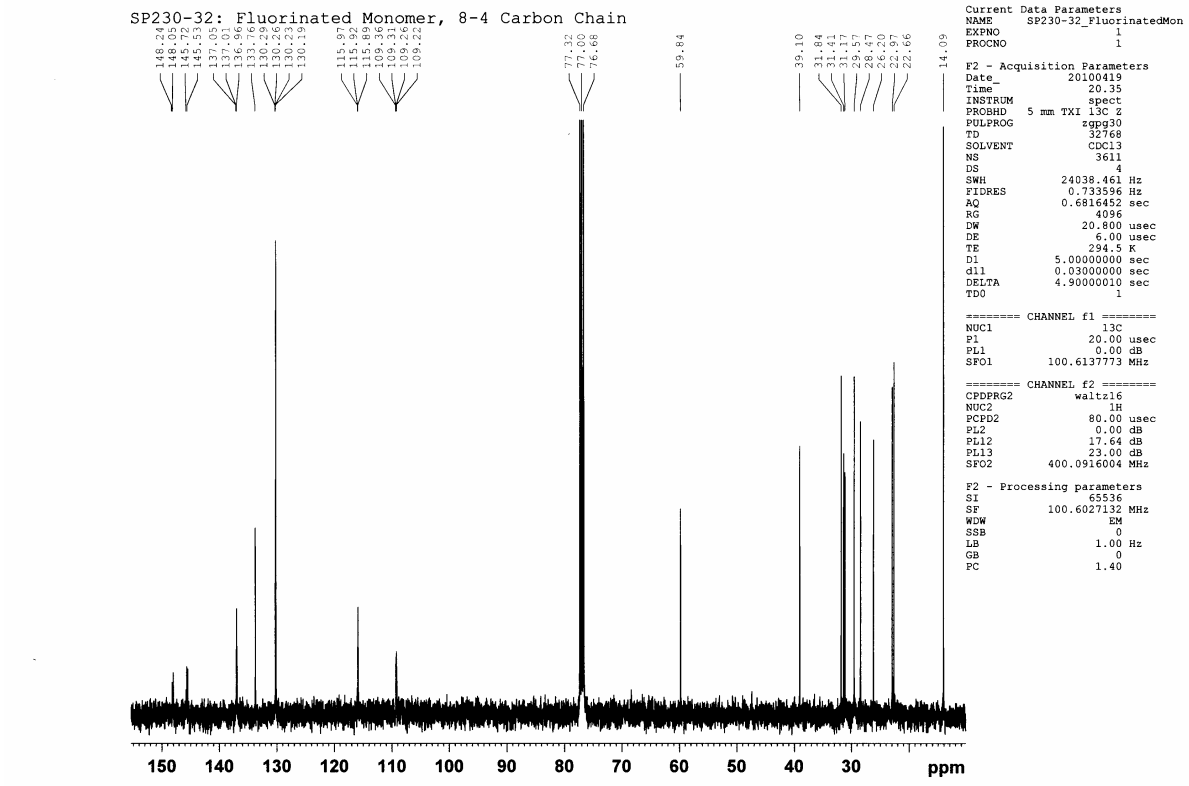

^{13}C NMR ($CDCl_3$, 100 MHz, δ): 146.89 (dd, $^{1}J_{CF}$ = 252 Hz, $^{2}J_{CF}$ = 19 Hz), 137.01 (t, $^{3,4}J_{CF}$ = 4.2 Hz), 133.76, 130.26 (m), 130.19, 115.92 (m), 109.29 (dd, $^{3}J_{CF}$ = 9.5 Hz, $^{4}J_{CF}$ = 4.4 Hz), 59.84, 39.10, 31.84, 31.41, 31.17, 29.57, 28.47, 26.20, 22.97, 22.66, 14.09.

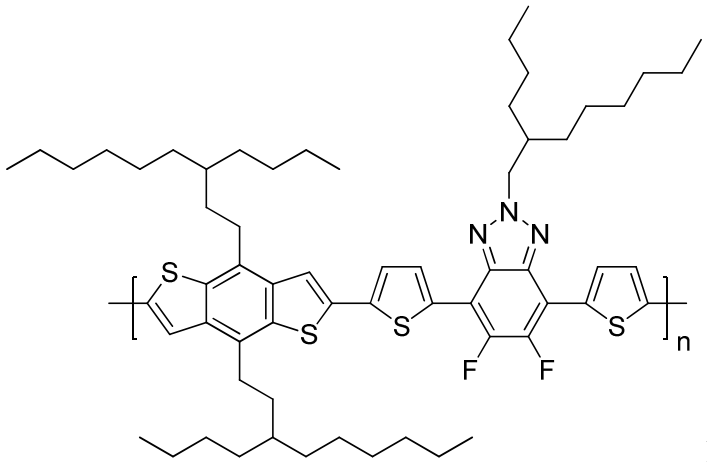

PBnDT-FTAZ

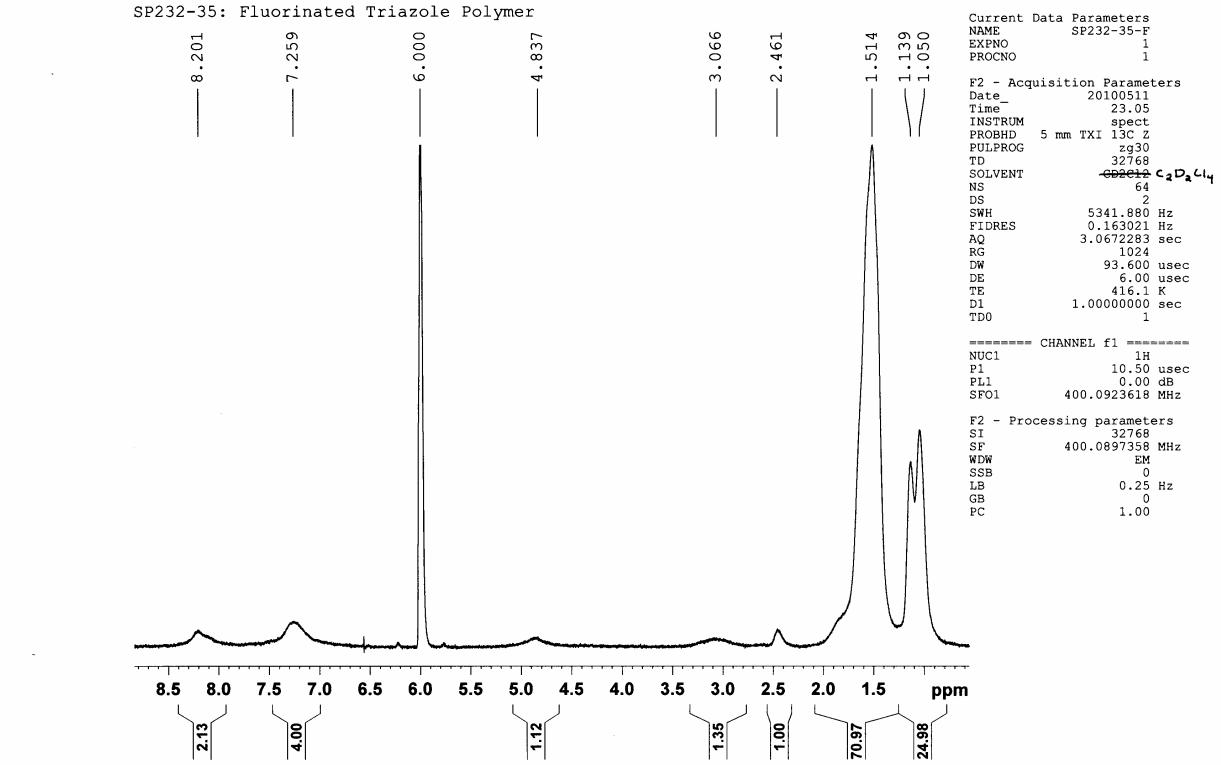

^{1}H NMR @ 400K ($C_2D_2Cl_4$, 400 MHz, δ): 8.20, 7.26, 4.84, 3.07, 2.46, 1.51, 1.14, 1.05.

Polymer Solutions

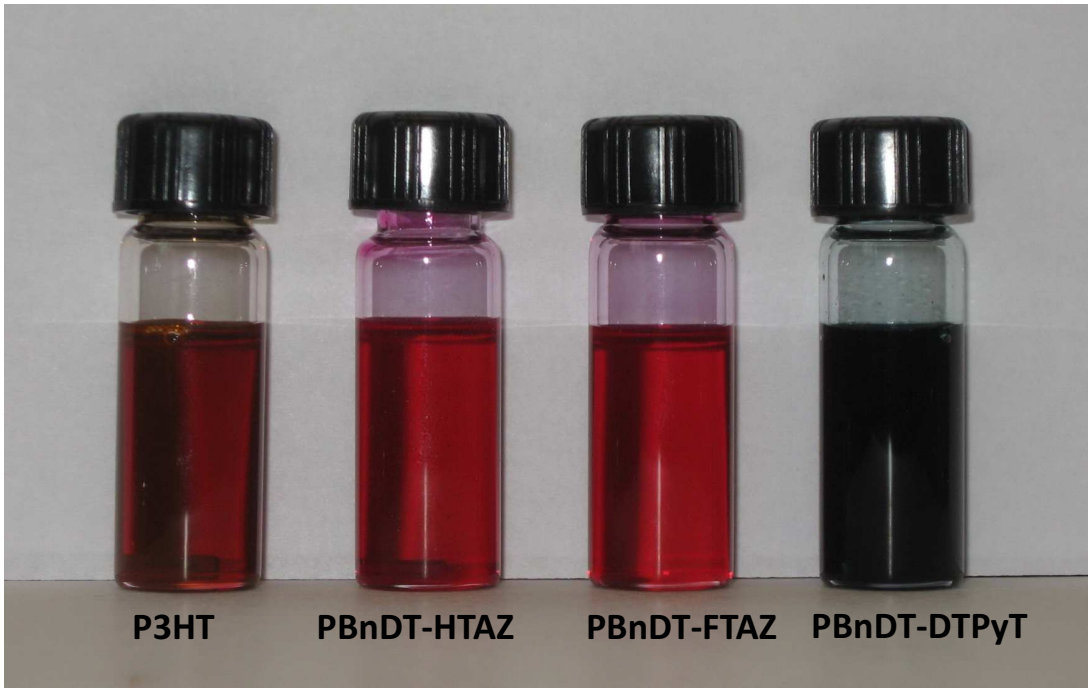

Figure A4.57. Polymer solutions, 0.75 mg/mL in dichlorobenzene. P3HT and low band gap copolymer PBnDT-DTPyT included as a reference.

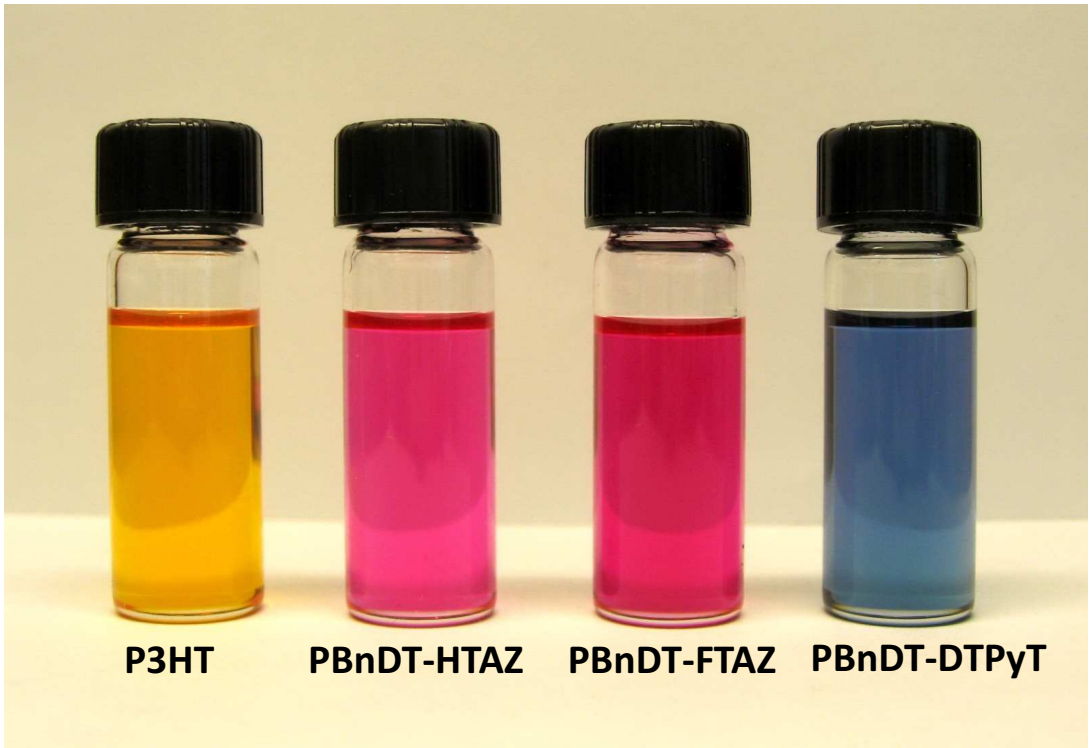

Figure A4.58. Polymer solutions, 0.025 mg/mL in dichlorobenzene. P3HT and low band gap copolymer PBnDT-DTPyT included as a reference.

CV – LUMO & SCLC Measurement

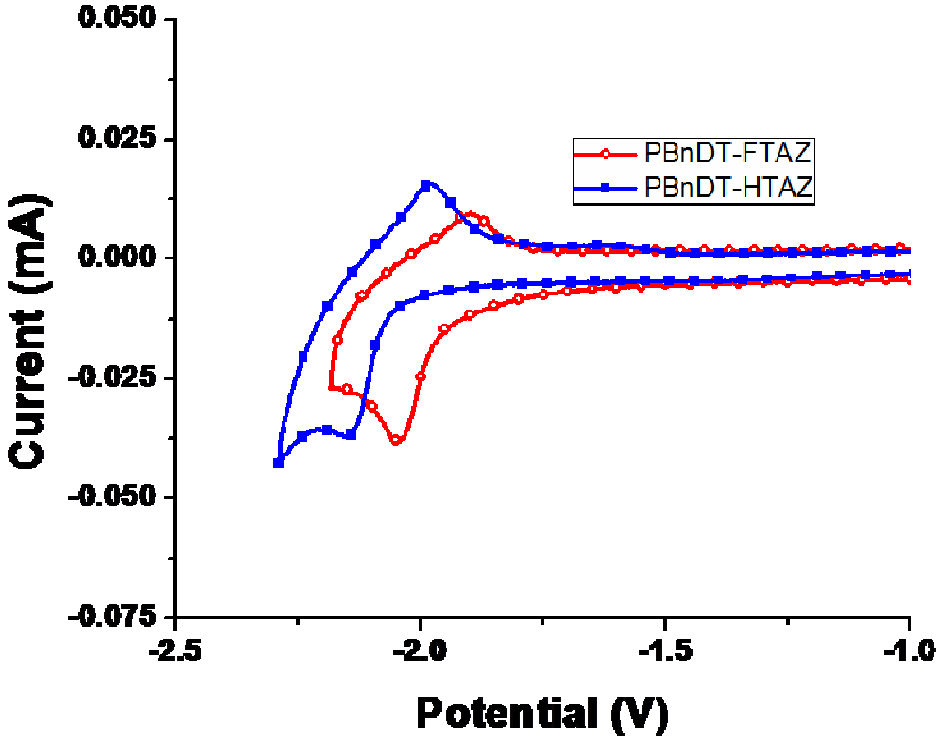

Figure A4.59. Cyclic voltammetry curves for the reduction of the two polymers. LUMOs for PBnDT-FTAZ and PBnDT-HTAZ are -3.05 eV, and -2.87 eV respectively.

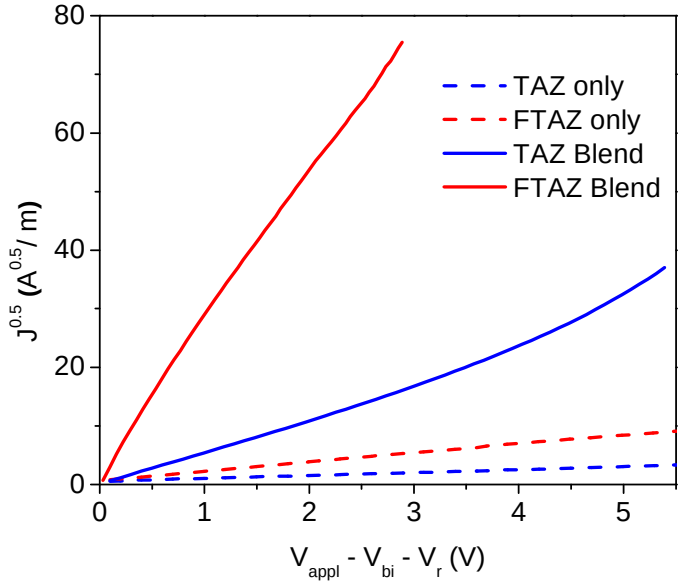

Figure A4.60. SCLC hole mobility measurements for each polymer, and 1:2 polymer:$PC_{61}BM$ blend.

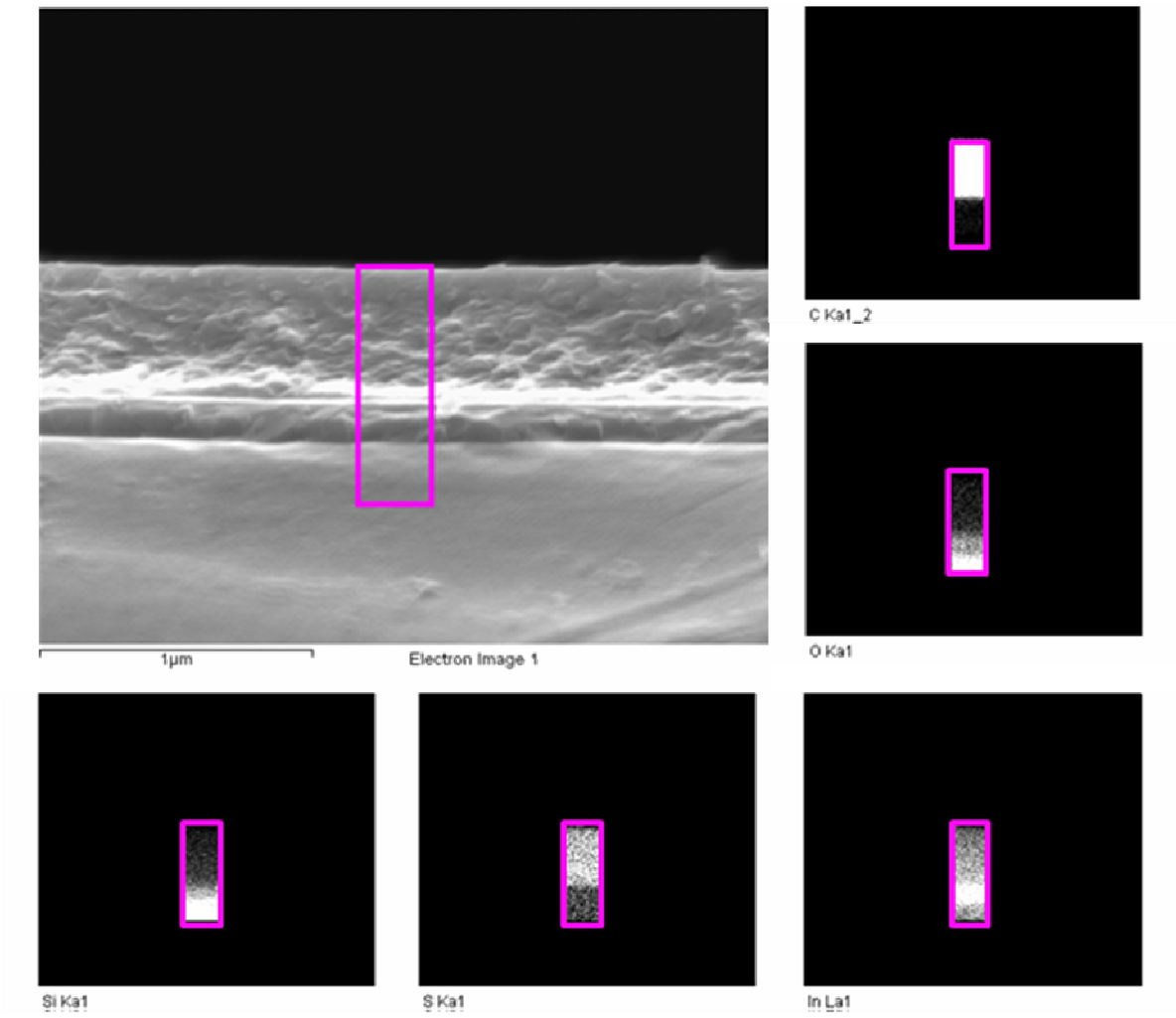

Figure A4.61. Energy dispersive spectroscopy confirms the elemental composition of the photovoltaic cell. No metal anode was evaporated on top. The small images, clockwise from the top are carbon, oxygen, indium, sulfur, and silicon. White color represents a high concentration of the atom. Indium measurement has a low signal to noise ratio, however, the highest concentration of indium is observed in the ITO layer.

Device Film Thickness Measurements (via SEM)

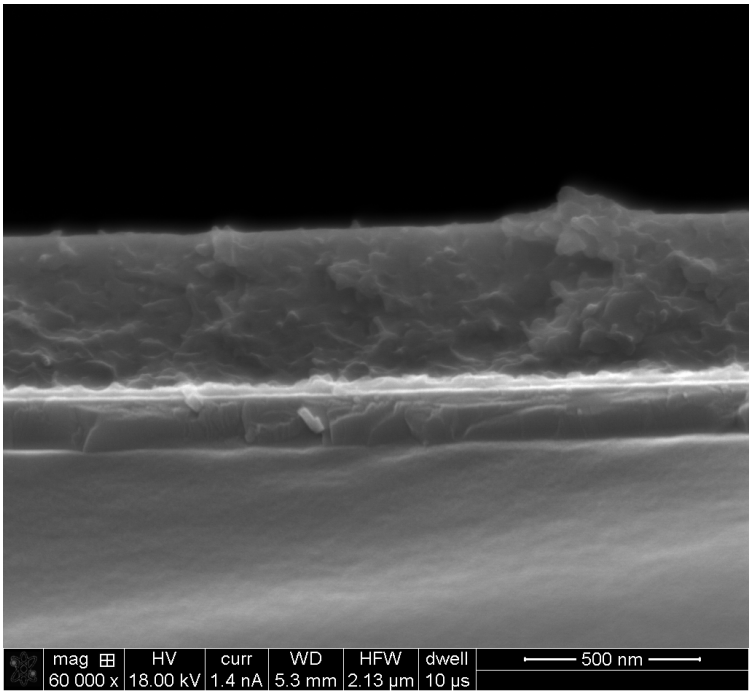

Figure A4.62. 400 nm PBnDT-FTAZ:$PC_{61}BM$ 1:2. In order from top to bottom, active layer, PEDOT:PSS, ITO, glass. ITO layer used as thickness reference (150nm).

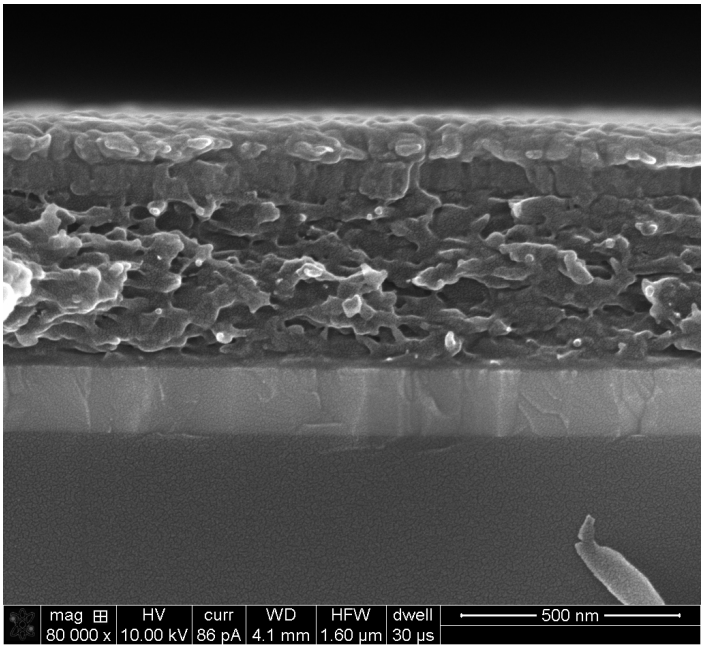

Figure A4.63. 310 nm PBnDT-FTAZ:$PC_{61}BM$ 1:2. In order from top to bottom, Aluminum/Calcium, active layer, PEDOT:PSS, ITO, glass. ITO layer used as thickness reference (150nm).

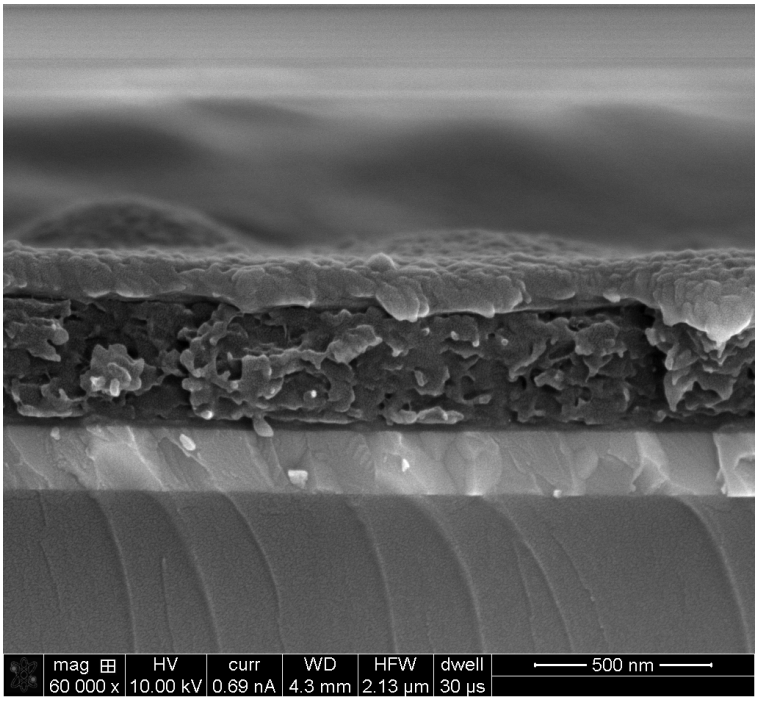

Figure A4.64. 250 nm PBnDT-FTAZ:$PC_{61}BM$ 1:2. In order from top to bottom, Aluminum/Calcium, active layer, PEDOT:PSS, ITO, glass. ITO layer used as thickness reference (150nm).

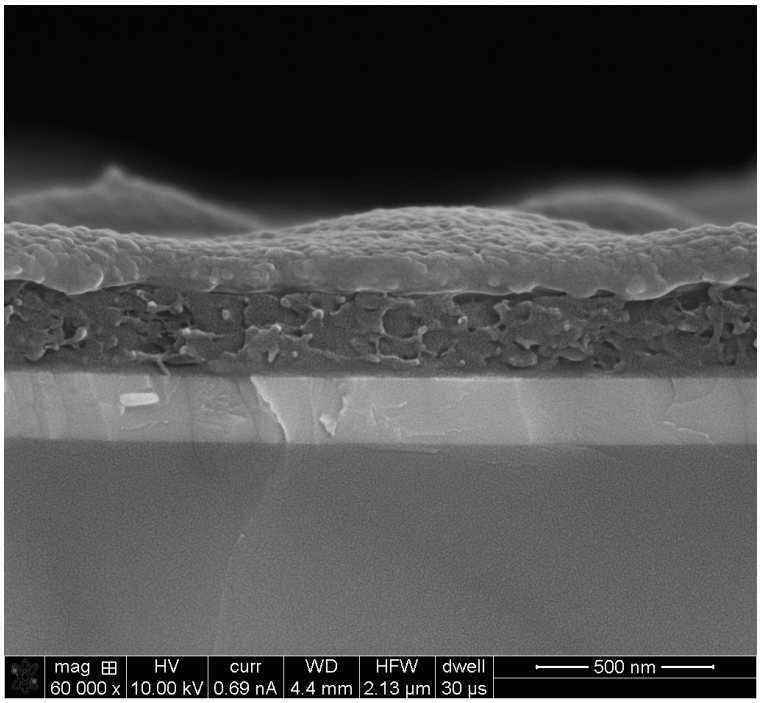

Figure A4.65. 160 nm PBnDT-FTAZ:$PC_{61}BM$ 1:2. In order from top to bottom, Aluminum/Calcium, active layer, PEDOT:PSS, ITO, glass. ITO layer used as thickness reference (150nm).

Appendix 5: Supporting Information for Chapter 5

NMR Spectra

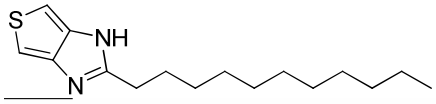

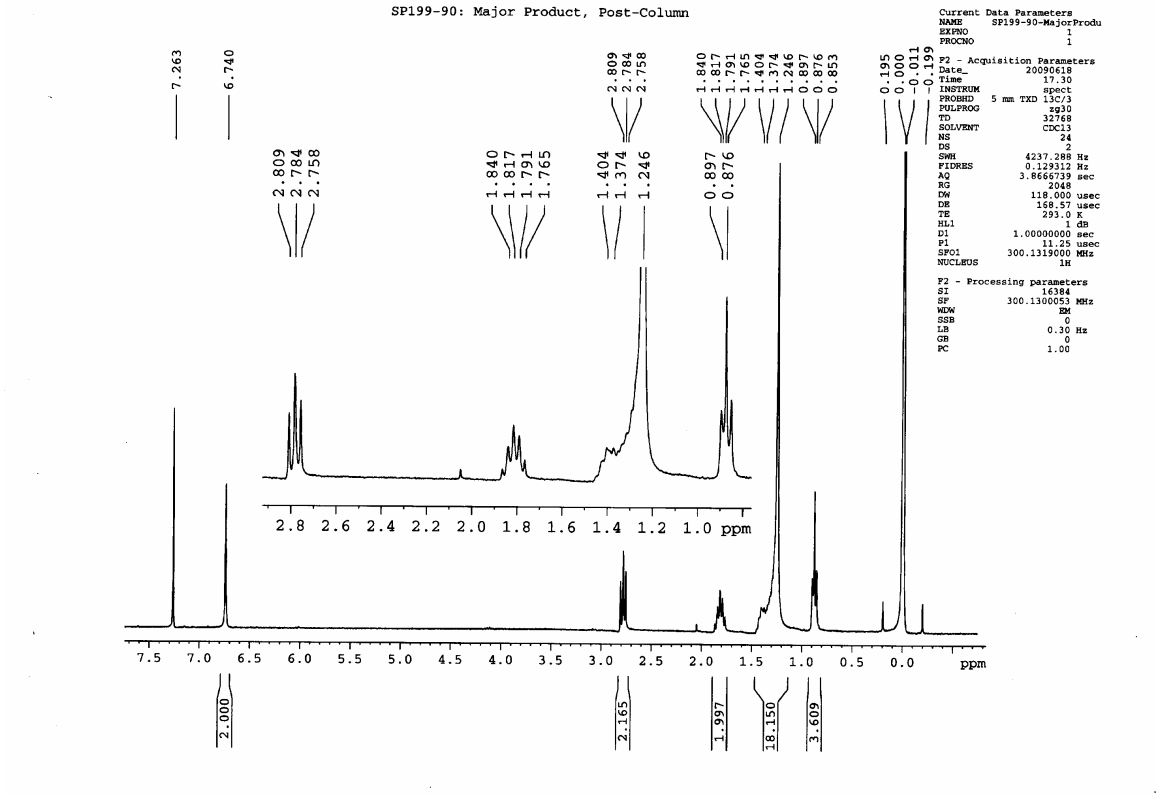

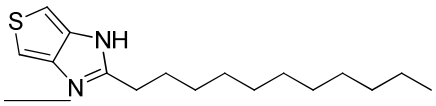
S
NH
N

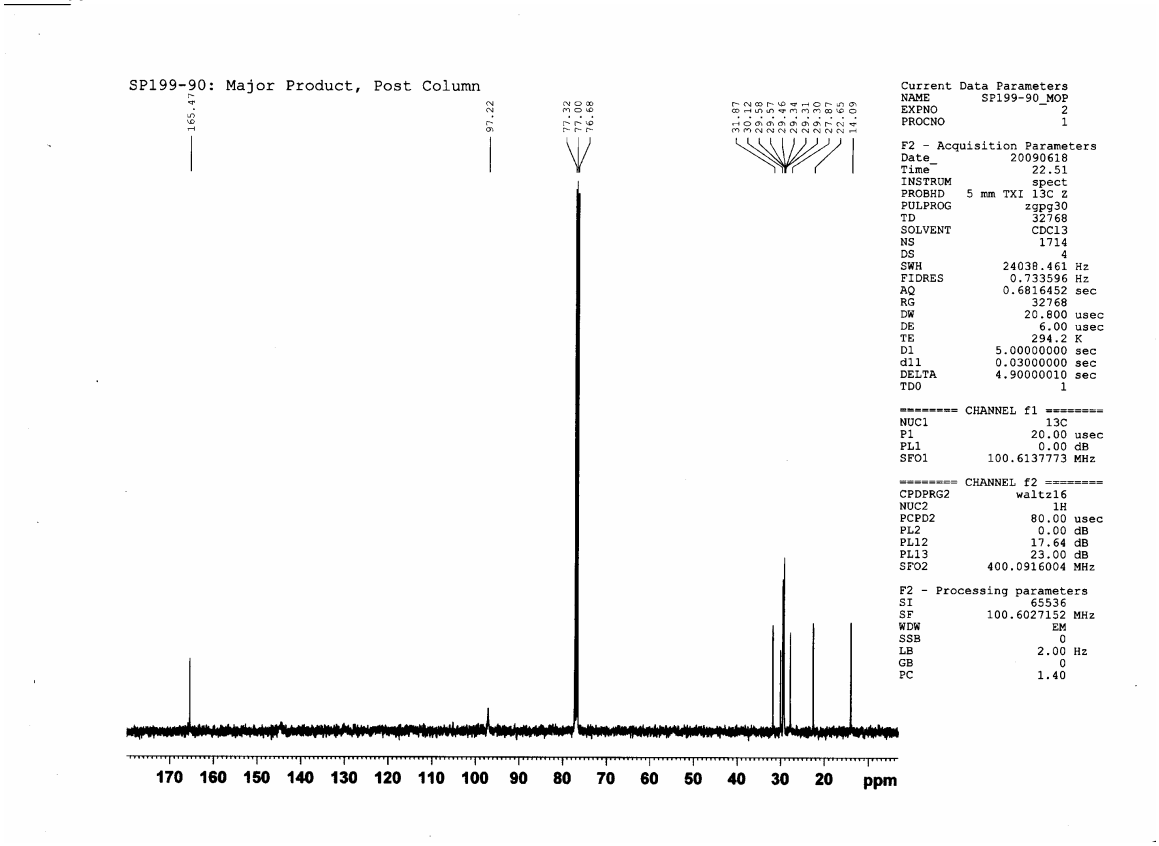
SP199-90: Major Product, Post Column
165.47
97.22
77.32
77.00
76.68
31.87
30.12
29.58
29.57
29.46
29.34
29.31
29.30
22.87
22.65
14.09
170 160 150 140 130 120 110 100 90 80 70 60 50 40 30 20 ppm
Current Data Parameters
NAME SP199-90_MOP
EXPNO 2
PROCNO 1
F2 - Acquisition Parameters
Date_ 20090618
Time 22.51
INSTRUM spect
PROBHD 5 mm TXI 13C Z
PULPROG zgpg30
TD 32768
SOLVENT CDCl3
NS 1714
DS 4
SWH 24038.461 Hz
FIDRES 0.733596 Hz
AQ 0.6816452 sec
RG 32768
DW 20.800 usec
DE 6.00 usec
TE 294.2 K
D1 5.00000000 sec
d11 0.03000000 sec
DELTA 4.90000010 sec
TD0 1
======== CHANNEL f1 ========
NUC1 13C
P1 20.00 usec
PL1 0.00 dB
SFO1 100.6137773 MHz
======== CHANNEL f2 ========
CPDPRG2 waltz16
NUC2 1H
PCPD2 80.00 usec
PL2 0.00 dB
PL12 17.64 dB
PL13 23.00 dB
SFO2 400.0916004 MHz
F2 - Processing parameters
SI 65536
SF 100.6027152 MHz
WDW EM
SSB 0
LB 2.00 Hz
GB 0
PC 1.40

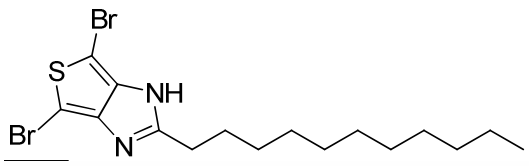
Br
S
NH
Br
N

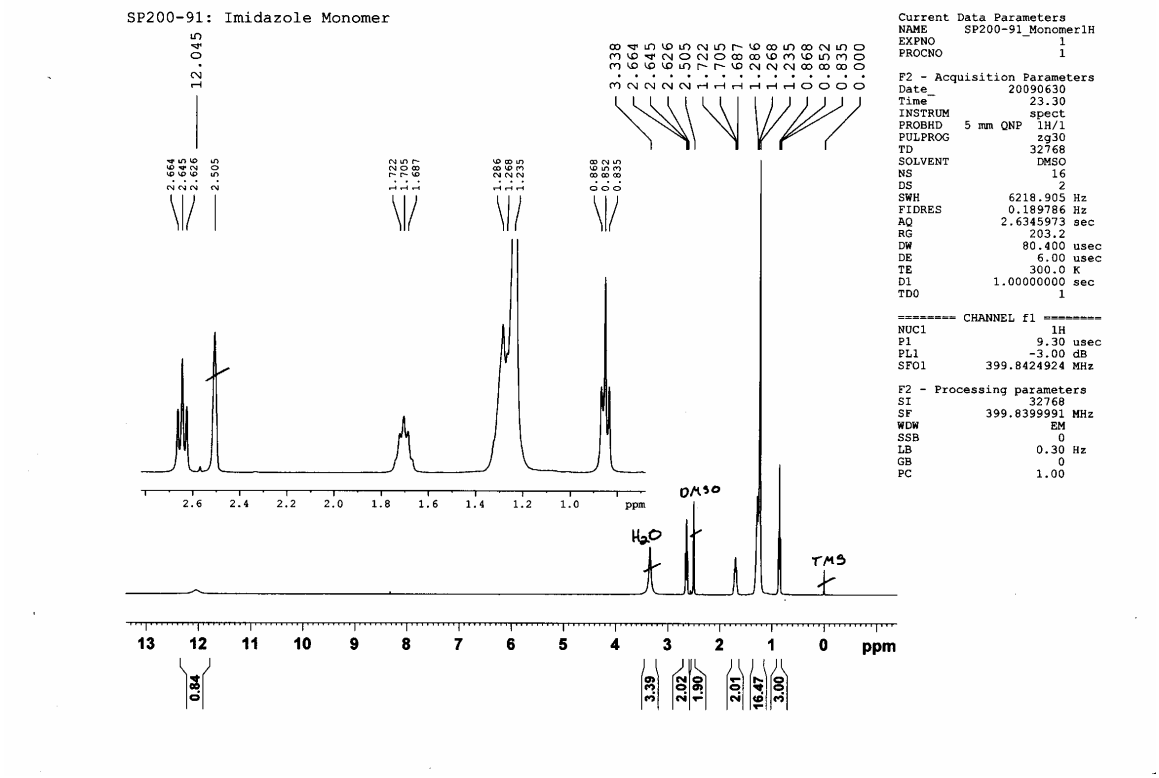
SP200-91: Imidazole Monomer
12.045
2.664
2.645
2.626
2.505
1.722
1.705
1.687
1.286
1.268
1.235
0.868
0.852
0.835
3.338
2.664
2.645
2.626
2.505
1.722
1.705
1.687
1.286
1.268
1.235
0.868
0.852
0.835
0.000
H2O
DMSO
TMS
ppm
0.84
3.39
2.02
1.90
2.01
16.47
3.00
Current Data Parameters
NAME SP200-91_Monomer1H
EXPNO 1
PROCNO 1
F2 - Acquisition Parameters
Date_ 20090630
Time 23.30
INSTRUM spect
PROBHD 5 mm QNP 1H/1
PULPROG zg30
TD 32768
SOLVENT DMSO
NS 16
DS 2
SWH 6218.905 Hz
FIDRES 0.189786 Hz
AQ 2.6345973 sec
RG 203.2
DW 80.400 usec
DE 6.00 usec
TE 300.0 K
D1 1.00000000 sec
TD0 1
======== CHANNEL f1 ========
NUC1 1H
P1 9.30 usec
PL1 -3.00 dB
SFO1 399.8424924 MHz
F2 - Processing parameters
SI 32768
SF 399.8399991 MHz
WDW EM
SSB 0
LB 0.30 Hz
GB 0
PC 1.00

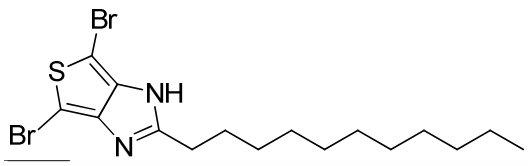
Br
S
NH
Br
N

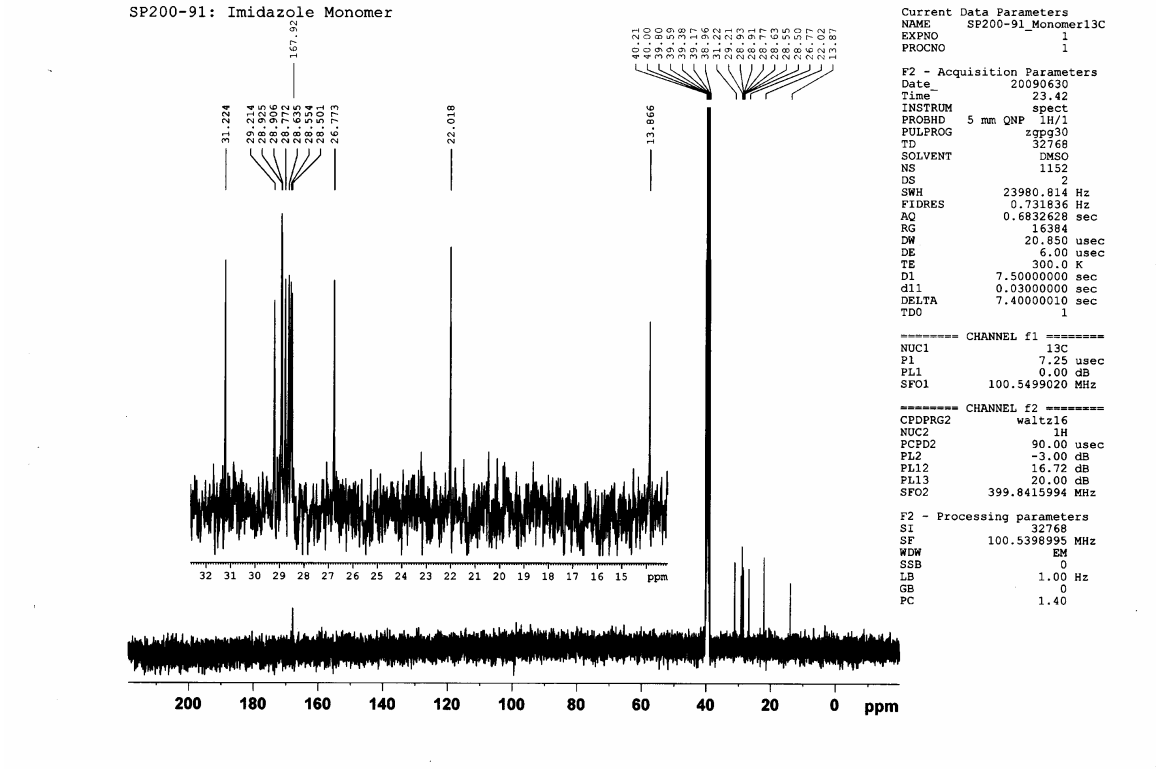
SP200-91: Imidazole Monomer
167.92
40.21
40.00
39.80
39.59
39.38
39.17
38.96
31.22
31.01
26.93
28.91
28.77
28.63
28.55
28.50
26.77
22.02
13.87
31.224
29.214
28.925
28.906
28.772
28.635
28.554
28.501
26.773
22.018
13.866
32 31 30 29 28 27 26 25 24 23 22 21 20 19 18 17 16 15 ppm
200 180 160 140 120 100 80 60 40 20 0 ppm
Current Data Parameters
NAME SP200-91_Monomer13C
EXPNO 1
PROCNO 1
F2 - Acquisition Parameters
Date_ 20090630
Time 23.42
INSTRUM spect
PROBHD 5 mm QNP 1H/1
PULPROG zgpg30
TD 32768
SOLVENT DMSO
NS 1152
DS 2
SWH 23980.814 Hz
FIDRES 0.731836 Hz
AQ 0.6832628 sec
RG 16384
DW 20.850 usec
DE 6.00 usec
TE 300.0 K
D1 7.50000000 sec
d11 0.03000000 sec
DELTA 7.40000010 sec
TD0 1
======== CHANNEL f1 ========
NUC1 13C
P1 7.25 usec
PL1 0.00 dB
SFO1 100.5499020 MHz
======== CHANNEL f2 ========
CPDPRG2 waltz16
NUC2 1H
PCPD2 90.00 usec
PL2 -3.00 dB
PL12 16.72 dB
PL13 20.00 dB
SFO2 399.8415994 MHz
F2 - Processing parameters
SI 32768
SF 100.5398995 MHz
WDW EM
SSB 0
LB 1.00 Hz
GB 0
PC 1.40

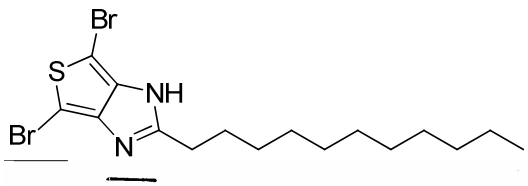

Display Report

Analysis Info

Analysis Name	D:\XMASS\Sample_07072009\121-200-91	Acquisition Date	7/7/2009 5:29:19 PM
Method	Linear	Operator	BioTOF
Sample Name		Instrument	BioTOF- NT
Comment	1-200-91; Price/You in 1mL MeOH/ACT; dil 1:10 in MeOH +ESI/BioToF w. i.s.		

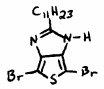

Acquisition Parameter

Capilary End Plate	n/a	Capilary Exit	n/a	detbias	n/a
EndP	n/a	Collision energy	n/a	Number of Averages	n/a

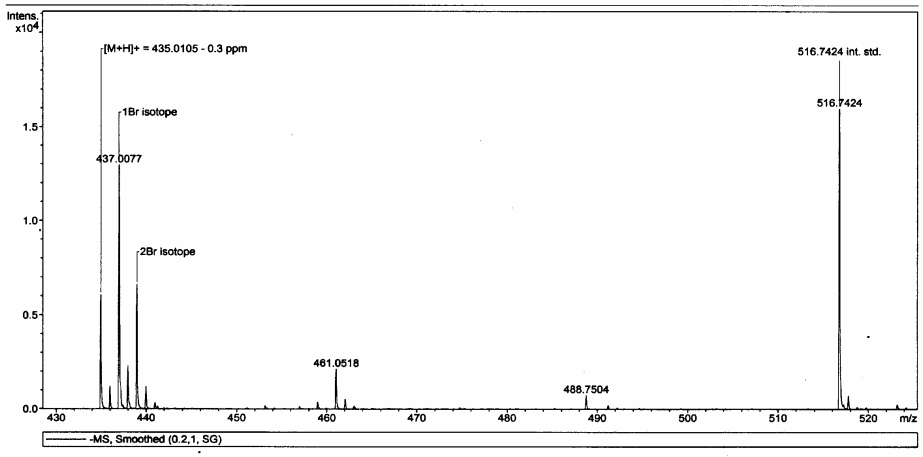

Bruker Daltonics DataAnalysis 3.2 printed: 07/07/2009 05:37:18 PM Page 1 of 1

References

(1) Tang, C. W. *Applied Physics Letters* **1986**, *48*, 183.

(2) Sariciftci, N. S.; Smilowitz, L.; Heeger, A. J.; Wudl, F. *Science* **1992**, *258*, 1474.

(3) Hummelen, J. C.; Knight, B. W.; LePeq, F.; Wudl, F.; Yao, J.; Wilkins, C. L. *The Journal of Organic Chemistry* **1995**, *60*, 532.

(4) Yu, G.; Gao, J.; Hummelen, J. C.; Wudl, F.; Heeger, A. J. *Science* **1995**, *270*, 1789.

(5) Irwin, M. D.; Buchholz, D. B.; Hains, A. W.; Chang, R. P. H.; Marks, T. J. *Proceedings of the National Academy of Sciences* **2008**, *105*, 2783.

(6) Shrotriya, V.; Li, G.; Yao, Y.; Chu, C.-W.; Yang, Y. *Applied Physics Letters* **2006**, *88*, 073508.

(7) Hains, A. W.; Marks, T. J. *Applied Physics Letters* **2008**, *92*, 023504.

(8) Waldauf, C.; Morana, M.; Denk, P.; Schilinsky, P.; Coakley, K.; Choulis, S. A.; Brabec, C. J. *Applied Physics Letters* **2006**, *89*, 233517.

(9) Gaynor, W.; Lee, J.-Y.; Peumans, P. *ACS Nano* **2009**, *4*, 30.

(10) Li, G.; Chu, C. W.; Shrotriya, V.; Huang, J.; Yang, Y. *Applied Physics Letters* **2006**, *88*, 253503.

(11) Bundgaard, E.; Krebs, F. C. *Solar Energy Materials and Solar Cells* **2007**, *91*, 954.

(12) Wienk, M. M.; Kroon, J. M.; Verhees, W. J. H.; Knol, J.; Hummelen, J. C.; van Hal, P. A.; Janssen, R. A. J. *Angewandte Chemie International Edition* **2003**, *42*, 3371.

(13) Gregg, B. A. *The Journal of Physical Chemistry B* **2003**, *107*, 4688.

(14) Barth, S.; Bassler, H. *Physical Review Letters* **1997**, *79*, 4445.

(15) Alvarado, S. F.; Seidler, P. F.; Lidzey, D. G.; Bradley, D. D. C. *Physical Review Letters* **1998**, *81*, 1082.

(16) Moliton, A.; Nunzi, J.-M. *Polymer International* **2006**, *55*, 583.

(17) Cook, S.; Furube, A.; Katoh, R.; Han, L. *Chemical Physics Letters* **2009**, *478*, 33.

(18) Ayzner, A. L.; Tassone, C. J.; Tolbert, S. H.; Schwartz, B. J. *The Journal of Physical Chemistry C* **2009**, *113*, 20050.

(19) Shaw, P. E.; Ruseckas, A.; Samuel, I. D. W. *Advanced Materials* **2008**, *20*, 3516.

(20) Loi, M. A.; Toffanin, S.; Muccini, M.; Forster, M.; Scherf, U.; Scharber, M. *Advanced Functional Materials* **2007**, *17*, 2111.

(21) Veldman, D.; İpek, O. z.; Meskers, S. C. J.; Sweelssen, J. r.; Koetse, M. M.; Veenstra, S. C.; Kroon, J. M.; Bavel, S. S. v.; Loos, J.; Janssen, R. A. J. *Journal of the American Chemical Society* **2008**, *130*, 7721.

(22) Scharber, M. C.; Mühlbacher, D.; Koppe, M.; Denk, P.; Waldauf, C.; Heeger, A. J.; Brabec, C. J. *Advanced Materials* **2006**, *18*, 789.

(23) Perez, M. D.; Borek, C.; Forrest, S. R.; Thompson, M. E. *Journal of the American Chemical Society* **2009**, *131*, 9281.

(24) Vandewal, K.; Tvingstedt, K.; Gadisa, A.; Inganas, O.; Manca, J. V. *Nature Materials* **2009**, *8*, 904.

(25) Mihailetchi, V. D.; Blom, P. W. M.; Hummelen, J. C.; Rispens, M. T. *Journal of Applied Physics* **2003**, *94*, 6849.

(26) Roncali, J. *Chemical Reviews* **1997**, *97*, 173.

(27) Wudl, F.; Kobayashi, M.; Heeger, A. J. *The Journal of Organic Chemistry* **1984**, *49*, 3382.

(28) Chen, H.-Y.; Hou, J.; Zhang, S.; Liang, Y.; Yang, G.; Yang, Y.; Yu, L.; Wu, Y.; Li, G. *Nature Photonics* **2009**, *3*, 649.

(29) Havinga, E. E.; Hoeve, W.; Wynberg, H. *Polymer Bulletin* **1992**, *29*, 119.

(30) Zhang, Q. T.; Tour, J. M. *Journal of the American Chemical Society* **1998**, *120*, 5355.

(31) McCullough, R. D.; Lowe, R. D. *Journal of the Chemical Society, Chemical Communications* **1992**, 70.

(32) McCullough, R. D.; Lowe, R. D.; Jayaraman, M.; Anderson, D. L. *The Journal of Organic Chemistry* **1993**, *58*, 904.

(33) Mayer, A. C.; Toney, M. F.; Scully, S. R.; Rivnay, J.; Brabec, C. J.; Scharber, M.; Koppe, M.; Heeney, M.; McCulloch, I.; McGehee, M. D. *Advanced Functional Materials* **2009**, *19*, 1173.

(34) Yap, B. K.; Xia, R.; Campoy-Quiles, M.; Stavrinou, P. N.; Bradley, D. D. C. *Nature Materials* **2008**, *7*, 376.

(35) Kline, R. J.; McGehee, M. D.; Kadnikova, E. N.; Liu, J.; Fréchet, J. M. J. *Advanced Materials* **2003**, *15*, 1519.

(36) Schilinsky, P.; Asawapirom, U.; Scherf, U.; Biele, M.; Brabec, C. J. *Chemistry of Materials* **2005**, *17*, 2175.

(37) Coffin, R. C.; Peet, J.; Rogers, J.; Bazan, G. C. *Nature Chemistry* **2009**, *1*, 657.

(38) Ma, W.; Yang, C.; Gong, X.; Lee, K.; Heeger, A. J. *Advanced Functional Materials* **2005**, *15*, 1617.

(39) Brabec, C. J.; Winder, C.; Sariciftci, N. S.; Hummelen, J. C.; Dhanabalan, A.; van Hal, P. A.; Janssen, R. A. J. *Advanced Functional Materials* **2002**, *12*, 709.

(40) Wang, X.; Perzon, E.; Delgado, J. L.; de la Cruz, P.; Zhang, F.; Langa, F.; Andersson, M.; Inganas, O. *Applied Physics Letters* **2004**, *85*, 5081.

(41) Thompson, B. C.; Fréchet, J. M. J. *Angewandte Chemie-International Edition* **2008**, *47*, 58.

(42) Peet, J.; Kim, J. Y.; Coates, N. E.; Ma, W. L.; Moses, D.; Heeger, A. J.; Bazan, G. C. *Nature Materials* **2007**, *6*, 497.

(43) Chen, C.-P.; Chan, S.-H.; Chao, T.-C.; Ting, C.; Ko, B.-T. *Journal of the American Chemical Society* **2008**, *130*, 12828.

(44) Hou, J.; Chen, H.-Y.; Zhang, S.; Li, G.; Yang, Y. *Journal of the American Chemical Society* **2008**, *130*, 16144.

(45) Wang, E.; Wang, L.; Lan, L.; Luo, C.; Zhuang, W.; Peng, J.; Cao, Y. *Applied Physics Letters* **2008**, *92*, 033307.

(46) Wienk, M. M.; Turbiez, M.; Gilot, J.; Janssen, R. A. J. *Advanced Materials* **2008**, *20*, 2556.

(47) Huang, F.; Chen, K.-S.; Yip, H.-L.; Hau, S. K.; Acton, O.; Zhang, Y.; Luo, J.; Jen, A. K. Y. *Journal of the American Chemical Society* **2009**.

(48) Huo, L.; Hou, J.; Chen, H.-Y.; Zhang, S.; Jiang, Y.; Chen, T. L.; Yang, Y. *Macromolecules* **2009**, *42*, 6564.

(49) Liang, Y.; Feng, D.; Wu, Y.; Tsai, S.-T.; Li, G.; Ray, C.; Yu, L. *Journal of the American Chemical Society* **2009**, *131*, 7792.

(50) Liang, Y.; Wu, Y.; Feng, D.; Tsai, S.-T.; Son, H.-J.; Li, G.; Yu, L. *Journal of the American Chemical Society* **2009**, *131*, 56.

(51) Park, S. H.; Roy, A.; Beaupre, S.; Cho, S.; Coates, N.; Moon, J. S.; Moses, D.; Leclerc, M.; Lee, K.; Heeger, A. J. *Nat. Photonics* **2009**, *3*, 297.

(52) Xiao, S. Q.; Zhou, H. X.; You, W. *Macromolecules* **2008**, *41*, 5688.

(53) Xiao, S.; Stuart, A. C.; Liu, S.; You, W. *ACS Applied Materials & Interfaces* **2009**, *1*, 1613.

(54) Westenhoff, S.; Howard, I. A.; Hodgkiss, J. M.; Kirov, K. R.; Bronstein, H. A.; Williams, C. K.; Greenham, N. C.; Friend, R. H. *Journal of the American Chemical Society* **2008**, *130*, 13653.

(55) Koeckelberghs, G.; De Cremer, L.; Persoons, A.; Verbiest, T. *Macromolecules* **2007**, *40*, 4173.

(56) Radke, K. R.; Ogawa, K.; Rasmussen, S. C. *Organic Letters* **2005**, *7*, 5253.

(57) Pan, H.; Li, Y.; Wu, Y.; Liu, P.; Ong, B. S.; Zhu, S.; Xu, G. *Chem. Mater.* **2006**, *18*, 3237.

(58) Sonar, P.; Zhang, J.; Grimsdale, A. C.; Mullen, K.; Surin, M.; Lazzaroni, R.; Leclere, P.; Tierney, S.; Heeney, M.; McCulloch, I. *Macromolecules* **2004**, *37*, 709.

(59) Heeney, M.; Tierney, S.; Thompson, M.; Giles, M.; Farrand, L.; Shkunov, M.; Sparrowe, D.; McCulloch, I. **2003**.

(60) Campaigne, E.; Bourgeois, R. C. *Journal of the American Chemical Society* **1954**, *76*, 2445.

(61) Blouin, N.; Michaud, A.; Gendron, D.; Wakim, S.; Blair, E.; Neagu-Plesu, R.; Belletete, M.; Durocher, G.; Tao, Y.; Leclerc, M. *Journal of the American Chemical Society* **2008**, *130*, 732.

(62) Brabec, C. J.; Cravino, A.; Meissner, D.; Sariciftci, N. S.; Fromherz, T.; Rispens, M. T.; Sanchez, L.; Hummelen, J. C. *Advanced Functional Materials* **2001**, *11*, 374.

(63) Gadisa, A.; Svensson, M.; Andersson, M. R.; Inganas, O. *Applied Physics Letters* **2004**, *84*, 1609.

(64) Mihailetchi, V. D.; Blom, P. W. M.; Hummelen, J. C.; Rispens, M. T. *J. Appl. Phys.* **2003**, *94*, 6849.

(65) Ma, W.; Kim, J. Y.; Lee, K.; Heeger, A. J. *Macromolecular Rapid Communications* **2007**, *28*, 1776.

(66) Ballantyne, A. M.; Chen, L.; Dane, J.; Hammant, T.; Braun, F. M.; Heeney, M.; Duffy, W.; McCulloch, I.; Bradley, D. D. C.; Nelson, J. *Advanced Functional Materials* **2008**, *18*, 2373.

(67) Mihailetchi, V. D.; Xie, H. X.; de Boer, B.; Koster, L. J. A.; Blom, P. W. M. *Advanced Functional Materials* **2006**, *16*, 699.

(68) Goh, C.; Kline, R. J.; McGehee, M. D.; Kadnikova, E. N.; Fréchet, J. M. J. *Applied Physics Letters* **2005**, *86*, 122110.

(69) Furuta, P.; Frechet, J. M. J. *Journal of the American Chemical Society* **2003**, *125*, 13173.

(70) Liu, B.; Bazan, G. C. *Nat. Protocols* **2006**, *1*, 1698.

(71) Zhang, M.; Tsao, H. N.; Pisula, W.; Yang, C.; Mishra, A. K.; Mullen, K. *Journal of the American Chemical Society* **2007**, *129*, 3472.

(72) Odom, Susan A.; Lancaster, K.; Beverina, L.; Lefler, Kelly M.; Thompson, Natalie J.; Coropceanu, V.; Brédas, J.-L.; Marder, Seth R.; Barlow, S. *Chemistry - A European Journal* **2007**, *13*, 9637.

(73) Lehmann, L. U. U.S., 2008; Vol. US 2008/0262183 A1.

(74) Scharber, M. C.; Mühlbacher, D.; Koppe, M.; Denk, P.; Waldauf, C.; Heeger, A. J.; Brabec, C. J. *Adv. Mater.* **2006**, *18*, 789.

(75) Jenekhe, S. A.; Lu, L.; Alam, M. M. *Macromolecules* **2001**, *34*, 7315.

(76) Zhu, Y.; Champion, R. D.; Jenekhe, S. A. *Macromolecules* **2006**, *39*, 8712.

(77) Pan, H.; Li, Y.; Wu, Y.; Liu, P.; Ong, B. S.; Zhu, S.; Xu, G. *Journal of the American Chemical Society* **2007**, *129*, 4112.

(78) Hou, J.; Park, M.-H.; Zhang, S.; Yao, Y.; Chen, L.-M.; Li, J.-H.; Yang, Y. *Macromolecules* **2008**, *41*, 6012.

(79) Price, S. C.; Stuart, A. C.; You, W. *Macromolecules* **2010**, *43*, 797.

(80) Zhou, H.; Yang, L.; Xiao, S.; Liu, S.; You, W. *Macromolecules* **2010**, *43*, 811.

(81) Bijleveld, J. C.; Zoombelt, A. P.; Mathijssen, S. G. J.; Wienk, M. M.; Turbiez, M.; de Leeuw, D. M.; Janssen, R. A. J. *Journal of the American Chemical Society* **2009**, *131*, 16616.

(82) Wang, E.; Wang, M.; Wang, L.; Duan, C.; Zhang, J.; Cai, W.; He, C.; Wu, H.; Cao, Y. *Macromolecules* **2009**, *42*, 4410.

(83) Shi, C. J.; Yao, Y.; Yang, Y.; Pei, Q. B. *Journal of the American Chemical Society* **2006**, *128*, 8980.

(84) Song, S.; Jin, Y.; Kim, S. H.; Moon, J.; Kim, K.; Kim, J. Y.; Park, S. H.; Lee, K.; Suh, H. *Macromolecules* **2008**, *41*, 7296.

(85) Qin, R.; Li, W.; Li, C.; Du, C.; Veit, C.; Schleiermacher, H.-F.; Andersson, M.; Bo, Z.; Liu, Z.; Inganaì^s, O.; Wuerfel, U.; Zhang, F. *Journal of the American Chemical Society* **2009**, *131*, 14612.

(86) Brown, P. J.; Thomas, D. S.; Köhler, A.; Wilson, J. S.; Kim, J.-S.; Ramsdale, C. M.; Sirringhaus, H.; Friend, R. H. *Physical Review B* **2003**, *67*, 064203.

(87) Pan, H.; Li, Y.; Wu, Y.; Liu, P.; Ong, B. S.; Zhu, S.; Xu, G. *Chemistry of Materials* **2006**, *18*, 3237.

(88) Kitamura, C.; Tanaka, S.; Yamashita, Y. *Chemistry of Materials* **1996**, *8*, 570.

(89) Hou, Q.; Zhou, Q.; Zhang, Y.; Yang, W.; Yang, R.; Cao, Y. *Macromolecules* **2004**, *37*, 6299.

(90) Piliego, C.; Holcombe, T. W.; Douglas, J. D.; Woo, C. H.; Beaujuge, P. M.; Fréchet, J. M. J. *Journal of the American Chemical Society* **2010**, *132*, 7595.

(91) Zhao, G.; He, Y.; Li, Y. *Advanced Materials* **2010**, *22*, 4355.

(92) Bijleveld, J. C.; Zoombelt, A. P.; Mathijssen, S. G. J.; Wienk, M. M.; Turbiez, M.; de Leeuw, D. M.; Janssen, R. A. J. *Journal of the American Chemical Society* **2009**, *131*, 16616.

(93) Zhang, F.; Jespersen, K. G.; Björström, C.; Svensson, M.; Andersson, M. R.; Sundström, V.; Magnusson, K.; Moons, E.; Yartsev, A.; Inganäs, O. *Advanced Functional Materials* **2006**, *16*, 667.

(94) Brabec, C. J.; Shaheen, S. E.; Winder, C.; Sariciftci, N. S.; Denk, P. *Applied Physics Letters* **2002**, *80*, 1288.

(95) Shaheen, S. E.; Brabec, C. J.; Sariciftci, N. S.; Padinger, F.; Fromherz, T.; Hummelen, J. C. *Applied Physics Letters* **2001**, *78*, 841.

(96) Beaujuge, P. M.; Amb, C. M.; Reynolds, J. R. *Accounts of Chemical Research* **2010**, *43*, 1396.

(97) Kim, J. Y.; Lee, K.; Coates, N. E.; Moses, D.; Nguyen, T.-Q.; Dante, M.; Heeger, A. J. *Science* **2007**, *317*, 222.

(98) Dennler, G.; Scharber, M. C.; Ameri, T.; Denk, P.; Forberich, K.; Waldauf, C.; Brabec, C. J. *Advanced Materials* **2008**, *20*, 579.

(99) Goodwin, A. P.; Mynar, J. L.; Ma, Y.; Fleming, G. R.; Fréchet, J. M. J. *Journal of the American Chemical Society* **2005**, *127*, 9952.

(100) Li, G.; Shrotriya, V.; Huang, J. S.; Yao, Y.; Moriarty, T.; Emery, K.; Yang, Y. *Nature Materials* **2005**, *4*, 864.

(101) Price, S. C.; Stuart, A. C.; You, W. *Macromolecules* **2010**, *43*, 4609.

(102) Zhou, H.; Yang, L.; Price, S. C.; Knight, K. J.; You, W. *Angewandte Chemie International Edition* **2010**, *49*, 7992.

(103) Zhou, H.; Yang, L.; Liu, S.; You, W. *Macromolecules* **2010**, *43*, 10390.

(104) Shockley, W.; Queisser, H. J. *Journal of Applied Physics* **1961**, *32*, 510.

(105) Balan, A.; Gunbas, G.; Durmus, A.; Toppare, L. *Chemistry of Materials* **2008**, *20*, 7510.

(106) Tanimoto, A.; Yamamoto, T. *Macromolecules* **2006**, *39*, 3546.

(107) Charushin, V. N.; Kotovskaya, S. K.; Romanova, S. A.; Chupakhin, O. N.; Tomilov, Y. V.; Nefedov, O. M. *Mendeleev Communications* **2005**, *15*, 45.

(108) Yang, L.; Zhou, H.; You, W. *The Journal of Physical Chemistry C* **2010**, *114*, 16793.

(109) Pagliaro, M.; Ciriminna, R. *Journal of Materials Chemistry* **2005**, *15*, 4981.

(110) Chen, D.-Y.; Hsu, Y.-Y.; Hsu, H.-C.; Chen, B.-S.; Lee, Y.-T.; Fu, H.; Chung, M.-W.; Liu, S.-H.; Chen, H.-C.; Chi, Y.; Chou, P.-T. *Chemical Communications* **2010**, *46*, 5256.

(111) Li, G.; Shrotriya, V.; Huang, J.; Yao, Y.; Moriarty, T.; Emery, K.; Yang, Y. *Nature Materials* **2005**, *4*, 864.

(112) Mihailetchi, V. D.; Xie, H. X.; de Boer, B.; Koster, L. J. A.; Blom, P. W. M. *Advanced Functional Materials* **2006**, *16*, 699.

(113) Pan, H.; Li, Y.; Wu, Y.; Liu, P.; Ong, B. S.; Zhu, S.; Xu, G. *Chemistry of Materials* **2006**, *18*, 3237.

(114) Tylleman, B. t.; Gbabode, G.; Amato, C.; Buess-Herman, C.; Lemaur, V.; Cornil, J. r. m.; Gómez Aspe, R.; Geerts, Y. H.; Sergeyev, S. *Chemistry of Materials* **2009**, *21*, 2789.

(115) Liang, Y.; Wu, Y.; Feng, D.; Tsai, S.-T.; Son, H.-J.; Li, G.; Yu, L. *Journal of the American Chemical Society* **2008**, *131*, 56.

(116) Sotzing, G. A.; Lee, K. *Macromolecules* **2002**, *35*, 7281.

(117) Pomerantz, M.; Gu, X. *Synthetic Metals* **1997**, *84*, 243.

(118) Greenlee, W. J., David; Maccoss, Malcolm; Mantio, Nathan; Chakravarty, Prasun; Walsh, Thomas.; Merck & Co. Inc.: 1995.

(119) Kenning, D. D.; Mitchell, K. A.; Calhoun, T. R.; Funfar, M. R.; Sattler, D. J.; Rasmussen, S. C. *The Journal of Organic Chemistry* **2002**, *67*, 9073.

(120) Hooley, R. J.; Rebek *Organic Letters* **2007**, *9*, 1179.

(121) Williams, J. H. *Accounts of Chemical Research* **1993**, *26*, 593.

(122) Feast, W. J.; Lovenich, P. W.; Puschmann, H.; Taliani, C. *Chemical Communications* **2001**, 505.

(123) Hou, J.; Park, M.-H.; Zhang, S.; Yao, Y.; Chen, L.-M.; Li, J.-H.; Yang, Y. *Macromolecules* **2008**, *41*, 6012.